UNIVERSITY OF
KWAZULU-NATAL

Electrical Engineering

Title: The use of an Auxiliary Spark Gap placed across the Surge arrester of a medium Voltage Transformer

Author: R Reddy (8830365)

Initiated By: Mr Tony Britten

University Supervisor: Dr Derek Hoch

DECLARATION OF OWN WORK

I declare that this dissertation is my own unaided work and the relevant sources that I have used or quoted, have been indicated accordingly in the text. The dissertation has being submitted for the Masters of Science in Engineering at the University of Kwazulu Natal. The work has not been submitted before for any degree or examination at any other university in South Africa.

The research work was conducted at the University of Kwazulu Natal under the supervision of Dr Derek Hoch in the Department of Electrical Engineering. The work forms part of an Eskom project (R99-00852) to report on the findings of the viability of using spark gaps for medium voltage transformer back-up protection.

Ravichandran Reddy

Date:

24th day of December 2007

ACKNOWLEDGEMENTS

I would like to thank the following people for their kind assistance, support and time dedicated to assist with this thesis

- Dr Derek Hoch for his tremendous technical guidance, support, knowledge imparted, supervision and patients
- Dr Hendri Geldenhuys and the late Mr Ian Ferguson for supervising and assisting me with references
- Mr Tony Britten for his technical comments and guidance.
- The Eastern Region management team especially Mr Prince Moyo and Mr Riaz Asmal for their support and encouragement to embark and complete the thesis.
- Miss S Ackah for her encouragement support and kind assistance in research material and with the compilation of this thesis document.

ABSTRACT

A possible lower cost alternative to medium voltage line arresters and parallel-connected surge arresters is the use of parallel-connected spark gaps across a metal oxide surge arrester. The function of the spark gap is to protect the transformer when the surge arrester fails. Clearly the breakdown voltage characteristics of such a gap need to be carefully co-ordinated with the transformer insulation and those of the arrester. Eskom (Electricity Supply Commission of South Africa) is the national electrical utility that provides the generation, transmission and distribution of electricity in South Africa. The majority of Eskom's electricity reticulation is done with either 11 kV or 22 kV electrical overhead networks. An unacceptable number of Eskom's pole mounted power transformers on these networks have failed over the past few years. The high failure rate of Distribution transformers in Eskom, South Africa has previously been highlighted and investigated in an MSc thesis, the most recent being the thesis completed at the University of Kwazulu Natal by Chatterton [6]. The thesis proposed possible solutions to the problem but experienced high implementation costs and particular technical issues before widespread implementation could prove viable for the Distribution System. The average transformer failure rate for the Distribution Eastern Region for the twelve month period taken as a moving average was calculated to be 5.19 % per annum at the end of November 2005 and 3.84 % at the end of November 2006. (Eskom Eastern Region Plant report, November 2006). International norms seem to indicate that a transformer failure rate of between 0.5% and 1.0% per annum is acceptable, Chatterton [6]. The reason for the increased failure rates during 2005 was attributed to incorrect Ground Lead Disconnect (GLD) specifications by one of the major surge arrester manufacturers. The incorrect GLD specifications have resulted in premature and nuisance operations. These were triggered by low intensity lightning storms as a result of the lower threshold trigger values. These premature operations have left numerous transformers vulnerable for periods as long as six months and have resulted in the transformer failures increasing from 2.4% quoted by Chatterton [6] in 2002 to 5.19% in 2005 and a reduction to 3.84 % in November 2006 once the problem was identified and the GLDs corrected. See annexure A, Figure A1 of the Plant report for November 2006 for performance details. Hence, this manufacturing flaw and the GLD's sensitivity to specification

necessitate further investigation into the spark gap as back-up protection. The spark gap therefore becomes more viable than line or double surge arresters due to its cost effectiveness and robustness. This thesis was based on an idea proposed by Eskom's (Industrial Association Resource Centre) IARC. The aim was to investigate the technical feasibility of using a spark gap to grade with a distribution class surge arrester whilst the surge arrester was operational. The purpose of the spark gap was to act as back-up protection when the arrester fails. Experimentation was undertaken via simulation using the FEMLAB software to model the most suitable gap and geometry for a given rod diameter. The breakdown characteristic of the rod was well understood and verified. Thus, the results obtained from the simulation were compared against the laboratory experiments for the same rod diameters and tip shapes used in the simulation. The results have been analyzed to determine whether the spark gap is a feasible solution for use with surge arresters to protect the transformer from induced strikes following arrester failure.

LIST OF SYMBOLS USED

The following is a list of symbols used in the thesis

$L1$ = Self-inductance of primary winding

$L2$ = Self-inductance of secondary winding

M = Mutual inductance between windings

$L8$ = Short-circuit inductance

C_m = Mutual capacitance

C_w = Capacitance from end to end in Farads

C_g = Capacitance to earth of the complete winding

I_g = Current to earth per unit length of winding at distance x from neutral

I_w = Current flowing in the turn to turn capacitance distance x from the neutral

r = Turns ratio of primary to secondary winding

E_T = Voltage to earth impressed on the line terminals

e_t = Voltage to earth at a point in the winding a distance x from the neutral end

l = length of winding, the same units as x

$v_{10\%}$ = The 10% flashover voltage

$v_{50\%}$ = The 50% flashover voltage

v_b = PM + $v_{50\%}$

PM = Protective margin

ϕ = arc of a circle produced by the Bruce profile

φ = The gradient of the E-field strength between plates

σ = The standard deviation of the statistical distribution of breakdown voltages

TABLE OF CONTENTS

LIST OF FIGURES

LIST OF TABLES

CHAPTER 1 INTRODUCTION

1.1 Background to the Dissertation

The high failure rates of Distribution level transformers in South Africa has previously been highlighted and investigated in two recent MSc thesis; the one performed at the University of Natal by Chatterton [6] and the second was completed at Stellenbosch University by Ahlschlager [personal communication]. Both these thesis projects proposed possible solutions to the problem but both experienced high costs and particular technical issues before widespread implementation within the Distribution System. The project is thus based on an original idea proposed by Ahlschlager. A possible lower cost alternative to parallel-connected surge arresters and line arresters is the use of a parallel-connected spark gap across an arrester. The function of the spark gap is to protect the transformer from lightning induced surges in the event of the surge arrester failing. Clearly the breakdown-voltage surge characteristics of such a gap need to be carefully analysed to ensure that the gap behaves as backup protection and the resulting reflected waves from the chopped wave does not cause transformer winding damage.

1.2 Literature Review of Works Produced On Spark Gaps

Extensive work has been done on the subject of spark gaps and the following references published in the IEEE Transactions on Power Apparatus and Systems was used to review the history of spark gaps: Linck [19], Amestrand [20], Linck [21]. These references have presented comprehensive technical data on the breakdown characteristics of such gaps. All the information from these references is based on tests carried out in clean air gaps. The paper written by Qureshi [30], addresses the performance of rod gaps, single and multiple when subjected to atmospheric pollution frequently found in arid and desert terrains. The paper discusses the influence of pollution on the breakdown voltage and breakdown time of protective air gaps. The rod radius and its end profile was changed to find the configuration which is least affected by pollution. In addition, practical protective gaps used across transformer bushings were tested to check their performance in clean and polluted conditions. Tests were conducted to further examine the effects of the rod tip radius on the breakdown voltage under dust pollution conditions. The performance of practical rod-rod (or bi-rod) gaps installed across medium voltage bushings and insulator chains were investigated using standard lightning impulses of both polarities. Qureshi [30], also studies the effect of atmospheric pollution on the performance of duplex (or multiplex) rod gaps as shown in

figure 2.2b below installed across bushings. Such gaps are used extensively by several transformer manufacturers and are being supplied to the electric power utilities worldwide. All of the published works investigated did not discuss the integration of a surge arrester and spark gap, where the spark gap is the backup overvoltage protection to the arrester.

1.3 Objectives of the Dissertation

The aim of this project was to investigate the feasibility of using a spark gap to co-ordinate with a distribution class 11kV or 22kV surge arresters whilst the surge arrester is operational. The investigation was done by simulating various geometries and gap sizes to determine which gap was best suited to be integrated with a typical Distribution transformer. The spark gaps purpose is to act purely as back up overvoltage protection, when the arrester fails. Experimentation was done by simulation studies using the **FEMLAB** package to model the electric field and hence the breakdown voltage characteristics. The simulations were performed with various gap sizes and geometries. The simulated results were compared and verified by performing laboratory experiments. These results were analysed to specify a single suitable gap or range of gaps and geometry to be paralleled with a Distribution Class surge arrester.

1.4 Dissertation Outline

The dissertation follows the outline below:

a) To undertake a comprehensive literature review of similar research data to develop appropriate, relevant theory to predict the performance of non-standard spark gap geometries under both standard and non-standard lightning impulse over voltages. This includes a thorough review of work previously completed within Eskom on this topic.
b) The literature review also discusses the performance of the transformer insulation when exposed to lightning impulse stressing.
c) Further explanations of how the volt-time curve is to be co-ordinated with that of the arrester and how the gap and arrester may influence each other are provided.
d) Simulation studies using FEMLAB on various geometries and gap distances with and without an earth plane are presented and analyzed in chapters that follow.
e) The simulation studies investigate factors that impact on the reliability of the proposed protection scheme.
f) The laboratory experiments used to verify the results of the simulation studies and confirm the choice of gap and gap settings are then presented.

CHAPTER 2 THE HISTORY AND THEORY OF SPARK GAPS

2.1 Introduction and history of Spark Gaps

2.1.1 Introduction

Spark gaps are used for protection of equipment against high voltage surges, for all voltage ranges, the advantage being that the *dielectric is recoverable*. Historically spark gaps ranged from the more commonly used arrester having Nitrogen in a ceramic body, with voltage ratings from 150 V to 1 000 V, to low pressure vacuum bottles with ratings of 1 V to 50 kV for railway equipment protection. Rod gaps, the focus of this thesis, are frequently used for over-voltage protection and insulation co-ordination in medium and high voltage networks. The main utilization of such gaps are:

(a) transformer protection against voltage surges,

(b) protection of insulators and cable terminations against harmful surface arcs,

(c) to produce chopped impulses for test purposes, and

(d) for the protection of workers busy on live line installation or maintenance.

2.1.2 The history of research on spark gaps

Extensive studies on large gaps typically, 500 mm to 2000 mm, at voltages of 115 kV and above have been performed and reported on by various IEEE working groups as follows:

a) IEEE Transactions on Power Apparatus and Systems, Vol 86, Linck [19]

- Rod diameters 10 mm to 25 mm
- Gaps 400 mm to 2,5 m
- Voltage levels in the report 115 kV to 345 kV

b) IEEE Transactions on Power Apparatus and Systems, Vol 93, Amestrand [20]

- Gap sizes tested 500 mm to 2000 mm
- Voltage range for test 500 kV – 2500 kV

c) IEEE Transactions on Power Apparatus and Systems, Vol 87, Linck [21]

• Voltage test ranging	320 kV to 450 kV
• Gap sizes	900 mm to 2000 mm

d) IEE, Proc. Part A, 1995, Kuffel [23]

As noted above, the published data are well above the voltage requirements for this investigation. However certain of the principles may be extended and applied. The only suitable source of data that was found in the range of test parameters in the published literature was on sphere gaps and a contribution on multiple gaps by Qureshi [30].

e) The familiar standard rod and sphere gaps suffer a basic weakness for protective gap applications. Rod gaps have a long time lag and are therefore difficult to co-ordinate with oil immersed apparatus. Sphere gaps do not have this disadvantage, but instead maybe drastically influenced by rain and other foreign particles in outdoor exposures, Linck [21].

Most spark gaps have typical accuracies of 3% for gaps less than half the diameter of the sphere and 5% for the gap larger than the diameter of the sphere for measurement. Spark gaps used for testing purposes are recognized in IEC 60052 [51]. As the gap gets larger, the field between the sphere becomes less uniform, and as a result the scatter in the data gets larger. The sphere gap is accurate and reproducible over its range, which extends to gaps equal to 0,5 X sphere diameter, after which it loses accuracy due to field distortion. It is also necessary to take into account humidity, temperature and pressure, all of which affect the breakdown voltage. A rod gap is a non-uniform gap, and is often quoted at +/- 8% accuracy for measurement. The tables for "sparking voltage against gap" in IEC 60060-2 [22] are still being used although the standard has undergone revision.

The simplest and most common spark gap is the rod-gap, used on outdoor equipment such as transformers, substations and bushings. Its simplicity is offset by a variable breakdown voltage with respect to time and polarity. For equipment protected by a rod gap, it is important to know its 'breakdown voltage against time' characteristics relative to that of the equipment being protected to ensure that the rod gap operates under the *specified surge conditions*. This is known as insulation co-ordination and is discussed in IEC 60028 [50].

2.2 Types of Spark Gaps

2.2.1 Open Spark Gaps

Spark gaps are found in some varieties. The most common spark gap is the rod gap as shown in Figure 2.1. This gap usually protects an insulator string, a bushing, a cable terminal, etc. Occasionally a ring-shaped electrode maybe used. These are suitable when a flashover wanders over the ring so that less damage is done to critical electrodes and insulators, Kreuger [47].

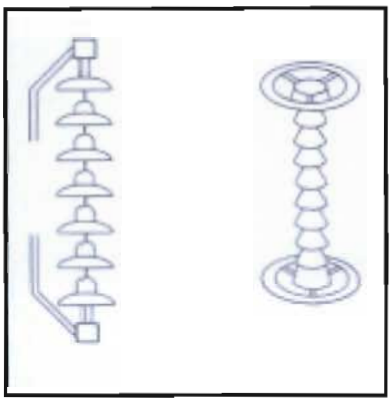

Figure 2.1 Open Spark Gaps, Kreuger [47]

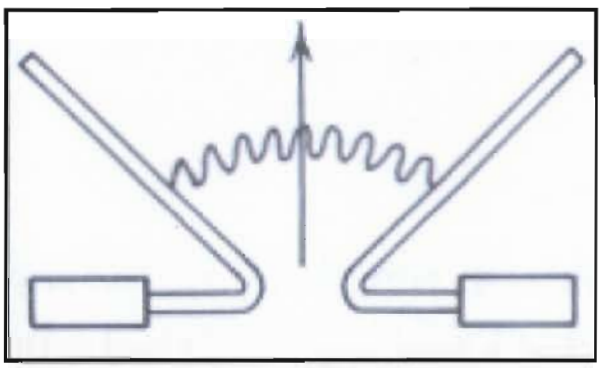

Figure 2.2a Arcing horns, Kreuger [47]

2.2.2 Arcing Horns

Arcing horns in Figure 2.2a are used at relatively low voltage levels. When an arc is formed, high currents pass the horns and cause a magnetic field. The arc undergoes an electrodynamic force and moves upwards. The arc is stretched and cools, the arc

voltage increases and the arc is eventually extinguished. This is a first step to a self-extinguishing arrester and is normally used to protect transformers.

2.2.3 Duplex Arrangement

Qureshi [30], discusses the effects of desert pollution on multiple rod gaps and the performance of duplex (or multiplex) rod gaps installed across bushings. These gaps are extensively used by several transformer manufacturers and are supplied to electric power utilities worldwide. It is interesting to note that merely the formation of a thin dust film on electrodes shifts breakdown levels towards the characteristics of polluted gaps. It is shown by Qureshi [30] that such pollution has a significant influence on the performance of rod gaps. This influence can be minimized by selecting rods of smaller diameters (± 10mm) and square cut end profiles. *Moreover, double sided rod gaps as shown in Figure 2.2b show greater immunity toward pollution as well as polarity effects as compared to single sided gaps.*

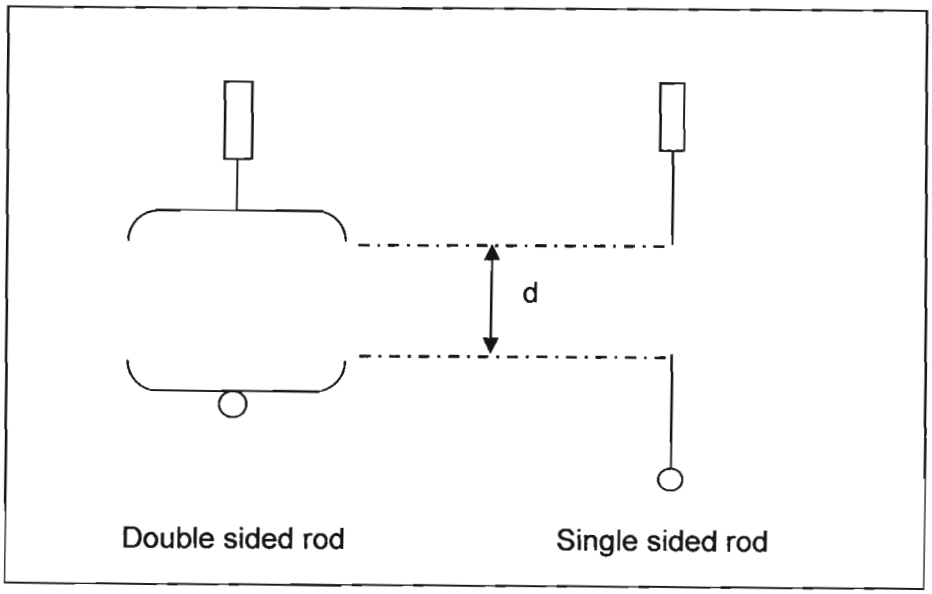

Figure 2.2b Double and single sided gaps

2.2.4 Wood Pole Basic Impulse Level Gap

The insulation level that provides optimal overall performance in high lightning areas for medium voltage networks has been proved on test sites. A range of basic impulse levels from 200 kV to 300 kV was found suitable for medium voltage networks. This level allows multiple flashovers for direct strikes and no flashovers for induced surges. It also limits the voltage and energy travelling down the line to a value that the surge arresters can dissipate without damage.

This BIL is achieved in the following way:

a) On suspension and intermediate structures, by the application of a BIL downwire and a 500 mm wood-path gap;
b) On stayed structures by the BIL of the insulators and the stay attachment point below hardware, provides the BIL.

2.3 Spark Gap Theory

2.3.1 Introduction

Th empirical method used for estimating the spark-over voltages of gaps of various geometries, based on the spark-over voltage of a rod-plane gap of the same length, indicates that the spark-over voltage depends on the spatial extent of the corona at the electrodes; this in turn depends on the nature of the electric field in the vicinity of the electrodes and hence their geometries. The details are explained in Chapter 5. A spark gap will have a very repeatable breakdown voltage for given atmospheric conditions. For mechanical reasons, uniform field gaps using Rogowski [31] or Bruce [26] profile electrodes are not used as much as sphere gaps where the sphere diameters are larger than the gap length. There is no convenient analytical expression for the breakdown voltage as a function of sphere diameter and gap, as there is for uniform field gaps. However, there exists empirical test data, which have been used in this thesis for comparision with the results obtained from the simulation and laboratory tests. Craggs [8], Kuffel [23] and Naidu [26] claimed that electrodes with separations of 112.5mm, 225mm and 375mm (see Figures 2.3 and 2.4 below), can be used for maximum voltages of 140kV, 280kV, and 420 kV respectively.

2.3.2 Electrode Geometry for Uniform Fields

2.3.2.1 Theory of the Rogowski Profiles

There are applications which require a uniform electric field between two electrodes such as breakdown voltage testing and large volume laser discharge cavities. The ideal infinite flat plates are somewhat difficult to realize in a laboratory of reasonable dimensions. Finite sized plates produce a uniform field at the middle of the plate, but a high field at the edges may create a problem in repeatability of breakdown voltage. Rogowski [31], and Naidu [26] report on techniques that starts by determining a realizable field, then constructing an electrode shaped such that the surface of the electrode creates an equipotential surface. Rogowski [31] started with an analytical solution of the field due to a finite plane plate parallel to an infinite plane. Bruce devised an empirical approach, which taken to the extreme, ensures that the field at a large distance from any charge distribution approximates the field from a point charge, i.e. a sphere, Naidu [26]. For example, consider the field between two finite flat plates. In the center region, the field is quite uniform. However, such electrodes if constructed, would create high field strengths at the edges of the plates and this would cause problems from a dielectric breakdown perspective. The solution is to construct electrodes that create an equipotential surface which is some distance from the flat plate electrode. Since it is further away, the field strength is lower, and breakdown is not as much of an issue. For an arbitrarily shaped electrode, determining the electric field, particularly in the dynamic case, is quite difficult and would normally need to be done by numerical techniques. However, for some special cases that happen to be useful, an analytical expression for the field can be developed. Naidu [26] showed that the gradient developed by Bruce, i.e. the electric-field strength, between the electrodes is greater than the gradient outside the

plane portion for any value of $\varphi = 1/2\pi$, where ϕ is the arc CD of the circle with centre 0 as shown in Figure 2.4 below

$$x = A(\phi + e^{\phi}\cos\varphi) \qquad (2.1)$$

$$y = A(\varphi + e^{\phi}\cos\varphi) \qquad (2.2)$$

In this situation, the above equation reduces to:

$$x = \frac{\alpha\varphi}{\pi} \qquad (2.3)$$

$$y = \frac{\alpha}{\pi}(\frac{\pi}{2} + e^{\varphi}) \qquad (2.4)$$

If $\varphi \leq 0.4\pi$, the field is greatest in the center region between the plates, and less everywhere else. If you make the electrode follow this contour, the breakdown voltage between the electrodes will be the same as if they were an infinite uniform field. Rengier, who worked with Rogowski [31], created electrodes by revolving surfaces for $\varphi = 1/2\pi$ and $2/3\pi$. Rengier found that the sparks always occurred within the central planar part and not the edges. Electrodes constructed with $\varphi = 5/6\pi$ always sparked at the edges. The $2/3\pi$ profile, while not as ideal as the $\varphi = 1/2\pi$ (or less) profile, will work adequately. The back surface of the electrode must also be smoothly curved, Cobine [7] and Craggs [8]. Figure 2.3 below shows a typical example of an electrode profile in a graphical format, showing equipotentials at intervals of 0.2, 0.4, 0.6, 0.8 and 1.0 as well as flux lines for a normalized case is shown.

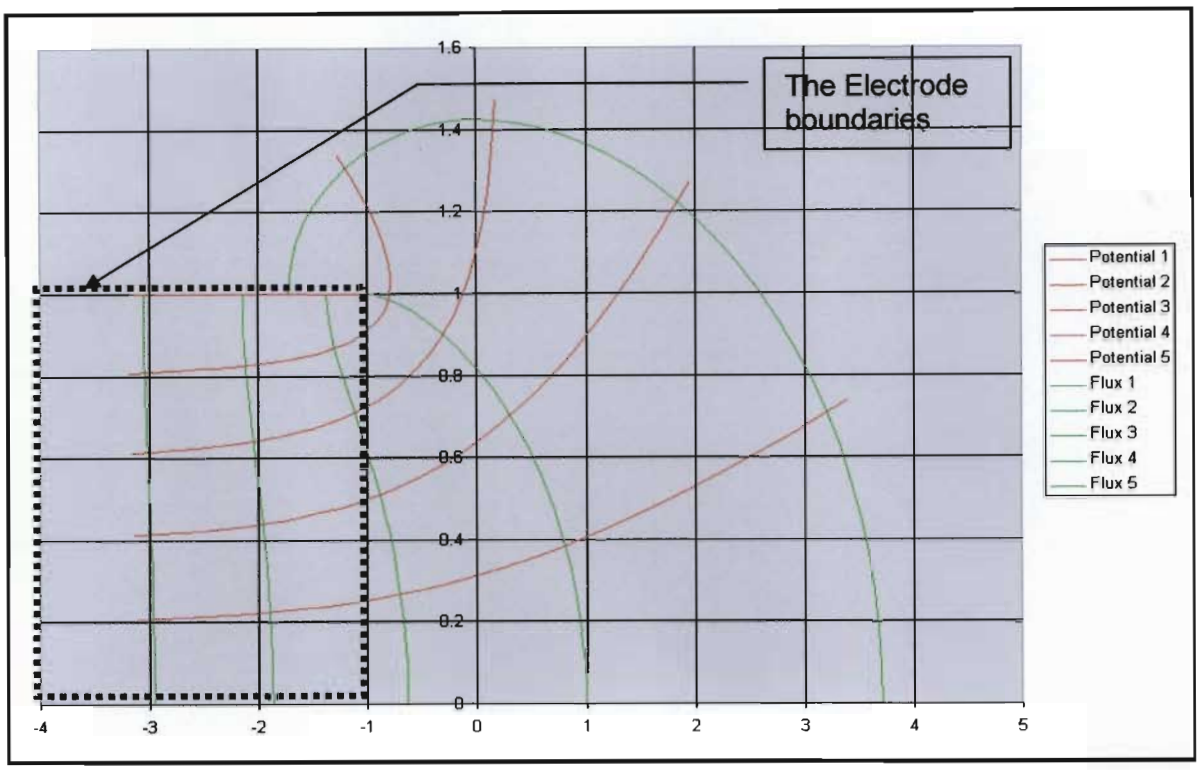

Figure 2.3 Electrode profiles showing equipotentials

2.3.2.2 Theory on the Bruce Profiles

Bruce referenced in Naidu [26] developed a series of electrode shapes that approximated an ideal uniform field. The Bruce profile shown in figure 2.4 of a revolution, starting with a flat plane in the center, with a sine curve used as a transition to a circular section at the edge.

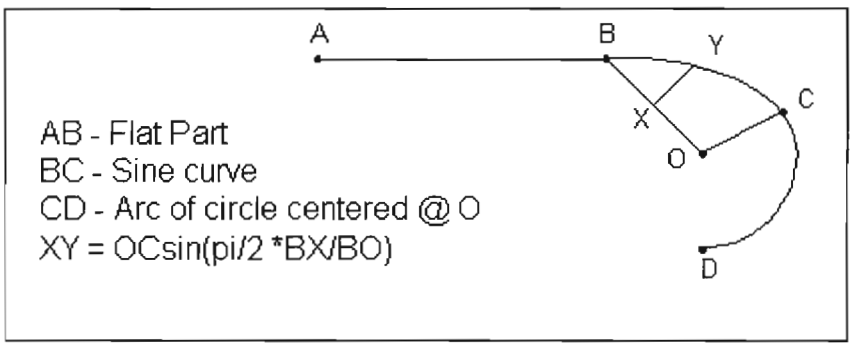

Figure 2.4 Bruce Profile

The idea is to have a large area of uniform field ie two flat plates with a gradually increasing radius of curvature to the edge. The Bruce profile was not originally developed with the intention of finding an analytical solution for the electrical-field analysis, but was empirically derived to reduce the edge effects, Naidu [26]

A comment made by Naidu [26], in connection with a discussion of uniform field gaps is that there is no significant difference in breakdown voltage between sphere gaps and the various uniform field gaps, given the fairly large uncertainty in all the measurements. In practice, breakdown measurements are made with spherical electrodes, because small changes in the surface of a uniform field electrode can cause field irregularities which in turn dramatically affect the breakdown voltages. Also, a deviation from parallelism of the opposing electrode faces can cause significant deviations from a large uniform field area. Spheres are easier to make and keep smooth, even though there is no proper analytical solution to the field between the electrodes. Furthermore, if there is a misalignment between the spheres, the region between the spheres is still geometrically the same.

2.4 Laboratory Set-Up for calibration Testing of Gaps

2.4.1 Recommended set-up for Sphere Gaps during Testing

2.4.1.1 Sphere Gaps Set Up

Sphere gaps can be arranged either vertically, typically with the lower sphere grounded (earthed), or horizontally. The surroundings have an effect on the breakdown voltage, as they alter the field configuration. Standard clearances are specified for spheres of various sizes in both configurations. These clearances reduce the effect of the surroundings to less than the specified accuracy of the 3% suggested in IEC 60052 [51].

2.4.1.2 Requirements for gap Set Up for calibration purposes

To minimise the effects of surrounding environmental factors the following set up explanation is illustrated in Figure 2.5 and 2.6 below, extracted from Naidu [26]. D is the diameter of the spheres; S is the spacing of the gap, $S/D \leq 0.5$. A is the height of the

lowest point of the HV sphere above the ground. B is the radius of clearance from surrounding structure. Table 2.1 and 2.2 below provide minimum distances for A, B and D, to be maintained to perform the tests.

Table 2.1 Test set-up dimensions for Sphere gaps

D (mm)	A (max)	A (min)	B (min)
≤ 62.5	7 X D	9 X D	14 X S
100 -150	6 X D	8 X D	12 X S
250	5 X D	7 X D	10 X S
500	4 X D	6 X D	8 X S
1000	3.5 X D	5 X D	7 X S
1500	3 X D	4 X D	6 X S
2000	3 X D	4 X D	6 X S

Table 2.2 Actual values applied

Sphere Diameter (cm)	A (max) meters	A (min) meters	B (min) for max gap (D/2) meters
≤ 62.5	7 X D	9 X D	14 X S
100 -150	60-75	0.80 -1.20	0.60
250	1.25	1.75	1.25
500	2.0	3.0	2.0
1000	3.5	500	3.5
1500	4.5	600	4.5
2000	6.0	800	6.0

The insulator supporting the upper sphere should be less than 0.5 D in diameter. The sphere itself should be supported by a conductive metal shank no more than 0.2 D in diameter and at least D in length. This is to ensure the sparking point is at least 2D from the lower end of the upper insulator.

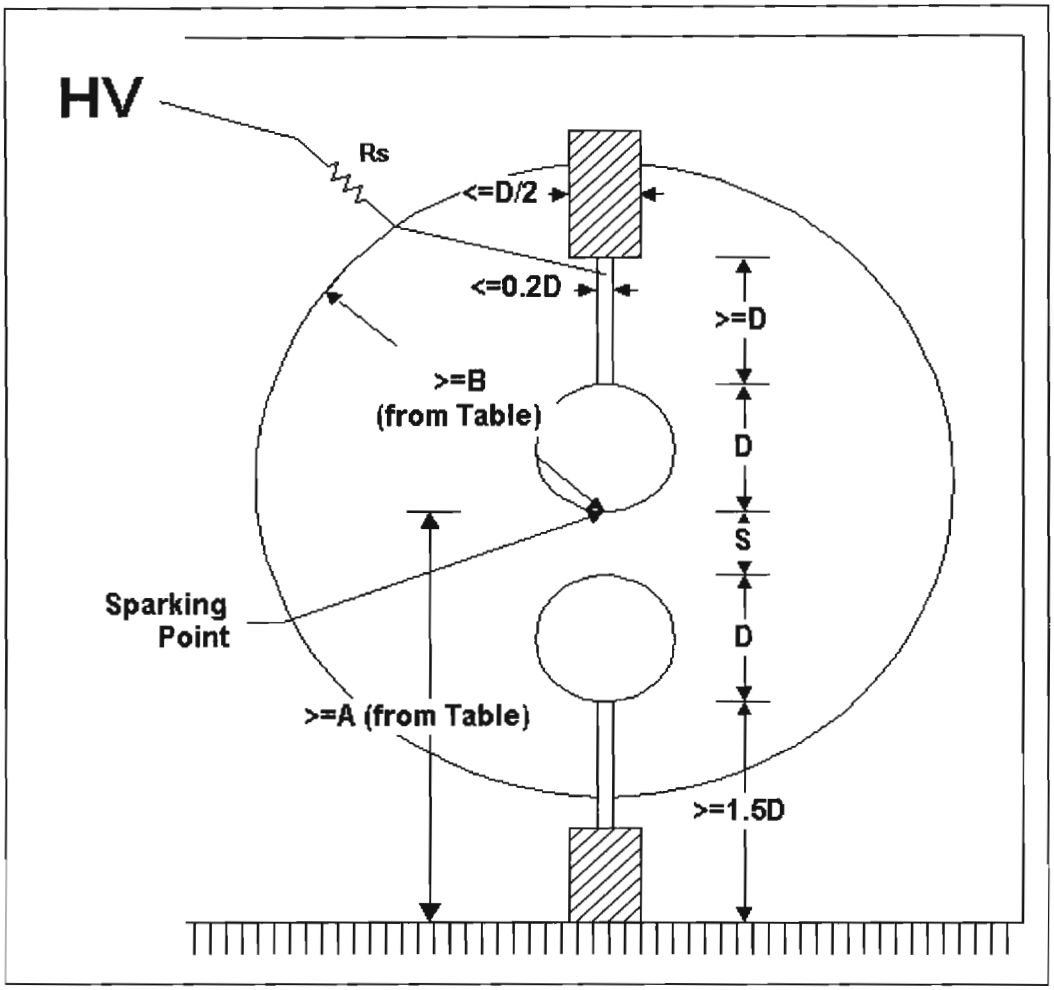

Figure 2.5 Vertical test set-up for sphere Gaps, Kuffel [23]

The high voltage lead shall not pass near the upper electrode. Ideally it should be led away from the shank to avoid crossing a plane perpendicular to the shank at least 1 D away from the sphere i.e. 2 D away from the sparking point, until it is outside of a sphere of radius B from the sparking point. The top of the lower electrode should be at least 1.5D above the grounded floor. Horizontal gaps are much the same as vertical gaps, except that both electrodes are insulated. The insulators should be longer, at least 2D long putting the sparking point at least 4D from the supports: 2D for the insulator, 1D for the shank, 1D for the sphere. Both spheres should be the suggested clearance from the floor or external objects as shown in Figure 2.6 below.

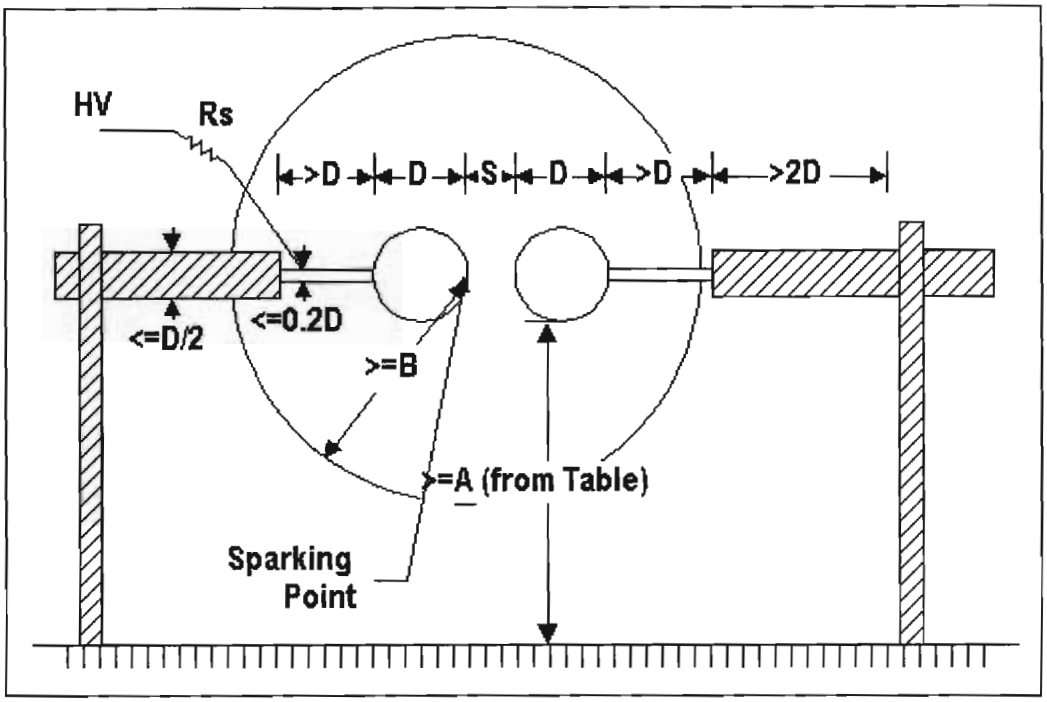

Figure 2.6 Horizontal Spark Gap Schematic Diagram, Kuffel [23]

2.4.2 Rod Gaps

2.4.2.1 Recommended set-up for Rod Gaps during Testing

International standards for rod gap testing usually specify two metal rods which are usually square in cross section. The round bar may be used but a square bar is preferred, the general area being either 12.5 mm^2 or 15.5 mm^2 and the end geometry cut perpendicular. The tables usually show rods with diameters of 12.7 mm, which reflects their British or American origin. The rods may be 150 mm to 750 mm long and the gap will range from 20 mm to 2000 mm. For impulse measurements horizontal mounting of the rod gap on insulators are recommended at 1.5 X S to 2 X S above ground, Naidu [26]. The purpose of calibrated tests sets is to ensure minimum impact of the environmental factors which does not apply to field application ie positive and negative impulse values may vary considerably. The significance of the large circle is to ensure standardized test results and prevent the influence of nearby objects. The radial distance **B** is specified so that the test is clear of any objects like walls, ceilings or metal, example, transformer tanks.

2.5 The advantages and disadvantages of using Spark Gaps

Open spark gaps are simple and inexpensive, but the disadvantages are so severe that they are used only as an extra safety measure where other measures have failed, Linck [19].

The disadvantages are:

a) A short–circuit follow through current after the gap has been tripped by an over voltage.

b) The scatter in the flashover voltage is large and can result in a failure risk as shown by the shaded area of Figure 2.7a below, Kreuger [47] if not carefully considered. The Spark gap on its own can be considered to have failed should it not operate within the pre-set protective margin values achieved by empirical means. Physically, it is difficult to fail as the flashover medium is air which has excellent self-recovery.

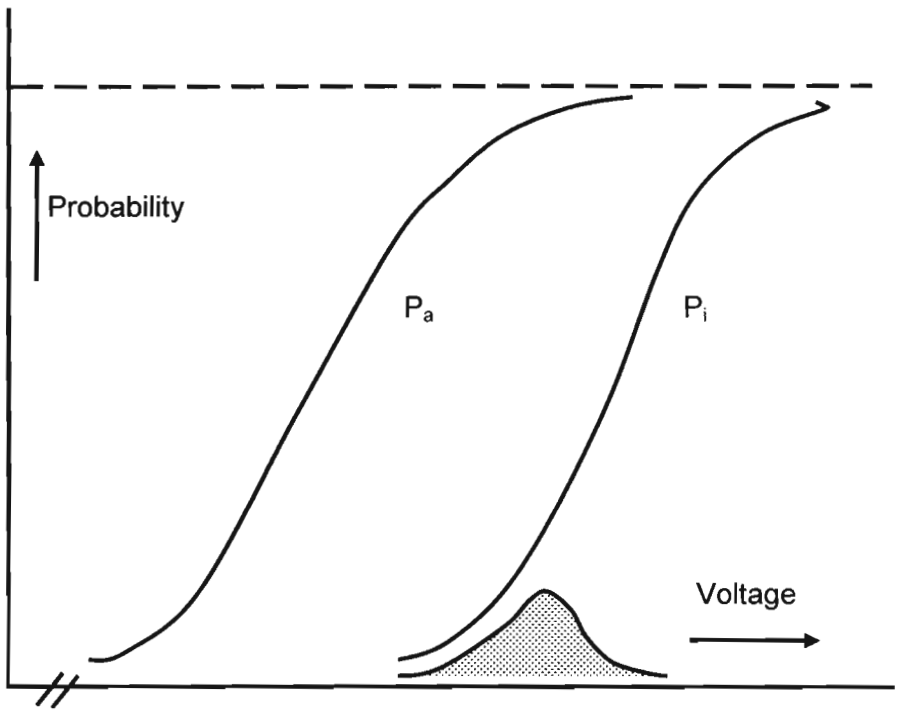

Figure 2.7a Failure risk and insulation construction breakdown probability, Kreuger [47]

The failure risk with no ignition of the arrester is given by $\mathbf{P_a}$ and the insulation construction breakdown probability by $\mathbf{P_i}$, Kreuger [47].

In practice, this risk analysis for failed surge arresters is complex to perform. New arresters as in curve $\mathbf{P_a}$ can be fairly well determined as a surge arrester restores after every breakdown. Curve $\mathbf{P_i}$ however is less accessible as each breakdown asks for samples of the non-restoring arrester. Therefore, in actual cases the upper protection limit (eg 98% responses) and the lower withstand level of the insulation (eg the BIL of the construction) are taken and a safety margin of 25% introduced. The safety margin includes variations in manufacturing and ageing Kreuger [47].

c) The breakdown to zero voltage takes place in an extremely short time, in the order of $0.1\mu s - 8\mu s$, see Figure 2.7b below. This steep front may create severe stresses in equipment such as transformers, Kreuger [47].

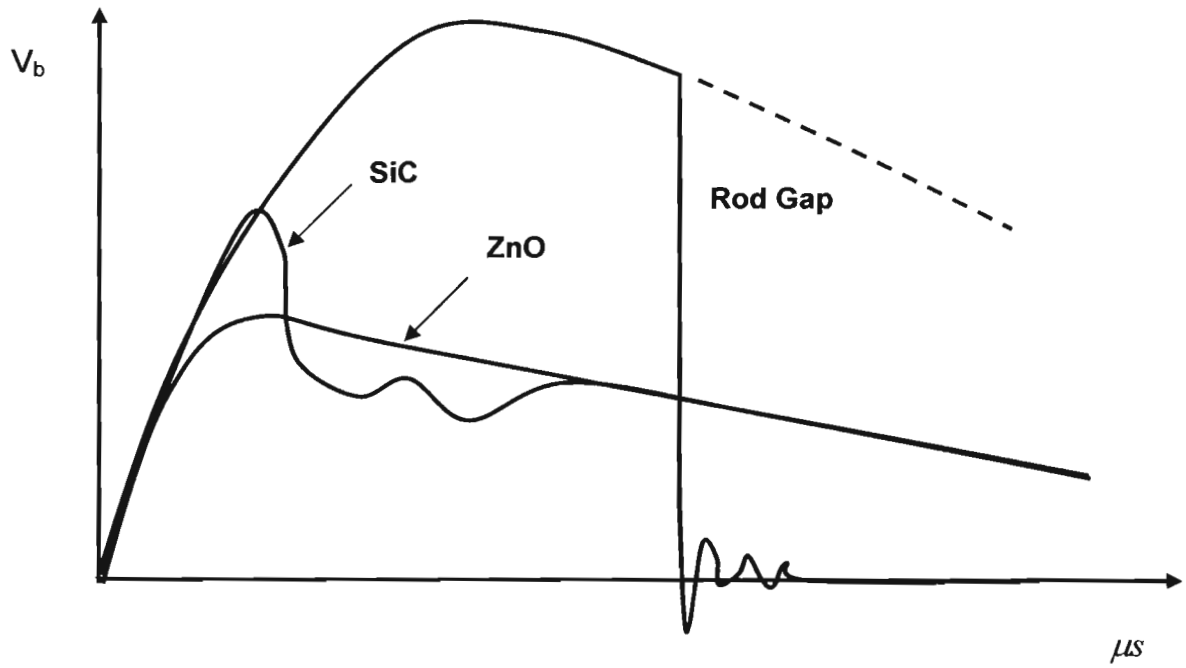

Figure 2.7b Steep chopped wave by rod gap, Kreuger [47]

The **power-follow through current** which has been described by Kreuger [47] as one of the major reasons for bushing failures is, of course, reduced to it's minimum in the surge diverter, where we are dealing with only half a cycle of power follow on current while, even with the rod gap, such a power follow through current leads not only to service interruption but also to secondary bushing failure. The breakdown characteristic shown in Figure 2.8 of a rod gap is unable to adequately protect the transformer. For steep wave fronts less than 1μs, only surge arresters are able to protect transformers for these steep surges.

The breakdown voltage increases appreciably for time less than1 μs . Most insulation constructions have a flat characteristic and are thus not well protected against steep waves. This may be particularly true for transfomers that are generally not insulated nor tested for steep wave fronts or chopped waves as shown in Figure 2.7b above and it is something that could be investigated in future.

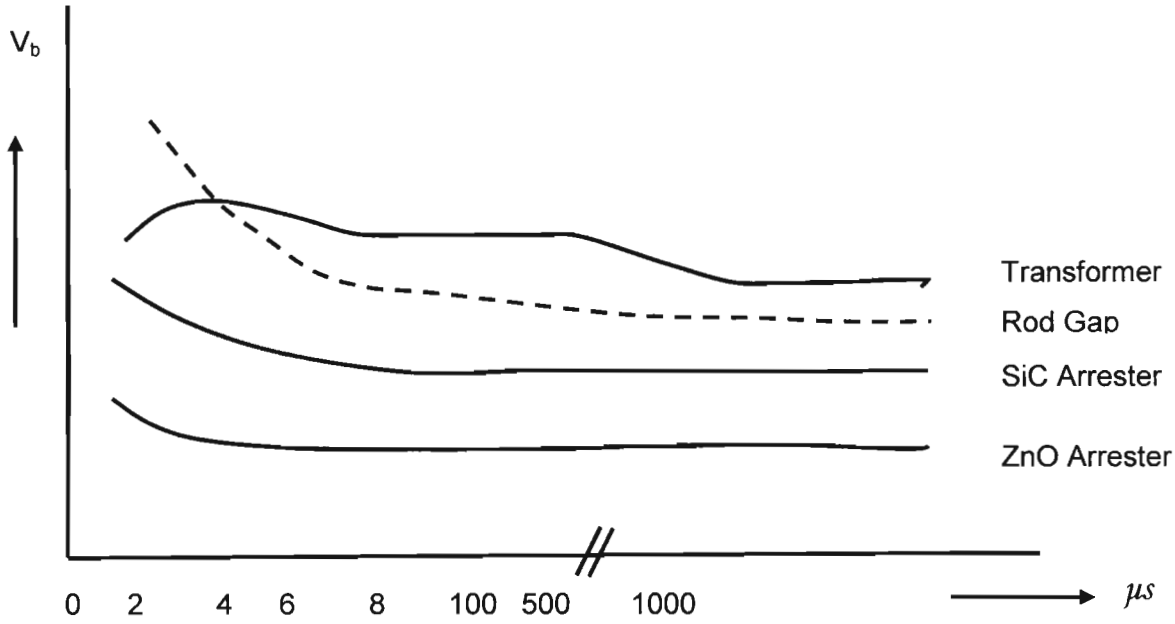

Figure 2.8 Transformer, rod gap and surge arrester Breakdown Characteristic, Naidu [26]

2.5.1 Volt-time Characteristics of Spark gaps

2.5.1.1 Theory of time lags for breakdown characteristics

There is a time difference between the application of a voltage sufficient to cause breakdown and the occurrence of the breakdown itself, Naidu [26]. This time difference is called time lag. The Townsend criterion for breakdown is satisfied only if one electron is present in the gap between the electrodes. For cases where an initial electron is not available, breakdown may not occur. The time which lapses between the applied voltage and the appearance of the initial electron is called the statistical time lag t_s of the gap. After the appearance of the electron, a time t_t (which is called the formative time lag) is required for flashover to occur.

2.5.2 Voltage Time Curve characteristics

The breakdown voltage of a particular insulation flashover voltage for a gap is a function of both the magnitude of voltage and the time of application of the voltage. The volt time or V-T curve is a graph showing the relation between the crest of flashover voltages and the time to flashover for a series of impulse applications for a given wave shape. For the construction of a V-T curve the following procedure is adopted. Waves of the same shape but of different peak values are applied to the insulation whose volt-time is required. If flashover occurs on the front of the wave, the flashover point gives one point on the V-T curve. If the flashover occurs just at the peak value of the wave; this gives another point on the V-T curve. If the flashover occurs on the tail side of the wave, this gives another point on the curve and in this case to find a point on the V-T curve, draw a horizontal line from the peak value of this wave and also draw a vertical line passing through the point where the flashover takes place. The intersection of the horizontal and vertical lines gives the point on the V-T curve. No volt time simulations or laboratory tests were done for this thesis. Practical laboratory tests values for polluted gaps have been taken from Qureshi [30], to show how the voltage time curve for an $8mm^2$ rod with a 40 mm gap would appear, see figure 10 below. All other aspects relating to the volt time characteristics are purely theoretical.

2.5.3 Insulation co-ordination by rod gap as back-up

The graph in figure 2.9 below indicates the operation of a spark gap and the grading times with other devices

Surge
Voltage
kV

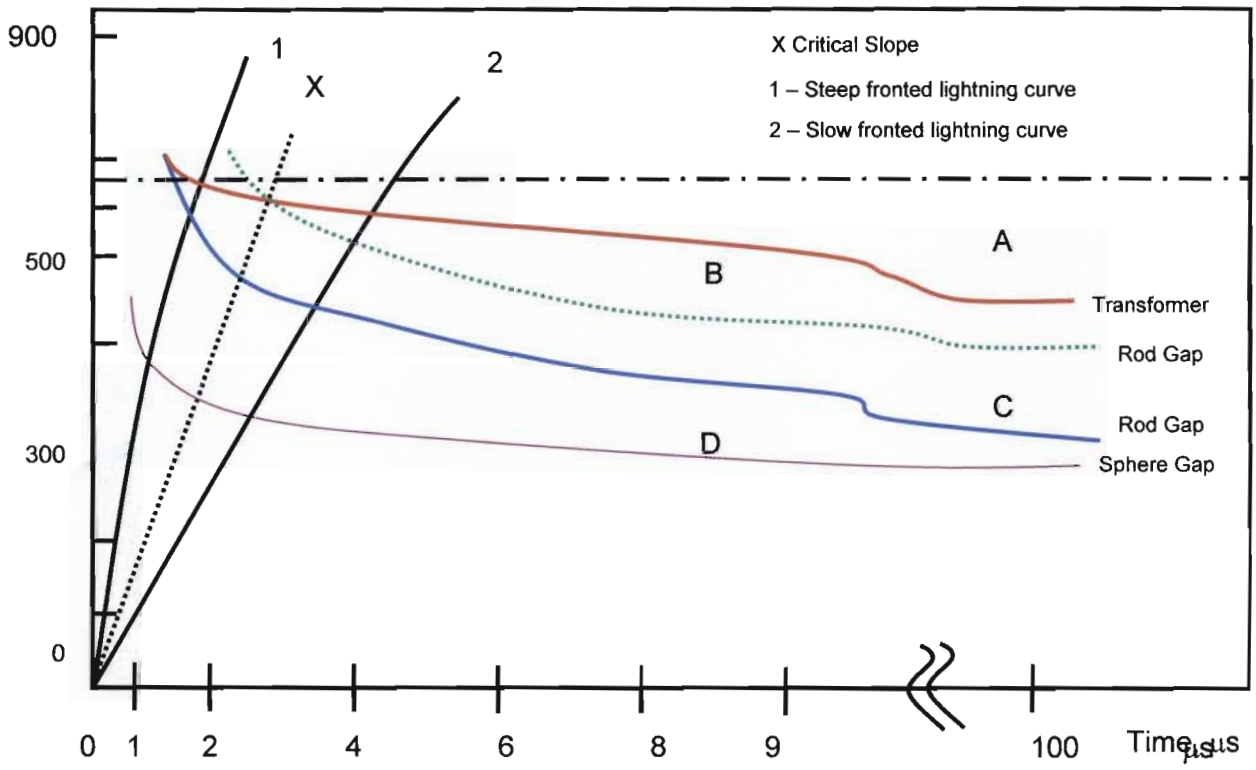

Figure 2.9 Impulse voltage time to flashover characteristics, Naidu [26]

- Curve 1, rod gap flashes and protects the transformer
- Curve 2, only the sphere gap could protect the transformer based on its characteristics in this instance.
- A – X0 kV BIL transformer withstand
- B - X1 cm rod type 1 gap flashover
- C - X2 cm rod type 2 gap flashover
- D – X3 kV sphere gap.

In Figure 2.9 above the BIL of the transformer curve A is protected from the wave fronts with steepness 1 and 2 in the following manner.

a) For surges smaller than 1 μs, the sphere gap will operate.
b) For surges greater than 1 μs, the rod gap with gap spacing X2 will provide protection over the protected range. Note that rod gap X1 does not provide protection for smaller time.
c) In terms of conduction switch on, the surge arresters will operate first and the spark gaps as a backup facility.

The above describes typical transformer characteristics for high voltage transformers to demonstrate the grading principle Naidu [26]. This principle of protective margin grading will be applied in this thesis to medium voltage in later chapters to select a suitable range of breakdown voltages for the sparks gaps

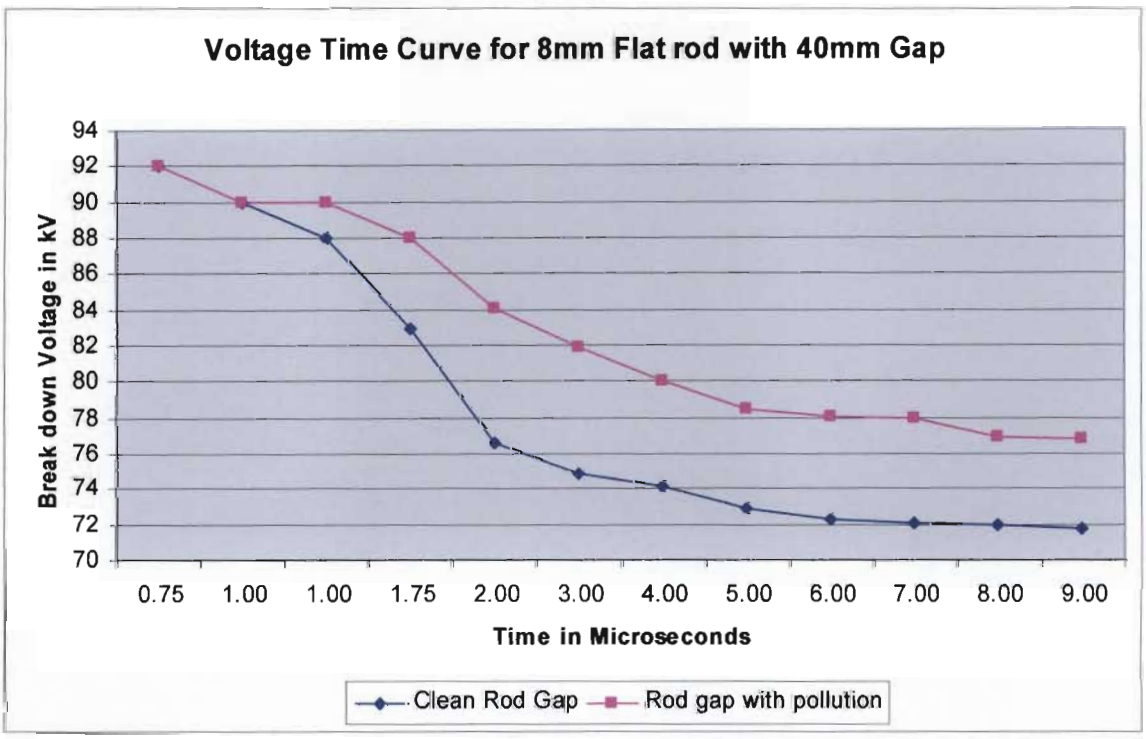

Figure 2.10 Modified Volt time curve for 8mm^2 Flat rod with 40mm gap

The Figure 2.10 above is derived from Figure (4)a in Qureshi [30], shows the time to breakdown in microseconds against the breakdown voltage in kV.

2.6 Choice of a suitable dead Time

The dead time setting on a high-speed auto-reclose relay should be long enough to ensure complete de-ionisation of the arc. For MV systems less than 66 kV the dead times can be anything less than 0.2 s, this is discussed further in Chapter 3, see figure 3.4.

The Eskom 11 kV and 22 kV network breakers will trip on a 40 A earth fault after 1.3 s and for a 6 A sensitive earth fault after a definite time of 10s. Eskom Eastern region uses a rapid trip criteria of 5 S which is extremely large compared to the deionization time required for the spark over which is in the millisecond range. The minimum time set on any recloser beyond the network breaker is 1 to 2 mS which again is a large time margin for complete breakdown of the gap to complete its de-ionisation process and avoid re-strikes.

Qureshi [30] showed that in the presence of dust pollution, smaller gaps can cause unnecessary interruptions of supply if they are not properly adjusted. It was also clear from Qureshi [30] that rods with cut ends ie flat rods and smaller diameters are preferred as these offer immunity towards pollution related influences.

2.7 Concluding remarks

The following critical aspects shall be considered in the theory and information presented in this chapter for use in the results and conclusion.

a) Most of the information presented is based on HV tests and very little test data is available on time lag and breakdown characteristics for medium voltage distribution as shown in Figures 2.7, 2.8 and 2.9.
b) Due to limited information, most of the data extractions are extrapolation of tests results done on HV Systems.
c) Appropriate data was used from Qureshi [30], but the tests were based on duplex gaps that were influenced by pollution.
d) All of the above information had to be analysed and suitable extrapolations done to hypothesize a result to complete the discussion.

The behaviour of shunt connected devices like surge arresters and rod gaps are given in Figures 2.9 and 2.10. A surge arrester protects the transformer insulation in the entire time region shown in Figure 2.9. The rod gap will protect the transformer insulation only if the rate of rise of the surge is less than the critical slope Curve X. Thus if the surge voltage rise is shown by curve 1, the rod gap flashes and protects the transformer. If the surge voltage rise follows curve 2, only the surge arrester can protect the transformer. It is generally known that for high voltages, surges of less than 1 μ S cannot be clamped by a rod gap. From the time curve plotted in Figure 2.10, taken from Qureshi [30], it is seen that the time lag for medium voltage is much larger than 1 μs , hence, the rod gap may be able to clamp the surges adequately.

Following the discussion above and the concerns of various authors, the rod gaps used for medium voltage systems will operate in the arc region of the flashover, ie relatively very high currents in the 1A or more range. When the voltage across the gap suddenly reduces to a few volts of 20 – 50 V, the current discharge at this stage, and the current density over the cathode region increases to high values of 10^3 to 10^7 A/cm^2 . Arcing is associated with high temperature ranges from a 1000 ^{0}C to several thousands of degrees and this shall result in damage to the plant and the metal tips of the gap. Naidu [26]. Hence, it should be clearly accepted that the gap will progressively become longer and the tip geometry vary in shape as each gap is operates and tips erode due to arcs. Thus this gap sensitivity must be considered when selecting a gap.

CHAPTER 3 LIGHTNING PROTECTION OF TRANSFORMERS

3.1 Lightning Surge Protection Practice in Eskom

3.1.1 Lightning Theory and Insulation Co-ordination

Lightning occurs when a charged thunder cloud is discharged to earth. The cloud usually contains positive charge at the top and negative charge at the bottom. This creates electric fields within the clouds and between the clouds and earth. The discharge is normally initiated from a point of high electric field stress i.e. 30 kV / cm or 10 kV / cm in the presence of water droplets in the cloud. The negative charge proceeds towards the ground in a series of steps and this is known as a downward leader stroke. The leader advances in steps of 50 to 100 m, in between intervals of a few to 100 microseconds.

When the leader stroke approaches the ground, it creates a high electric field between the leader tip and the ground and this initiates an upward travelling positive charge streamer. When the two meet a conducting channel is established between the cloud and the ground, a heavy discharge known as a return stroke takes place. The thunder associated with the lightning is due to the rapid expansion of air when heated in the return stroke. The process can repeat itself producing multiple strokes.

The return strokes carry large current in the thousands of amps, typically 150 kA, and the average values are of the order of 20 kA. The duration of the current varies from tens of microseconds to several thousands (in multiple strokes). The amplitude (peak value) of current, ranges from about 50 kA to 130 kV, roughly distributed as follows: 50 % > 15 kA, 10 % > 50 kA, 1 % > 130 kA, 80 % of the strokes are of negative polarity. The duration of the current varies from tens of microseconds to several thousands (i.e. 50 % of the discharges) and 50 kA/sec (for about 10 % or more of the discharges), Naidu [26]

Insulation co-ordination is achieved when the insulation strengths of all components of the electricity system are adequately designed to withstand the electrical stresses of surges within selected reliability margins.

The conditions that system components are designed to meet are:

a) To withstand indefinitely the normal and maximum system operating voltages at supply frequency.
b) To withstand temporary supply frequency over-voltages up to the rated short duration power frequency withstand voltage.
c) To withstand lightning impulse over-voltages up to the rated withstand level
d) To restore the insulation level after a flashover.

3.1.2 Supply Frequency Voltages and Over-Voltages

3.1.2.1 Over-voltages

An over-voltage is a voltage whose value is abnormally high in relation to the network operating voltage. It may be caused by either:

a) atmospheric conditions, in which case it is external to the network,
b) switching operations or resonance phenomena, in which case the cause is said to be internal,
c) or the untimely opening of the circuit-breaker during transformer magnetisation.

3.1.2.2 Switching Over-voltage

This is caused by maintenance work on the networks during which circuit-breakers or fuses interrupt inductive or capacitive loads.

The design, material and specific creepage length of phase insulators influence the performance of a system in terms of:

a) To withstand indefinitely the normal and maximum system operating voltages at supply frequency.
b) To withstand temporary supply frequency over-voltages up to the rated short duration power frequency withstand voltage.

3.1.2.3 Lightning Impulse Over-Voltages

This is caused by atmospheric discharge (from lightning), and may be generated:

a) Either directly, when lightning strikes the transformers feed line conductors,

b) Or indirectly, when lightning strikes the ground or metallic structures near the line, thus generating induced current and an increase in the ground potential.

CSIR and Eskom TSI studies have concluded that the effect of lightning on the performance of MV overhead power lines can be minimised if the 300kV BIL insulation co-ordination philosophy is adopted. The disturbances due to lightning can be due to either direct strikes or induced voltages from adjacent strikes, Gaunt [14]

a) **Direct strikes**

Direct strikes to an unshielded line nearly always cause flashovers to earth of one or more conductors at the pole closest to the strike. If insulation levels are low, flashover may occur at several structures while if the insulation levels are high, flashover may occur at only one structure. Severe impulse voltages may be transmitted to the attached equipment depending on the line insulation value. The amount of energy of the impulse may exceed the capability of the surge arrester at the attached equipment point and hence result in damage to the attached equipment. The probability of damage to attached equipment eg transformers are high for a direct strike to the line pole where the equipment is attached. The higher the insulation level of the line the greater will be the probability of damage to the attached equipment and line poles, Gaunt [14]

b) **Induced voltages**

Induced voltages rarely exceed 200 kV with a maximum order of 250 to 300 kV. As the induced voltages in different phases are of similar in amplitude and identical wave shape, flashovers between phases are not expected. Flashover to ground will occur if the insulation strength to ground is smaller than that of the induced voltage. The amount of flashovers due to induced voltages will depend on the actual insulation values. The lower the insulation value below 300kV, the higher the number of flashovers due to induced voltages, Gaunt [14]

3.2 Line Hardware Damage

Most damage to line hardware is caused by the power arc that develops after flashover; however surges and flashovers may also cause damage. The surge or impulse will cause an initial breakdown of the air and ionisation, which will allow a follow through arc to

develop. The arc current will cause erosion of the line hardware at the arc root. Hardware damage will be reduced by rapid operation of the protection equipment and removal of the supply voltage, Gaunt [14]

3.2.1 Surge Arresters Used To Limit Damage to Attached Equipment

Equipment connected to a power line will be damaged if the surge voltage exceeds the BIL of the equipment. This will be the case for the majority of direct strikes and the higher induced surges. To reduce the equipment damage surge arresters are utilised on the equipment. These surge arresters will clamp the voltage to a value lower than the equipment BIL. Provided the surge energy is less than the arrester capability and the equipment BIL has not deteriorated the arrester will protect the equipment. The energy in a direct strike will normally exceed the energy capability of a surge arrester. Should the strike occur at the pole of the attached equipment the probability of destroying the arrester and damaging attached equipment is high. Should a direct strike be on the line away from the attached equipment there is still a high probability of the energy in the traveling wave exceeding the surge arrester rating if no BIL down wire is applied to the intermediate poles. The BIL downwire used on Eskom poles effectively reduce the BIL to the 250 kV to 300 kV insulation level, Gaunt [14]

3.2.2 Bonding of Metal Hardware on Wood Structures

The practice of electrically connecting all the hardware and insulator 'dead' ends is known as bonding. Small leakage currents (due to pollution contamination on the insulator surface) may cause the burning or degradation of unbonded cross-arms and poles. Bonding the 'dead' ends of phase insulators and stay wires has now changed as latest field tests have disproved the theory that this practice can prevent damage and a wood pole gap is now maintained between bonded hardware and the stay wire. The bonding wire coupled with the circumferential strapping will also act as part of the BIL system and reduce the probability of cross-arm and pole splitting, Geldenhuys [15].

3.2.3 Stay Insulators for MV Structures

The insulation level of the conventional porcelain stay insulators is low. Porcelain stay insulators may be considered as adding value to the system only in terms of providing protection to the public against a live stay condition from a broken conductor coming into

contact with the stay. The porcelain stay provides very little additional lightning surge insulation. Strain structures are not fitted with BIL downwires since the stay-wire fulfills this purpose. To achieve a higher BIL on a strain structure than the porcelain insulator provides, glass fibre longrod type stay insulators may be used, or stays fitted in such a way that there is a suitable wood path in series, Geldenhuys [15].

3.3 Transformer and Surge arrester BIL Used in Eskom Distribution

3.3.2 Medium Voltage Transformer BIL

The preferred MV voltage level in Eskom is 22 kV due the flexibility offered by this voltage at a marginal extra cost of insulation as compared to the 11kV voltage level. The additional basic insulation level (BIL) provided by the 22kV insulation also improves the general lightning performance of MV overhead lines. The BIL of the line is defined as the "*peak value of a positive voltage surge having a 1.2/50 us waveform for which the probability of withstand is 90%*", SCSASABE7 [36]

Table 3.1 Rated lightning impulse withstand voltage

Nominal System Voltage kV rms	Highest System Voltage kV rms	BIL SABS (kV)	BIL IEC (kV)
6.6	7.2	75	60
11	12	95	75
22	24	150	125
33	36	200	170

Data taken from SANS 1019 and IEC 60071-1 [49]

Table 3.2 indicates that the BIL levels adopted in South Africa are typically higher than international norms as guided by IEC 60071-7. Eskom uses the SABS ratings and hence all 11 kV transformers are based on a 95 kV BIL and 22 kV on a 150 kV BIL. If there are a number of surge arresters in close proximity on the line it effectively reduces the BIL of that line. Hence, when considering a protective margin for a rod gap, to be used as a back-up protection, the highest BIL rating is to be considered and from table 3.1, called the high value and for this thesis shall be taken as 150 kV being the most commonly used voltage implemented on the Eskom reticulation lines.

3.3.3 MV Surge Arrester BIL

Table 3.2 Eskom MV Surge arrester Specifications,

Specification	11 kV Surge Arrester	22 kV Surge Arrester
MCOV	10.2 kV	19.2 kV
Discharge Current	10 kA	10 kA
Residual Voltage	40 kV	80 kV
Energy absorption (per MCOV)	2.5 kJ/kV	2.5 kJ/kV

Taken from SCSSCAAN5, [36]

3.4 Determination of a Gap with a Suitable Protective Margin

The protective level is the breakdown voltage values that are chosen such that the transformer will not experience any spill surges. For rod gaps, the wave reflection theory is discussed in chapter 4. Figure 4.2 shows graphically the magnitude of the surges that will be experienced by an unprotected transformer winding. The analysis shows graphically the impact that a chopped wave impulse has on the transformer winding and in particular the voltage distribution profile. The information from this analysis is used to determine the stress points in the winding and aids in selecting of a protective margin that is within the "safe" limits of the windings insulation capability.

For the purposes of this thesis a range of breakdown values have been considered. The values were determined based on a reliable margin of protection (MP) for insulation co-ordination studies and is defined in IEEE [48] working group standard as:

$$\%MP = \left(\frac{BIL}{VD + V_A} - 1 \right) X100 \qquad (3.1)$$

Where

BIL is the insulation level of a transformer in kV

V_D is the discharge voltage of the surge arrester in kV

V_A is the inductive volt drop due to the windings in kV

Hence considering equation 3.1 above, typically for high lightning density countries such as South Africa, a MP of 20% is recommended.

Considering, the MCOV ie the maximum continuous overvoltage is the highest root mean square (rms) power frequency voltage that an arrester can withstand continuously. After exposure to the specified tests by the relevant specifications, the arrester should be able to return to its normal temperature with this MCOV voltage rating applied continuously NRS 039 [27]

The value adopted for the PM range for this thesis will be taken as the specified 22 kV surge arrester rating values. The higher voltage value will be taken as a 22 kV transformer BIL of 150 kV. The 150 kV is supported by showing theoretically in chapter 4 and Figure 4.2 how the value is achieved by analyzing the abrupt termination of a rectangular wave. The result agrees with a maximum value less than 100 kV for breakdown times smaller than 15 μS, Wedmore [40]. Hence the 150 kV limit is attenuated to a value that can be easily managed. The gap value selected will therefore be able to breakdown within a margin of 20% above the lower $V_{50\%}$ value and 20% below the higher $V_{50\%}$ value. It is also a criterion that the $V_{50\%}$ values, lower and higher, do not fall outside the $V_{10\%}$ range.

Therefore the most optimal range for the spark gap to operate within for the purposes of this thesis would be chosen as follows:

$V_{50\%}$ value higher-end = (150 kV – 20%) = 120 kV

$V_{50\%}$ value lower-end = (80 kV + 20 %) = 96 kV

3.5 Transformer Protection Using Surge Arresters

3.5.1 The Need for Transformer Protection

The over-voltage experienced at equipment structures discussed above, often damages the electrical equipment when the wave fronts exceeds the insulation level for which the equipment was sized, see figure 3.1 below. The transformer has the same insulation level as the other equipment but may undergo a higher level of stress when an over-voltage occurs. Indeed, it acts as a high input impedance in pulsed operating conditions. It therefore provides the best point of wave reflection and is consequently one of the most exposed live parts on the network. This is why it is necessary to protect the transformer from the outside environment and limit over-voltage to an acceptable level, i.e. by ensuring there is a Protective Margin in relation to the devices insulation level. The best way of doing this is to install surge arresters close to the transformers connection points. Schneider [37]

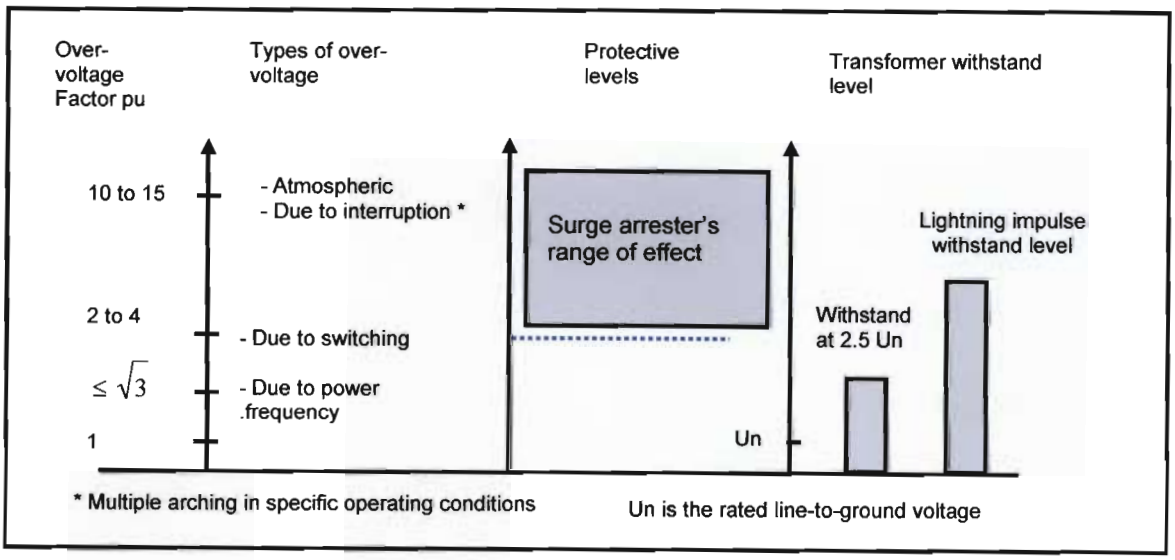

Figure 3.1 Over-Voltage Withstand Of the Transformer and Surge Arrester, Schneider [37]

3.5.2 The Ideal Solution to the Problem is the Surge Arrester

The surge arrester is a static device designed to limit the amplitude of over-voltage, which may be generated at a given point on the network.

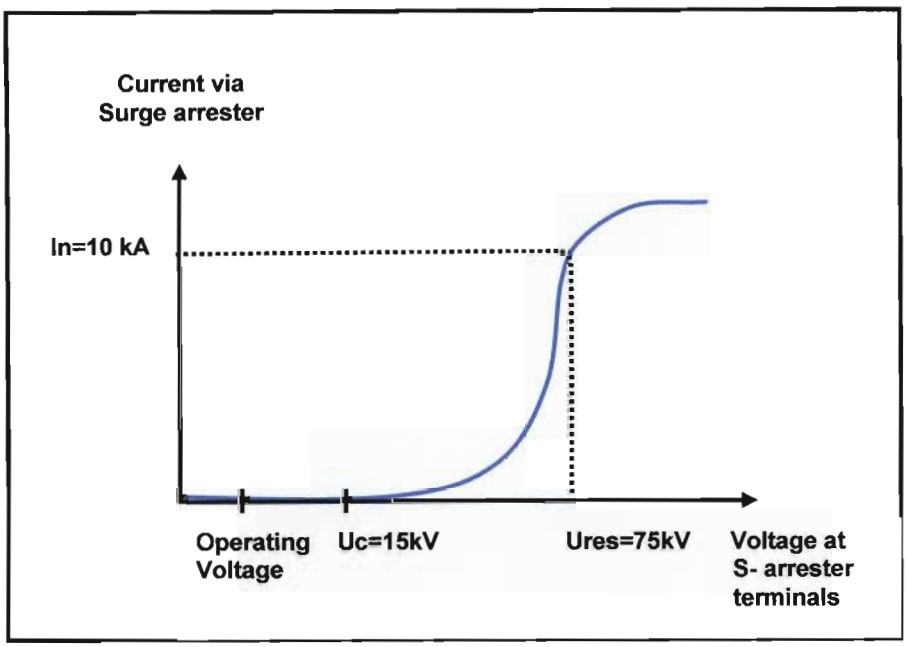

Figure 3.2 Dynamic behavior of surge arrester, Schneider [37]

Figure 3.2 above shows the dynamic behaviour of a surge arrestor. Once an overvoltage is experienced, the metal oxide block become conductive and discharges current to earth. The surge arrester is permanently connected to the network, close to the transformer terminals. When an over-voltage wave is propagated over the network and becomes greater than the surge arresters limitation voltage, the resistance of the surge arrester becomes temporarily very low, allowing limited current to be discharged via an earth conductor to earth and hence limiting the voltage at the transformers terminals. It spontaneously recovers its insulation strength once the voltage normalizes. This solution offers an advantage in terms of network operation since it does not involve interrupting the supply.

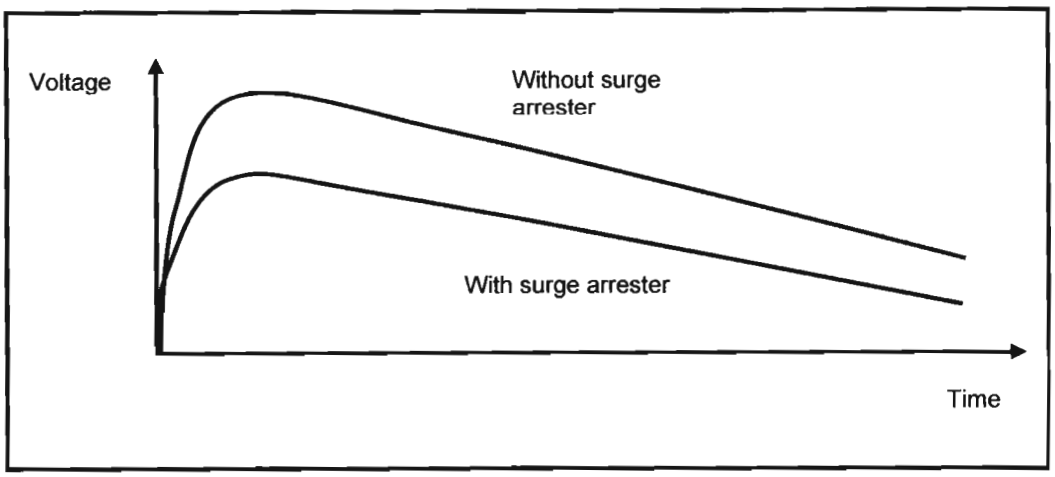

Figure 3.3 Behavior of surge arrester to Over-voltage conditions. Schneider [37]

In fig 3.3 above it is noted that the surge arrester effectively decreases the voltage across the terminals of the equipment being protected. It is also noted that unlike the spark gap impulse wave, the discharge profile does not change with the addition of the surge arrester. This is import to ensure even distribution of voltage stresses that will ensure that the transformer winding insulation levels are maintained.

3.5.3 Choice of Surge Arrester

To justify the use of a surge arrester, it is necessary to assess the risk of lightning strikes using various parameters such as:

a) The lightning impact level

b) the type of network,

c) The topology of the site.

The following expression was developed by Gaunt [14]

$$Ns = Ng(28H^{0.6} + W) \times L \times 10^{-3} \qquad (3.2)$$

Where, Ns is the number of direct lightning strikes to a line

Ng, is the annual ground flash density in $km^{-2}\,yr^{-1}$

H is the average line height in meters

W is the line width in meters, L is the line length in km

Equation 3.2 above is to be used to determine the number of direct lightning strikes to a line, based on its physical dimensions. This information is important to rate the surge arrester. To define a surge arrester it is necessary to know the network's characteristics, and notably the neutral point connection conditioning the choice of constant operating voltage. The transformer manufacturer is usually unaware of the network parameters; furthermore, probability calculations differ according to the type of network and the country.

The main electrical sizing criteria for surge arresters are:

a) The maximum constant voltage Umcov, dependent on the rated voltage Un and neutral point connection,
b) Earth fault factor
c) The rated current (e.g. 10 kA),
d) The residual voltage at In (8/20 µS wave),
e) Creepage distance 31 mm / kV

3.5.4 Surge Arrester Specification and Configuration

a) It is essential to install phase-earth surge arresters when equation 3.2 is applied and Ns > 2-3 strikes / km^2 / year.
b) Double surge arrester configuration are suitable for high lightning areas typically 8-9 strikes / km^2 / year

In the research by Chatterton [6], it was found that even with arresters from different manufacturers, the use of the double arrester configuration would decrease the energy absorbed per arrester and hence reduce the risk of failure of the individual arresters protecting the transformer. This means that Eskom field staff can use different manufacturer arresters in parallel. This would be especially for times when replacing failed arresters or a faulty transformer under breakdown conditions and electrical supply of the customer has to be restored to as soon as possible. It was, however, proposed to perform arrester matching by ensuring that the both arresters were from the same manufacturer to ensure even power dissipation.

3.5.5 Surge Arrester Attachment

If the distance between the surge arrester and the transformer to be protected is significant, the incident wave will be reflected at the terminals of the transformer. The reflected wave causes voltage doubling, discussed in chapter 4 that may be well above the surge arrester's level of protection. In this situation, the surge arrester no longer ensures its protective role. It is consequently imperative to consider the following:

a) For the 11 and 22 kV transformers, surge arresters are to be installed on the tank
b) Connect the earth of the surge arrester directly to the mass of the transformer; in this way the transformer over-voltage will be limited by the surge arrester.

3.6 The Effects of Power arc from Spark Gaps on System Performance

3.6.1 Requirements for a protective device in parallel with a surge arrester

a) It should not usually flashover for the power frequency overvoltage
b) The Volt-time characteristics of the device must lie below the withstand voltage of the protected apparatus insulation. The marginal difference between the above two should be adequate to allow for the effects for distance, polarity, atmospheric conditions, and changes in the characteristics of the devices due to ageing.
c) It should be capable of discharging high energies contained in surges and recover the insulation quickly.
d) It should not allow power frequency follow-on current to flow.

3.6.2 Studies on Over-voltage Protection, with arresters and spark gaps

Distribution transformers in rural networks have to cope with frequent lightning induced over-voltages and thus must be protected using spark gaps or surge arresters. The over-voltage protection type has an influence on the system behaviour and on the interruptions and voltage sags experienced by power system customers. Heine [18], presented measurement results showing the effect of over-voltage protection on established faults in an un-earthed medium voltage overhead line network. Detailed results of fault frequencies and fault types are shown in Heine [18]. Although this information is not relevant to Eskom's systems, the results do illustrate effectively the

disadvantages of spark gaps. Heine [18], further, established a probability function to describe the influence of over-voltage protection on voltage sags experienced in the network. This latter aspect is important when limiting the effects of interruptions and voltage sags for sensitive customers.

Heine's [18] key results of the measurements revealed the following:

a) Feeders with spark gaps faulted ***six times*** more frequently than the feeders with surge arresters.
b) Feeders having spark gaps showed a high number of ***changed fault types***. Faults developed from an earth fault to a two-phase-to-ground short circuit. This means an increase in the share of short circuits and voltage sags.
c) In feeders having spark gaps, the number of voltage sags of magnitude $U_{sag} < 70\%$ was about ***three times higher*** than the sag frequency of surge arrested feeders.

An earth fault changes to a two-phase short circuit typically within 10 cycles. This means that the prolonging of the delay time of the earth fault protection would not prevent this incident. The operation of a spark gap causes an earth fault. When one spark gap in the system sparks over, the other spark gaps should not operate during this earth fault. Further, an arc in one spark gap should not be able to spread to an adjacent spark gap. Based on the measurements performed here, there is a relatively high possibility that the electric arc of one spark gap does spread to other phases. If the main power quality improvement is to limit the number of short interruptions, surge arresters should be installed in an unearthed network instead of spark gaps.

Eskom's reticulation network protection settings are based on philosophies mainly using the Alstom Prag manual on network protection and automation guide [41]. The Eskom System will easily cope with the follow - through power arc due to the settings applied. Section 3.5 provides the results to support this hypothesis.

3.7 The reaction for the protection system to the Rod Gap

3.7.1 Dead Time in the 11 kV and 22 kV networks

Several factors affect the selection of system dead time as follows:

a) System stability and synchronism
b) Type of load
c) Circuit breaker characteristics
d) Fault path de-ionisation time
e) Protection reset time

3.7.2 Factors influencing MV Auto-Reclose

From the various factors that determine the selection of dead time, the focus of this section will be on the type of load and fault path de-ionisation time. These are the only protection time that will be discussed further. Figure 3.4 shows the dead time characteristics that the breaker must have to avoid nuisance tripping for a power follow through arc produced by the spark gap.

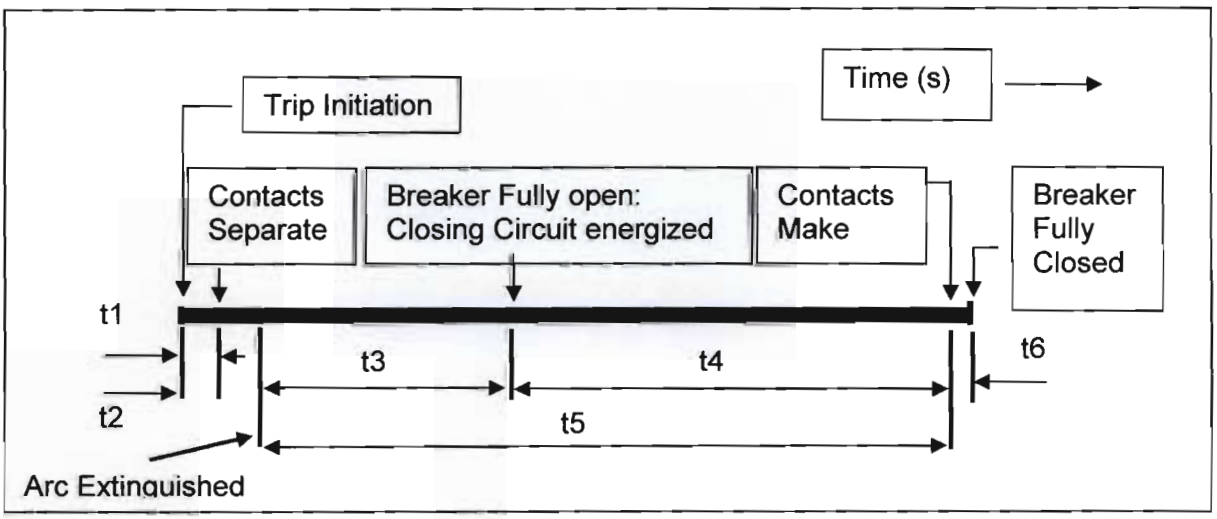

Figure 3.4 Graphical Protection time line for breaker

It is noted that t2 is the time from the instant the trip is initiated until the arc is extinguished

Table 3.3 Protection times

Time	OIL 11 kV [s]	Vacuum 22 kV [s]	SF6 33 kV [s]
t1	0.06	0.038	0.04
t2	0.1	0.053	0.07
t3	0.08	0.023	0.03
t4	0.16	0.048	0.08
t5	0.24	0.28	0.11
t6	0.02	0.07	0.12

The successful high speed reclosure of a breaker requires the interruption of the fault by the circuit breaker to be followed by a time delay long enough to allow the ionized air to disperse. This time shown in table 3.3 above is dependent on the system voltage; cause of fault and weather conditions for 11 kV and 22 kV systems, ***0.1s-0.2s*** is adequate for single lightning strikes but not in the case of multiple strikes.

It is important to know the time that must be allowed for complete de-ionisation of the arc, to prevent the arc re-striking when the voltage is re-applied. The de-ionisation time of an uncontrolled arc, in free air depends on the circuit voltage, conductor spacing, and fault currents, fault duration and wind speed. Of these, the circuit voltage is the most important, and as a general rule, the higher the voltage the longer the time required for deionisation. Typically for 132 kV t = 0.3 S and for medium voltage 11 and 22 kV, $t \leq 0.2$ S. These values are given in Table 3.4 below.

Table 3.4 Minimum deionisation time for arcs based on voltage

Line Voltage (kV)	Min De-energizing Time (Seconds)
Up to 66	**0.20**
110	0.28
132	0.30
220	0.35
275	0.38
400	0.45
525	0.55

If single-phase tripping and auto-reclosing is used, capacitive coupling between the healthy phases and the faulty phase tends to maintain the arc and hence extend the

dead time required. This is not a problem on short MV lines, hence will not be discussed further. Prag manual on network protection and automation guide [41].

3.7.3 Earth fault created by Rod gap Sparkover

A rod gap that sparks over is seen by the protection as an earth fault. It is common to fit sensitive earth-fault protection to supplement the normal protection in order to detect high resistance earth faults. This protection cannot possibly be stable for through-faults, and is therefore set to have an operating time longer than that of the main protection. This longer time may have to be taken into consideration when deciding on a reclaim time. A broken overhead conductor in contact with dry ground or a wood fence may cause this type of fault. It is rarely if ever transient and may be a danger to the public. It is therefore common practice to use a contact on the sensitive earth fault relay to block auto-reclosing and lock out the circuit breaker. Where high-speed protection is used, reclaim times of 1 second or less would be adequate. However, such short times are rarely used in practice, to relieve the duty on the circuit breaker. Typical SF6 times to operate are 5s

3.8 Concluding remarks

It was established in this chapter that a protective margin (PM) of:

$V_{50\%}$ value higher-end = (150 kV – 20%) = 120 kV (3.3)

$V_{50\%}$ value lower-end = (80 kV + 20 %) = 96 kV (3.4)

Would be suitable for the 11kV and 22 kV MV networks in Eskom. These values have been used to decide on the specific range that the rods were to be simulated using FEMLAB and then tested in the laboratory. The typical test voltage used in the simulation was 110 kV and this was also used for the lab tests.

The time for the breaker pick-up as explained above is a few seconds typically 5s which in comparison with the rise and fall times of the chopped waves in the millisecond range is not visible to the protection and hence will not cause any protection tripping. For longer sustained power follow through faults at the gap, outside the dead time, nuisance trips can be expected, an imposition of the Spark Gap that can be managed.

CHAPTER 4 IMPULSE SURGE ON TRANSFORMER WINDINGS

4.1 Introduction to Surge Distribution in Transformer Windings

Surges that enter the power system via the over head line travel towards the terminal equipment and are reflected at the terminal point. The reflection phenomena of the traveling wave, its magnitude and direction will determine the damage that can be caused to a transformer winding. This section attempts to determine this effect by simulating a wave resulting from a spark gap. The theory for analysis is based on results from tests done on an ideal rectangular wave to simulate the chopped wave generated by a rod gap.

The rod gap is a simple and cheap form of protection but it does not meet the complete requirements of a protective device as the spark over characteristics of the rod gap depends on the atmospheric conditions, polarity and wave shape. If no current limiting resistance is provided to limit the current after sparkover, the sparking current may be very high and the applied impulse voltage collapses suddenly to zero thus creating a steep step voltage as seen in Figure 2.7, which could damage the transformer windings. The discussion that follows is based on an ideal "chopped wave" effect on transformer windings as a result of the abrupt termination of a rectangular wave or impulse due to the operation of a rod-rod gap. The conditions presented by atmosphere pressure, temperature effects and pollution is not part of this scope. The resulting waveform hence will be the maximum possible value that can be achieved. These values can be de-rated to cater for the environmental conditions listed, Wedmore [40].

4.2 Theory of Surge Distribution in Windings

The transient impact of a rectangular wave at normal operating frequencies of 50 Hz neglecting the resistance in a transformer winding can be approximated to be that of a pure inductance. The effects of the small capacitances present being negligible. At much higher frequencies, however, the reactance due to the inductance becomes very large, while the reactance due to the turn-to-turn capacitances becomes progressively small, with the result that currents set up by impressed voltages of higher frequency tend to take the capacitance path, Wedmore [40]. If for instance a rectangular travelling wave reaches a transformer, the initial voltage distribution is as shown in **Figure 4.1 and 4.2** and depends entirely on the capacitances present, since the front of a rectangular wave represents a part of a cycle of very high frequency. Subsequently, however, the

distribution depends entirely on the inductance, as the wave, apart from its front, represents uniform voltage, that is, zero frequency. Now the distribution of inductance in a transformer is practically uniform and, therefore, the final distribution of voltage is also uniform. The initial distribution of voltage, however, is not uniform owing to the fact that there is an appreciable capacitance to the core and tank in addition to the turn-to-turn capacitances. The capacitance currents to earth (core and tank) must flow through the turn-to-turn capacitances, and these result in an increase of voltage at the line end of the windings. Between these two conditions, the non-uniform initial distribution and the uniform final distribution, oscillations occur and dangerous voltages and voltage gradients may arise. The question as to whether dangerous internal voltages are likely to arise depends on the characteristics of the winding under consideration, *the terminal conditions of the neutral end of the winding*, and the frequency of the applied surge due to the capacitance. If the frequency of oscillation is equal or approximately equal to the natural fundamental frequency or one of the natural harmonic frequencies, of the transformer winding, there is danger that high local voltages and voltage gradients may be set up that will result in winding damage, Wedmore [40]. Note that the neutral ends of Eskom MV transformers are isolated due to the Delta-star configuration as shown in figure 4.0 below. However due to the transference of surge effects explained by Kelly [45], the impact of the surge needs to be considered.

4.3 Methods for Improving the Voltage Distribution in the Windings

Eskom's Distribution pole mounted transformers are of the Delta-Star (DynN11) configuration with the secondary winding effectively earthed via an earth electrode V_N.

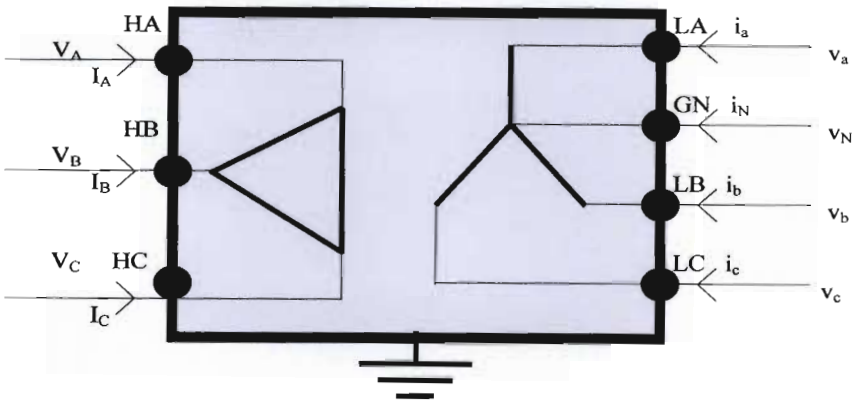

Diagram showing the Terminal connections of a Δ-Y transformer

Figure 4.0 Terminal connections of a Delta-Star transformer

The discussion that follows will be based on a star-star, with earthed secondary windings as no analytical information was available on the delta-star configuration. As the surge passes over to the secondary winding that is grounded, the transference mechanism of such a surge will apply to the Delta-star configuration and is therefore discussed and analysed further in this chapter.

4.4 Characteristics of Normal Voltage on the Distribution Transformer

The initial Voltage distribution of the transformer windings with the neutral point earthed is dependant on the end to end as well as earth capacitance of the complete winding in Farads. As seen in figure 4.1 below, the initial voltage distribution is very dependant on the values of C_w and C_g as is derived using equation 4.1 below.

$$\alpha = \sqrt{\frac{Cg}{Cw}} \qquad (4.1)$$

Where:

C_w = Capacitance from end to end in Farads

C_g = Capacitance to earth of the complete winding

Figure 4.2 shows the voltage as a percentage of applied voltage on windings neutral earthed. This is important as it show the input profile of the surge voltage wave which will later be compared with the output profile.

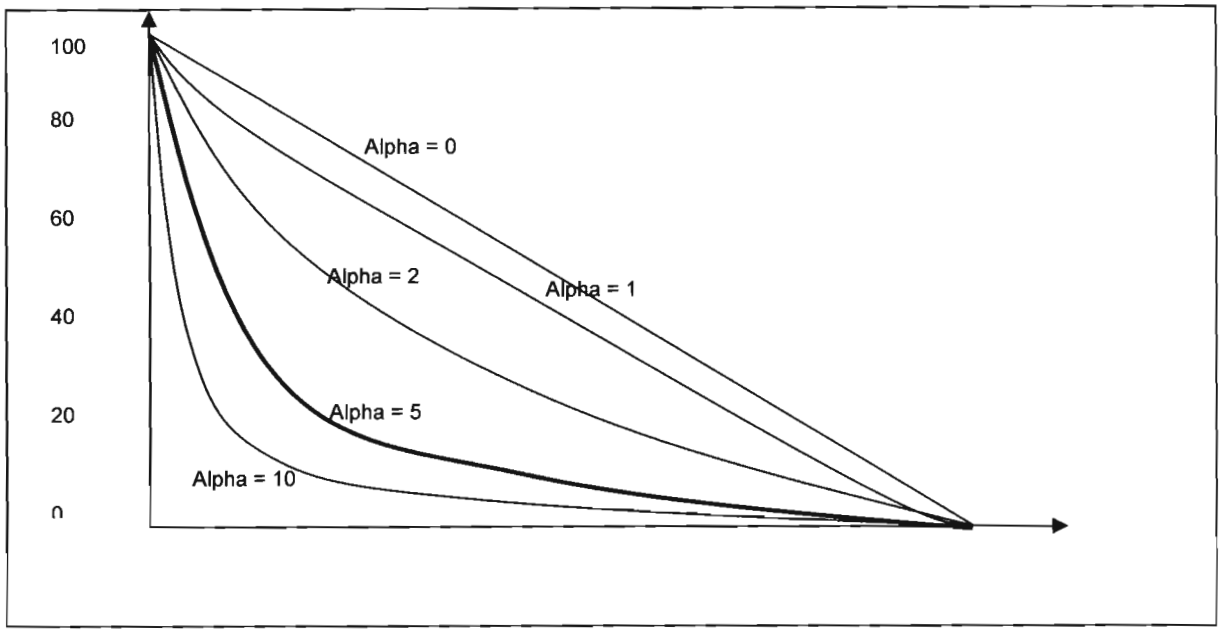

Figure 4.1 Initial Voltage distribution on windings neutral point earthed

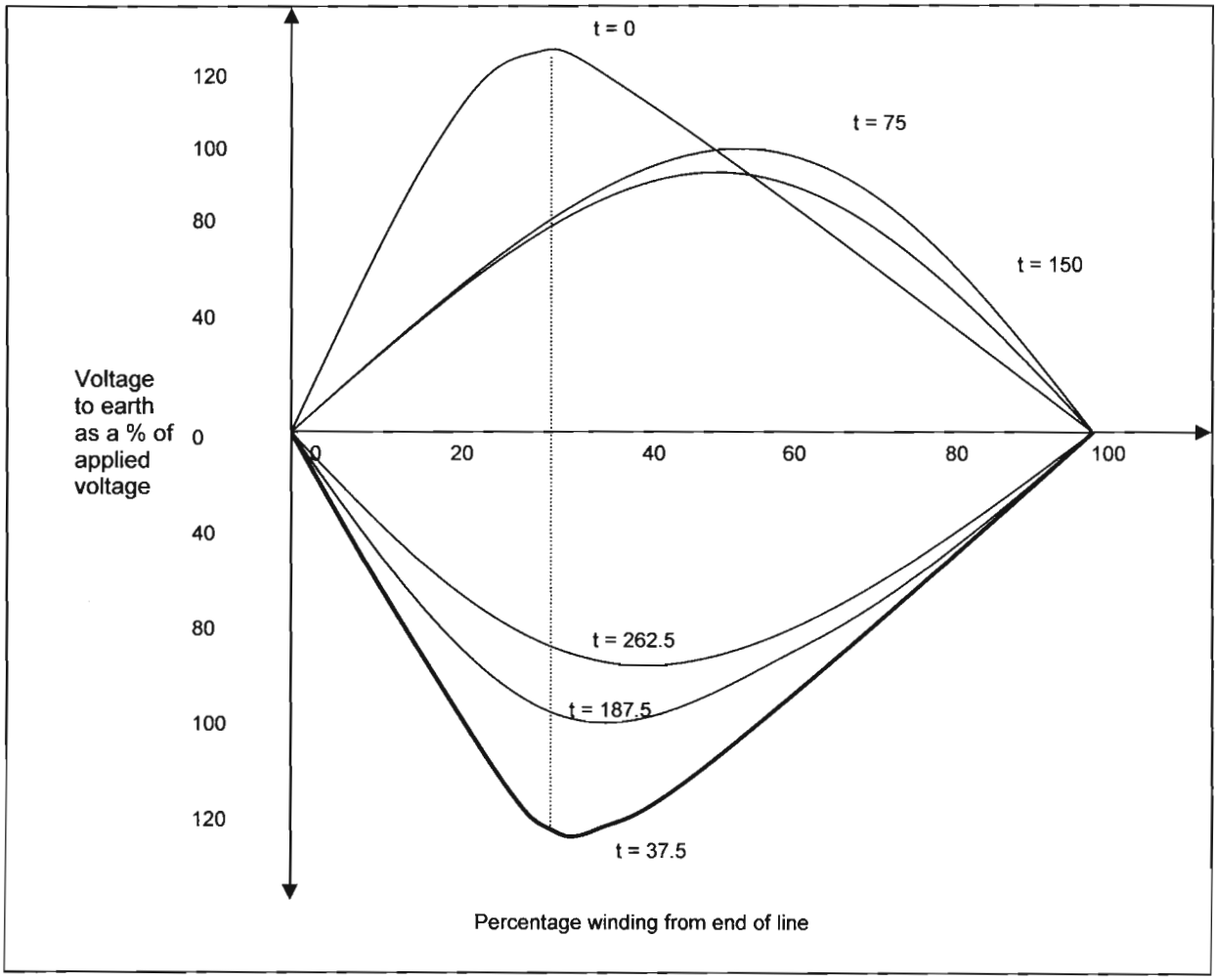

Figure 4.2 Voltage as a percentage of applied voltage on windings neutral earthed

4.5 The Nature of Oscillations Set Up In the Primary Winding

The impact of the impulse voltage is greatly influenced by the connection of the windings. The individual harmonics may also be influenced by the connection of the secondary windings. The oscillations can be transferred magnetically to the secondary winding, so that the voltages set up within the secondary winding depend on the distributed winding constants and the turns ratio. The duration of these oscillations is limited only by the damping factors involved, and they may continue for some hundreds of microseconds. In the case of three-phase transformers the possibility of transference of these oscillations is limited. Delta-connected windings can oscillate only in even harmonics, but these cannot be magnetically transferred since they do not create a resulting flux in the iron transformer core. The transference of these components can, therefore, only take place in star-star connected transformers, but, for the same reason, even in this case only odd harmonics can be transferred. If equal impulses are applied to a transformer on all three phases, this transformer component is always zero, since the impulse voltages cause equal and opposite fluxes in the iron core and therefore do not create a magnetic field, Wedmore [40].

4.6 The Mechanism of Transference of Surges to the Secondary Windings

The equivalent circuits which are based on Palueff's findings are described in detail and has simplified the transference problem to such an extent that it was now open to numerical treatment, and since the calculations in the report are, to a large extent, based on Palueff's assumptions, it is useful to state shortly his method of treatment, Wedmore [40].

It is shown in Wedmore [40] that the whole phenomenon of transference can be subdivided into four components:-

a) At the moment of voltage impact the secondary winding assumes a potential to earth which is produced purely electrostatically and which is determined by the position of the two windings in the electrostatic field set up at the moment of voltage impact. This voltage component occurring at the secondary terminals depends, therefore, solely on the mutual capacitance **(C_w)** between both windings and their capacitances to ground **(C_g)**; it is, therefore, independent of the turns ratio.

b) The electrostatically impressed voltage sets up oscillations in the secondary winding which are determined by its distributed constants.

c) The voltage impact causes free oscillations of the primary winding which can be subdivided into space and time harmonics according to the ordinary theory of the behaviour of a transformer winding when subjected to an impulse. These oscillations can be transferred to the secondary winding by means of the electrostatic and magnetic fields set up, so that the induced voltages depend on the distributed winding constants and the turns ratio of the transformer.

d) The unidirectional final voltage distribution along the primary winding is transferred electromagnetically to the secondary winding. The induced voltage is directly proportional to the turn's ratio.

4.7 The solution for abruptly chopped wave

The theoretical treatment has been based on approximated equivalent circuit from Wedmore [40], in which the distributed winding constants of a transformer are represented as lumped impedances. These equivalent circuits consist of self and mutual inductances and capacitances of the transformer windings, whereas the ohmic resistances of the windings are neglected. Bewley referenced in Wedmore [40] has, however, in the case of a transformer with secondary load, shown that the effect of ohmic losses is very small. Since the present calculations are carried out for transformers on no-load the impedances connected to the secondary transformer terminals consist only of the capacitances of the windings to earth. The absence of any ohmic resistance causes the solution to be oscillatory and without appreciable damping.

4.8 The effects of Chopped Waves on the Transformer Windings

The numerical solution for the chopped wave has been developed as follows:

The initial distribution of voltage due to the wave front, which may be considered as a cycle of very high frequency. It is permissible therefore to calculate this distribution as though the applied voltage were alternating. This simplifies the calculation as it avoids time variables.

From the equivalent circuit three equations are developed and solving these will result in the following for winding with the neutral connected to earth. The max voltage gradient

$$E = \frac{\alpha}{l} \qquad (4.2)$$

Where

$$\alpha = \sqrt{\frac{Cg}{Cw}} \qquad (4.3)$$

α Represents the ratio between the maximum and average voltage gradient and the equation is shown above in 4.2

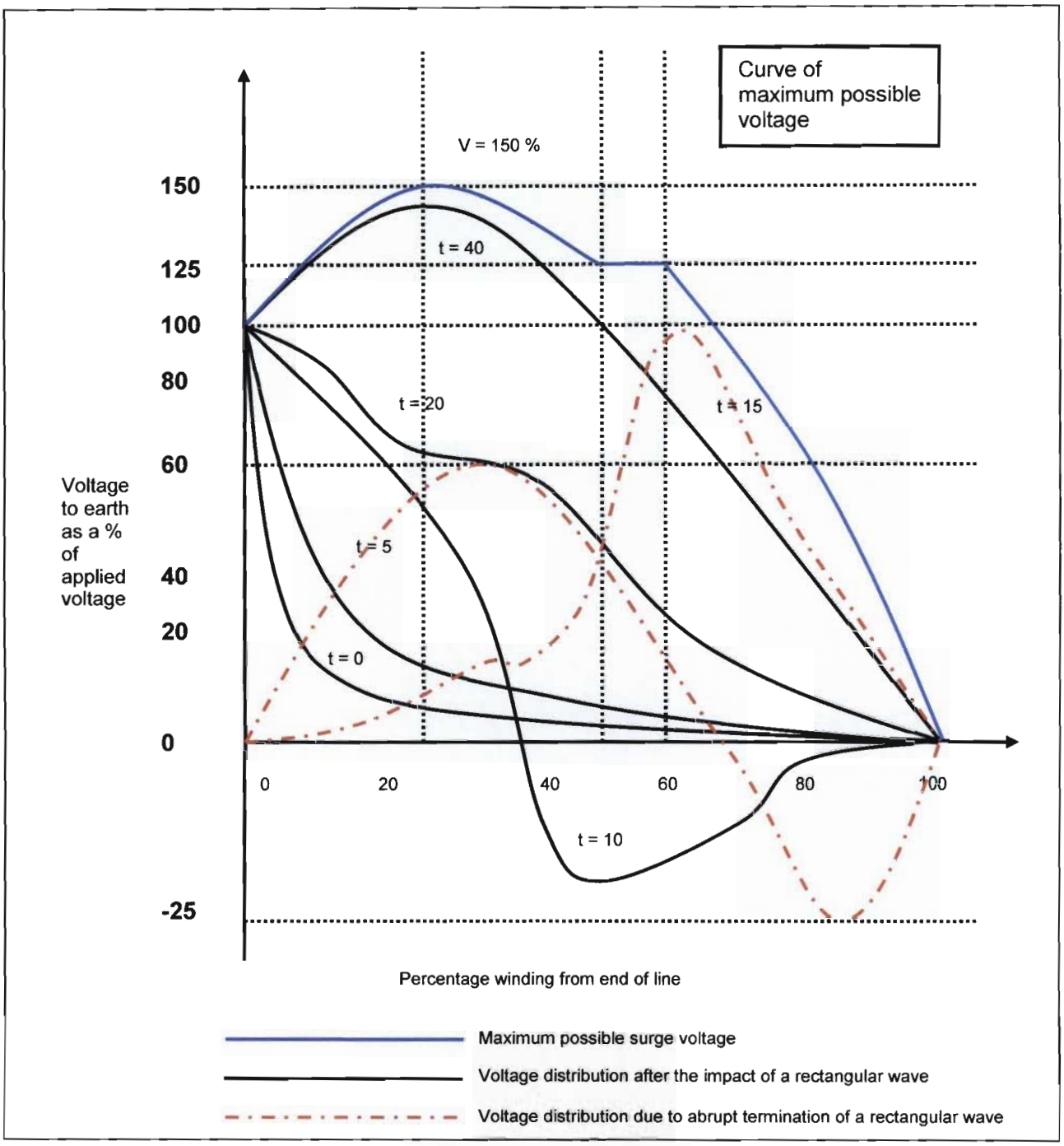

Figure 4.3 Abrupt terminated impulse voltage on transformer windings

The above graph is taken from Wedmore [40]. The point demonstrated here is that the maximum voltage reached is 150 kV for a 100 kV applied input surge of the chopped wave type. This is similar to the electrical characteristics produced by a spark gap chopped wave that will be generated when the surge is extinguished by the gap.

4.9 Concluding remarks

To accurately model the behaviour of a pole mounted transformer under lightning conditions, a detailed high frequency (HF) model is required. The nonlinear behaviour and the frequency dependence must be taken into account at high frequencies. The effect of the frequency dependent copper and iron losses and the effect of stray capacitance are not taken not account by the ATP transformer model, Leuven [42]

The transformer is a complex arrangement of closely spaced coils around an iron core. This arrangement introduces capacitances (inter winding and winding to ground) and inductances. At high frequencies the capacitance of the winding comes into effect. Transformers have a number of resonant frequencies, with one dominant frequency in the 5-30 kHz range and other resonances at other frequencies. Lightning surges may excite these resonance and cause voltage amplification inside the windings, Woivre [43]

A comprehensive background literature survey of the high frequency modelling of transformers is provided by Kelly [45]. The work provides information on the HF transformer model (based on performance in the laboratory, mathematical processing in Mathlab and EMTP simulation results) for the transfer of overvoltages from the primary to the secondary side. The HF model presented could be used as a transformer based on the coupled coils level representation to be implemented in EMPT is provided by Chimklai [39].

It was proved that for shell type transformers that the windings behave as a linear system without saturation effects in the period of time immediately following the beginning of the impulse, Woivre [43]. A simple capacitive model is used to demonstrate that the lower the capacitance of the winding, the higher the resultant overvoltage.

It was also found by Morched [44], that the modelling of the distributed stray capacitances along the windings with lumped capacitances connected across the terminal of the transformer could not reproduce the behaviour of the transformer beyond the first resonance frequency.

When modelling a transformer for lightning surge studies on a network, a lumped capacitance may be used to represent the transformer. This only applies when the

voltage transfer from the MV to the LV side is not important. The constraints of using a lumped capacitance value representation of a transformer as discussed in Woivre [43], and Morched [44] are important. A capacitance value of 1nF was used by Holdalen [46] to represent the transformer.

The reflection and transmission of a travelling wave at junction points of unequal impedances are of great importance in surge protection of transformers. The travelling wave is modified by transformer parameters and results in a voltage rise. From The above discussions and Figure 4.3 it is shown that a travelling wave is modified at the transition point ie at the transformer terminal but the max possible voltage remains at 100 kV and could reach a maximum of 150 kV, depending on the frequency of the surge and transformer parameters. Figure 4.3 shows that the maximum voltage distribution for a Medium voltage transformer is 150 kV irrespective of the parameters for the worst case lightning induced surges. Modelling of a transformer winding also proves to be difficult as shown in the latter discussion from the works of Woivre [43] and Morched [44], hence further support why the value of 150 kV was adopted as the safe high point that is also well supported by SANS 1019 and IEC 60071-1 [49] for transformer specifications purposes. All 22kV distribution transformers are constructed and tested at 150 kV BIL, hence it is safe to design the spark gap based on this maximum value of 150 kV.

CHAPTER 5 Breakdown Mechanisms in Insulating Gases

5.1 Introduction

Electric insulating materials or dielectrics are materials in which electrostatic fields can remain almost indefinitely. These materials thus offer a very high resistance to the passage of direct currents. However they cannot withstand an infinitely high voltage. When the applied voltage across the dielectric exceeds a critical value the insulation will break down and be permanently damaged. The failure of gas insulation is discussed in terms of gas filled regions stressed by the application of a voltage between two metal electrodes, immersed in the gas. There are two types of gaseous failure:

5.2 Complete Failure

An insulating gas becomes highly conductive with a collapse of voltage across the electrodes. This kind of failure is known as breakdown, sparking, sparkover or flashover. An arc, glow or transitory type of discharge depends on the nature and condition of the gas and the ability of the external source to sustain a continuous discharge.

5.3 Incomplete Failure

This partial insulation failure is also known as a corona discharge. It is characterised by a localised region or regions becoming conductive. The voltage across the electrodes remains high and only small intermittent current flows. This occurs in highly non-uniform fields and the localised high conductivity regions occur in the high field regions. Corona usually occurs when the following criteria are met:

$$\frac{E\max}{Eave} \geq 5 \qquad (5.1)$$

In high non-uniform fields, these are two critical voltages i.e. the corona inception voltage and the spark over voltage. The breakdown on the spark gap will be determined using this criterion, Kuffel [23].

5.4 Types of Gaseous Electric Fields That Are Considered.

a) **Uniform fields**, in which the field strength is constant throughout the electrode, gap as an example, the parallel plate arrangement in Figure 5.1.

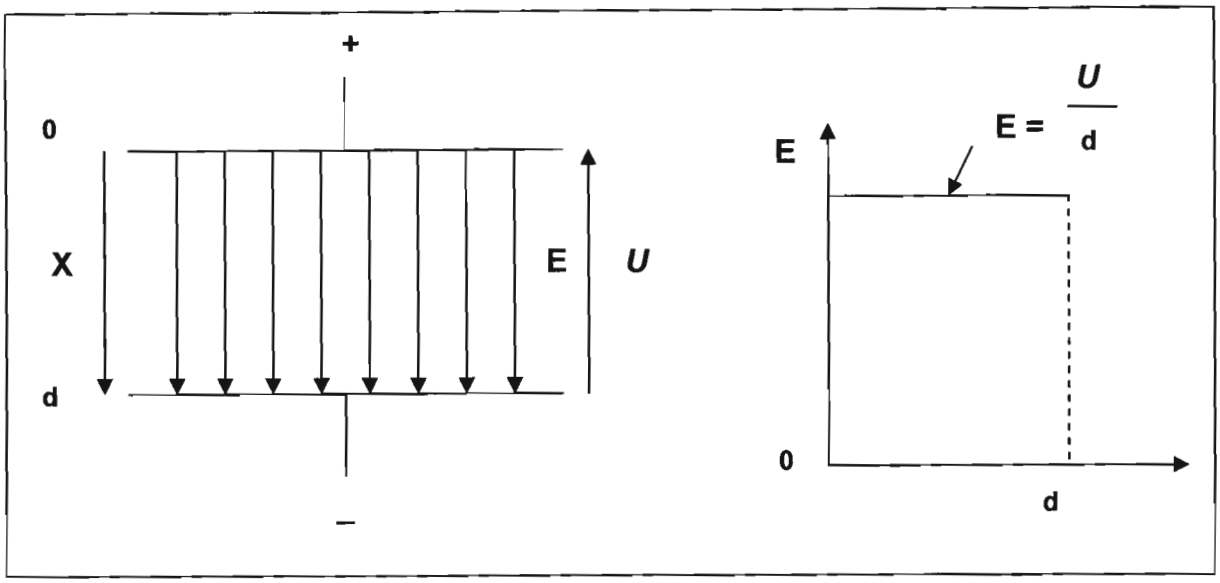

Figure 5.1 Uniform Fields

b) Quasi-uniform fields, when the electric field varies with position in the gap but corona discharge does not occur, an example being a Co-axial cylinder arrangement,

C) Non-uniform fields, where corona discharges occur before breakdown. The degree of non-uniformity depends on the gas pressure, but normally corona precedes breakdown if equation 5.1 holds true. Examples are rod-rod gaps, rod plane gaps and transmission lines.

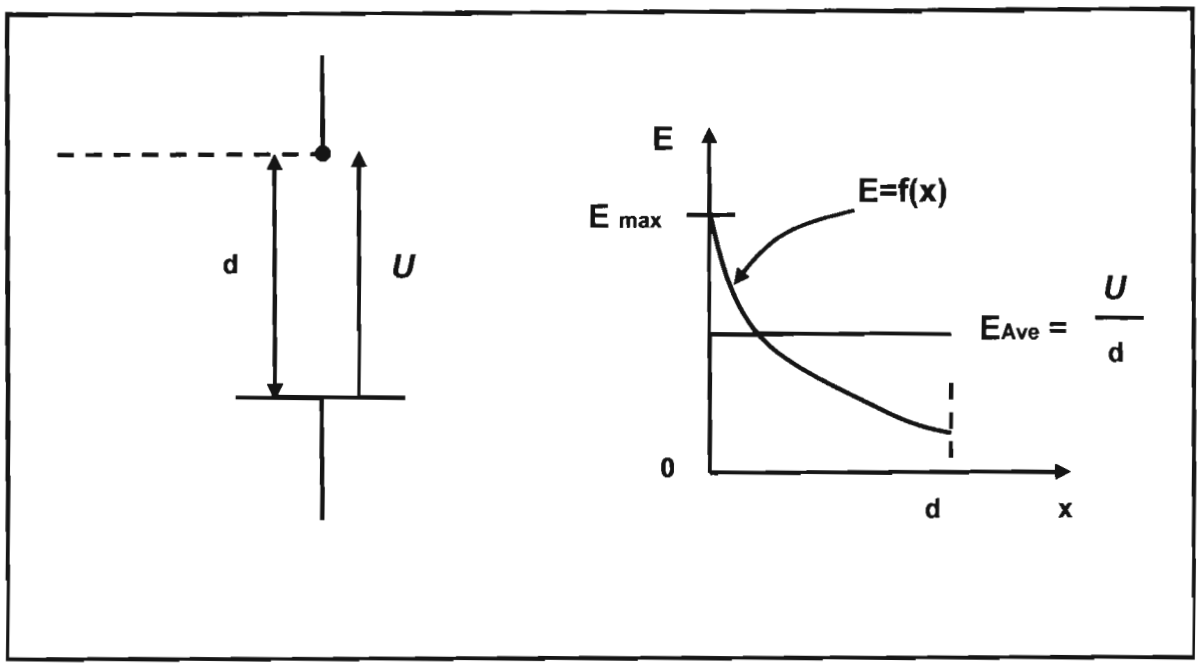

Figure 5.2 Behaviour of Non-Uniform Fields

Insulation systems are designed to operate without corona discharges under normal operating conditions and insulation failure theories are simplest in uniform field configurations. Experimental studies under uniform field conditions are useful in testing insulation failure theories. Quasi-uniform fields occur in practical insulating systems like direct engineering application. Non-uniform fields are found in many practical applications and failures under such conditions are the most difficult to study, but most required, Kuffel [23].

5.5 Fundamental Processes in Insulation Failure

When a gas filled region is subject to an electric field, no current except capacitive current will flow, unless there are free electric charges present in the gas. When a voltage is applied between metal electrodes in air at atmospheric pressure, a small current will flow due to the presence of electron ion pairs produced by natural background radioactivity from cosmic radiation. The ion pairs are generated at an extremely slow rate and a current of $1.6 \times 10^{-19} \times 10^{4}$ A $= 1.6 \times 10^{-15}$ A flows. This negligible leakage current will flow if all the released charges are collected at the electrodes, Kuffel [23].

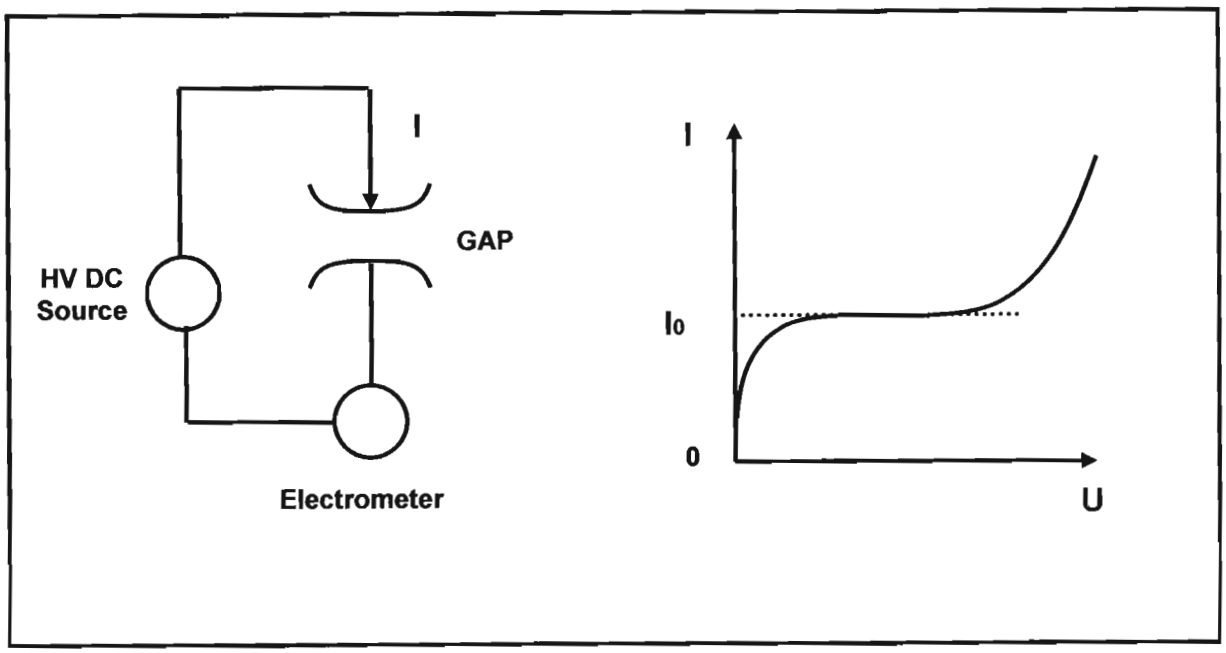

Figure 5.3 Leakage Current Flow

If the applied voltage is high enough, the free electrons involved in leakage current flow can initiate processes that lead to insulation failure. The free electrons are accelerated in the electric field and they collide and transfer their energy to molecules. As the electric field strength is increased, the electrons gain more energy, sufficient enough to ionize the molecules thus creating more free electrons Kuffel [23].

5.6 Motion and Energy of Charged Particles in a Gas

A gas with some free electrons will acquire velocities through collisions with gas molecules that are in random thermal motion. In the absence of an electric field, the motion of electrons will be random if the electrons are uniformly distributed. If there is a non-uniform distribution of electrons in gases, then the electrons will diffuse to achieve a more uniform distribution. So the diffusive motion will be superimposed on the random motion. In the presence of an electric field, the electrons will move along field lines between collisions and will acquire a velocity in the direction of the field. This velocity is known as the *drift velocity* Kuffel [23].

So in the presence of an electric field, the electron velocities will have three components i.e.

a) Random thermal velocity
b) Diffusion velocity ie from regions of high electron concentration to regions of lower electron concentration.
c) Drift velocity in the direction of the field.

The drift velocity is the most dominant. Similar considerations apply to positive ions and negative ions. The drift is dependent on pressure, ambient temperature and field strength. For a pressure of 760 torr, field strength of 30 kV/ cm and temperature 20°C, the drift velocity of the electrons is ~10^5 m/s and that of positive or negative ions ~ 10^3m/s.

The electron or ion drift velocity is an average value. At any instant, the particles have a wide range of velocities that are described in terms of statistical distribution. The distribution follows a BOLTZMANN – MAXWELL function. ie

$$f(u) = \frac{dNu}{N} \qquad (5.2)$$

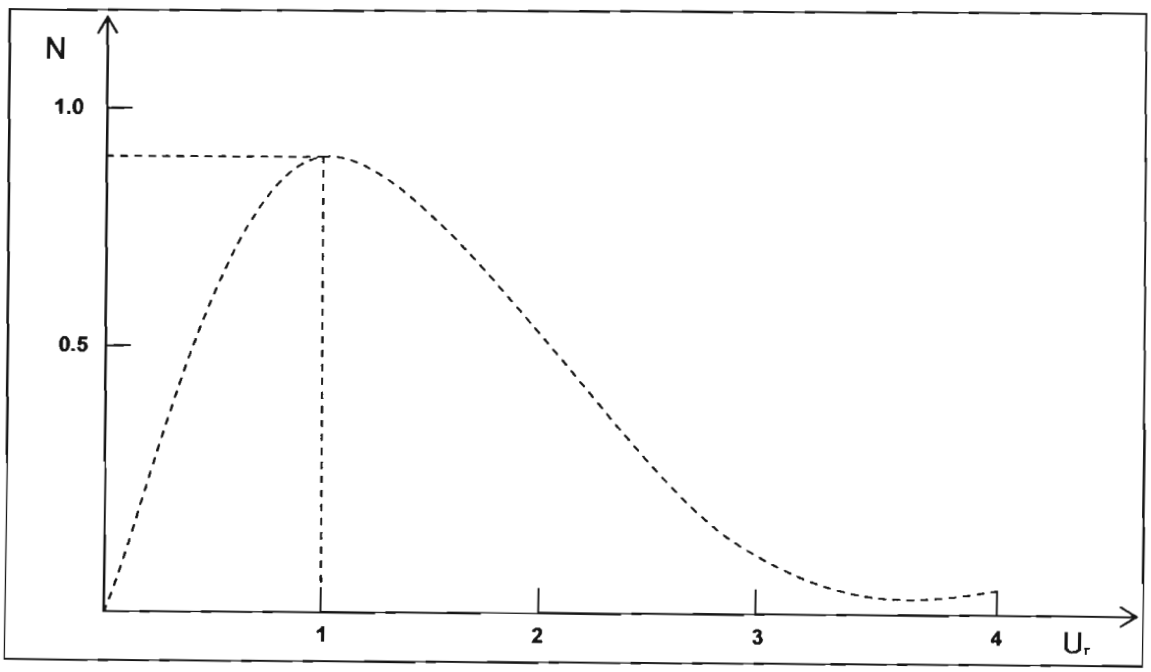

Figure 5.4 Molecular velocities in common gases at 20°C < 760 torr

If

$$\frac{U}{up} = ur \qquad (5.3)$$

Then

$$f(_{ur}) = \frac{4}{\pi} ur^{2} e^{-ur^{2}} \qquad (5.4)$$

Therefore at

$$_{ur} = 1$$

$$f(1) = 0.83 \qquad (5.5)$$

Table 5.1 Typical mean molecular velocities, 20°C < 760 torr

Gas	Electron	H_2	O_2	N_2	Air	CO^2	SF_6
U m/s $X10^3$	100	1.76	0.44	0.47	0.465	0.375	0.199

The electrons that participate in inelastic collisions are only a small fraction of the total number in the high energy field of the distribution. Table 5.1 above shows the molecular velocity for the various gases. , Kuffel [23].

5.6.1 The energy parameter

$$= \frac{E}{N} \qquad (5.6)$$

In most electrons–molecule collisions, the controlling factor is the amount of energy gained by the electron from the electric field in between collisions. The distance molecules or electrons travel in-between collisions are known as the free path (λ). It is a random quantity and its mean value depends on the density of the gas. Assuming that a

molecule of radius r_1 and a particle of radius r_2 are to collide and assuming that they behave as solid spheres, then a collision will occur when the centre of the two will come within a distance of $r_1 + r_2$ .of each other, Kuffel [23].

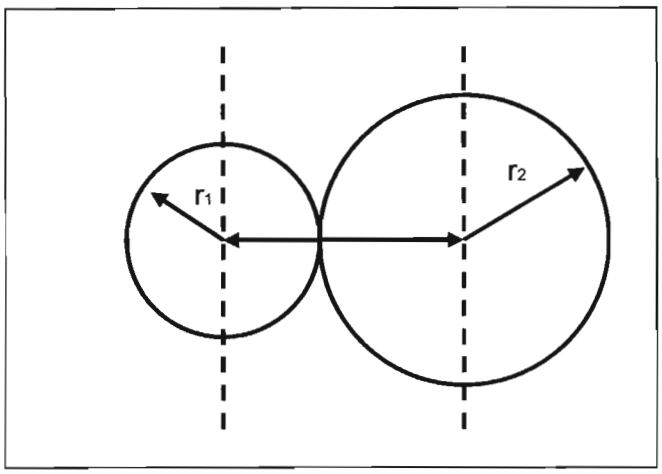

Figure 5.5 Area of Collision Presented By Molecule

The area of collision presented by molecule is

$$\pi\ (r_1 + r_2)^2 \qquad (5.7)$$

And if N = number of molecule involved,

Then effective area of interception per Volume is

$$N\ \pi\ (r_1 + r_2)^2 \qquad (5.8)$$

By definition, mean free path λ,

$$\lambda = \frac{1}{N\pi(r1 + r2)^2} \qquad (5.9)$$

But

$$\pi\ (r_1 + r_2)^2 = \sigma = \text{collision cross section}$$

Therefore

$$\bar{\lambda} = \frac{1}{N\lambda} \qquad (5.10)$$

Q = effective cross-section or collision cross section presented by molecules or particles in a unit volume of gas for all collisions for density N molecules/volume. If W = energy gained by an electron of charge e moving in a electric field E, through a mean free path λ, Then for an ideal gas

$$w \infty \frac{E}{P} \qquad (5.11)$$

$\frac{E}{P}$ is convenient because P is more measurable than N. However, E is meaningful only if the temperature at which the pressure was measured is known eg. if

t =20°C $\Longrightarrow$ T = 293K, for K = 1.3, then

$$\frac{E}{P_{20}} = \frac{E}{NKT_{20^0 c}} \qquad (5.12)$$

5.7 Fundamental Processes at molecular level

5.7.1 Electron-Molecule Collision Processes

a) **Excitation**

The orbiting electron in the molecule is raised to a higher energy level then it normally occupies when the molecule is in its ground state. This is an unstable state, and the process utilizes the excess energy by emitting a photon. The lifetime of an excited state is ~ 10^{-2} μS or less. In some gases, molecules can remain in the excited state for longer periods and these are known as metastable states.

Equations representing excitation and de-excitation processes are:

Excitation $A + e^- \Rightarrow A^* + e^-$ (5.13)

Photon emission $A^* \Rightarrow A + h\gamma$ (5.14)

Where:

e $\Rightarrow$ electron

A $\Rightarrow$ atom/molecule colliding with the electron

A* $\Rightarrow$ excited atom / molecule

hλ $\Rightarrow$ photon energy. The released light has wavelength frequency of the wave form, c = velocity of light

h $\Rightarrow$ Planck's constant (6.626×10^{-34} Js)

If the gas is monatomic dissociation may accompany the excitation

$XY + e^- \Rightarrow X + Y^* + e^-$ (5.15)

$Y^* \Rightarrow Y + h\gamma$ (5.16)

b) **Collision Ionisation**

Occurs when the kinetic energy of the electron is at least equal to the ionization energy of the molecule/atom with which collides:
i.e.

$A + e^- \Rightarrow A^+ + 2e^-$ (5.17)

The atom / molecule is ionized, releasing an electron, providing two free electrons, if the gas is not monatomic dissociation may occur along with ionization i.e.

$XY + e^- \Rightarrow X + Y^+ + 2e^-$ (5.18)

If the colliding electron has sufficient energy it can also give rise to a positive excited ion i.e.

$$XY + e^- \Rightarrow X + Y^{+*} + 2e^- \qquad (5.19)$$

$$Y^{+*} \Rightarrow Y^+ + hr \qquad (5.20)$$

c) **Attachment**

This occurs if a colliding electron occupies one of the free energy levels in the outmost shell and converts the molecule into the negative ion.
i.e.

$$A + e^- \Rightarrow A^- \qquad (5.21)$$

This is process is know as direct attachment.

Attachment is most likely to occur in electronegative gases. There are atoms or molecules lacking one or two electrons in their outer shell e.g. the halogens with one electron missing and O, S, Se, with two electrons missing in the outer shell.

Ionisation and attachment are competing processes (i.e. ionization tends to increase the number of free electrons while attachment tends to reduce them) , Kuffel [23].

d) **Recombination**

This occurs when an electron collides with a positive ion and assumes the place of the electron that was removed when the ion was formed – leading to the formation of a neutral molecule. The molecule will be in an excited state and it will reach the ground state by emitting a photon.
i.e.

$$e^- + (XY)^+ \Rightarrow (XY)^* \Rightarrow XY + h\gamma \text{ radiation} \qquad (5.22)$$

The resulting radiation is called recombination radiation. The rate at which recombination occurs is proportional to the product of the number of free electrons or negativity per unit volume and the number of positive ions per unit volume. The recombination process is particularly significant at high pressure where diffusion is relatively unimportant, Kuffel [23].

For equal concentrations of positive ions (n_+) and negative ions (n.), the rate of recombination is

$$\frac{d_{n+}}{dt} = \frac{d_{n-}}{dt} = -\beta n + n \qquad (5.23)$$

Where β = the recombination rate

The final equation is

$$t1/2 = \frac{1}{ni0\beta} \qquad (5.24)$$

The recombination coefficient is pressure dependent

e) **Detachment**

This occurs when negative ion loses its extra electron to become a neutral molecule. The released electron is free and can therefore ionize by collision. In photo-detachment, the energy necessary to separate the electron is provided by a photon.
i.e.

$$A + h\gamma \Rightarrow A + e^- \qquad (5.25)$$

In dissociative detachment the reverse of dissociative attachment takes place
i.e.

$$X_Y^- \Rightarrow XY + e^- \qquad (5.26)$$

5.7.2 Photon Process

Many of the ionization processes lead to the emission of photons which in some cases lead to release of more free electrons through photoionistaion (or photoemission from the cathode.)

a) **Photoionisation**

A photon can ionize a molecule or atom if its energy (ie $h\gamma$) is at least equal to the ionization energy of the molecule or atom.

$$A + h\gamma \Rightarrow A^{+} + e^{-} \qquad (5.27)$$

b) **Photoemission**

Occurs when a photon impinging on the electrode surface if its energy is at least equal to the work function of the electrode material i.e

$$h\gamma \geq W_{\phi} \qquad (5.28)$$

Work functions of common elements

Table 5.2Typical work function values

Element	Ag	Al	Cu	Fe	W (Tungsten)
W_{ϕ} (ev)	4.74	2.98-4.43	4.07-4.7	3.91-4.6	4.35-4.6

Table 5.2 above shows the work functions for the various metals, Copper and Iron are very close.

c) **Quenching –Destruction Of The Excited States By Collision**

ie.

$$A^{*} + M \Rightarrow A + M \qquad (5.29)$$

Probability of quenching occurring increases with pressure at a given temperature, Kuffel [23].

5.7.3 Other Process

a) **Electron Emission from Electrode Surface**

This is caused by photons or positive ions or metastable molecules impinging on an electrode (cathode) surface.

b) **Space –Charge Field Distortion**

Space charge field is an electric field produced by a large number of charge carriers (i.e. electrons, positive ions and negative ions) concentrated in a small volume. This field can be comparable to the applied field and its distorting effect on the applied field can accelerate insulation failure or inhibit it, Naidu [26].

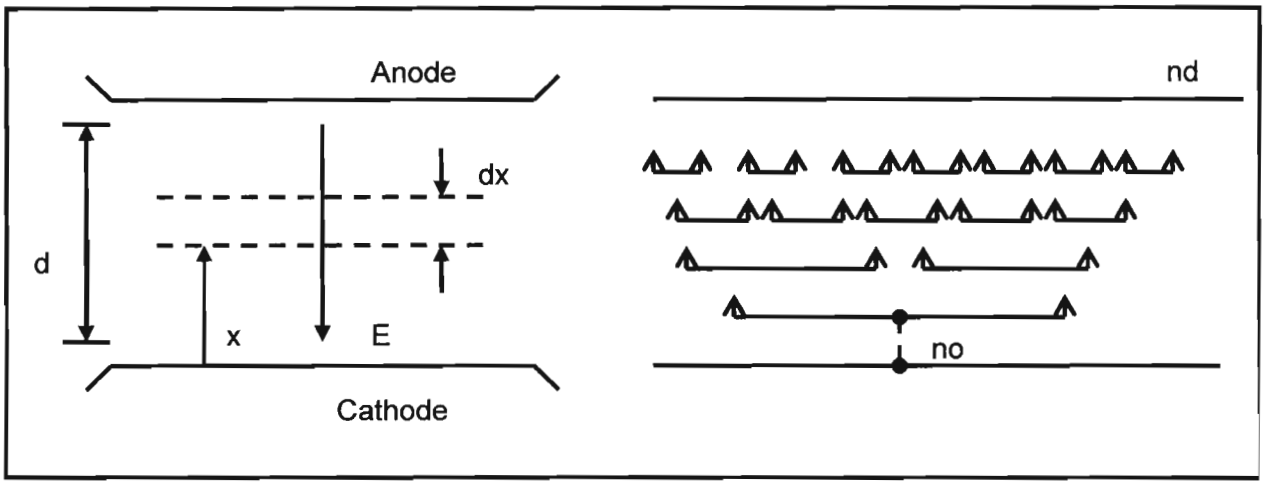

Figure 5.6 Electron Multiplications in an Avalanche

c) **Electron Multiplication in an Avalanche**

The avalanche will continue to grow until the electrons either reach the anode or travel into region of the gap where the field is not high enough to support Collisional ionization. If the field conditions are appropriate, then the avalanche growth leads to breakdown. There are two main theories that are used to explain breakdown mechanisms in gases i.e. the Townsend breakdown mechanism and the streamer or Raether breakdown mechanism, Naidu [26].

5.8 The Townsend Mechanism

Townsend's original experiments involved measurement of the growth of the average current to breakdown in a uniform field gap at dc voltages. The current was found to increase linearly with voltage to a constant value Io which corresponded to the background and uv radiation (saturation) current.

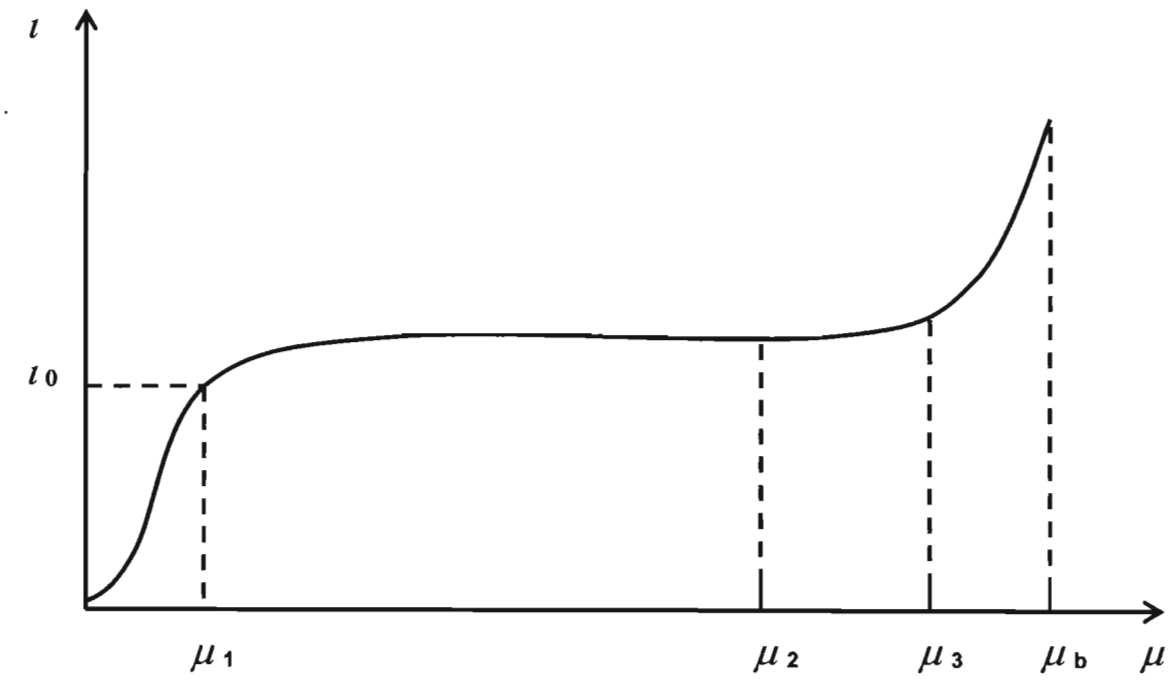

Figure 5.7 Current growth in the ionization process

The observed increase in current beyond μ_2 was attributed to ionization by electron at increased field values to cause ionization producing more electrons. This is know as primary ionization or the α -process. A coefficient α was introduced whereby α = *Townsend's first ionization coefficient* defined as number of electrons produced by an electron moving a unit length in the direction of the field. The primary growth α -process equation, Naidu [26].

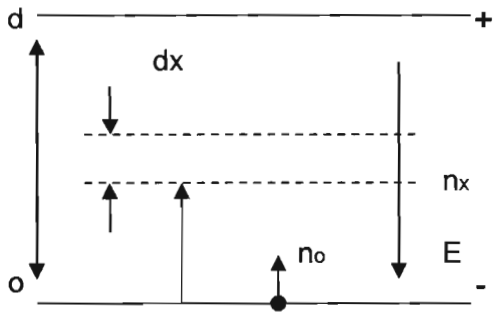

Figure 5.8 Townsend's first ionization process

Let n_o = number of electrons from the cathode per second. At x distance from the cathode, the number of electrons will be n_x due to ionizing collision (avalanche growth). Let dn_x = number of electrons traversing x = α dx

Then the initial current at the cathode will be

$$I=I_o \exp(\alpha d) \qquad (5.30)$$

5.9 The Breakdown Process

Collisional ionization is the most significant process in insulation failure mechanisms. Assuming that a free electron released by cosmic radiation or background activity is present in a gap, under an electric field. If this electron is not captured in the attachment process then it is likely to cause ionisation of a gas molecule through collision. So there will be two free electrons and a positive ion. The two electrons will each cause further ionization (assuming no attachment), and soon there will be three positive ions and four electrons, Naidu [26].

5.10 Breakdown Criteria

Since $nx = n_0 e^{(\alpha.\eta)x}$ in uniform fields

Where nx is the number of electrons in an avalanche head at a distance x from the cathode n_0 =initial number of electrons Then for breakdown to occur

$$(\alpha - \eta)d \geq 19.5 \qquad (5.31)$$

This condition is fulfilled when avalanche has traversed the gap (i.e. x = d). One of the most important laws in high voltage technology, see Figure 5.8 above. For pd> (pd) min, the reduced mean free path electrons make more frequent collisions energy gained between collisions is lower increased voltage necessary for breakdown to occur. For pd < (pd) min increased mean free path electrons can cross the gap without making collisions more electrons must be released to increase chance of breakdown higher voltage necessary (pd) min corresponds to point of highest ionisation efficiency, Kuffel [23].

5.11 Factors Affecting Uniform Field Breakdown

At high pressure the materials become significant in processes of releasing electrons (by high fields- effects on the feedback process) the electrode material influences emission from the surfaces. Rating of materials in the order of decreasing electrical strength: tungsten, molybolem, tantalum, stainless steel, iron, nickel. Surface contaminating reduces breakdown. Other factors include area of electrode surface, temperature, frequency of applied voltage, Naidu [26].

5.12 Effective Area

The concept of the area effect demands the definition of an electric active electrode area. One possibility is to determine the area stressed by the electric field of at least 90 % of the highest electric field strength of the whole surface. This area is defined here as the "Effective Area". Numerical field simulations were carried out using the knowledge of the above theory for both arrangements. The coplanar profile has the advantage of a

homogenous field distribution. However, a critical point exists at the border area. At this point the electric field strength is increased according to the homogeneous field strength of the coplanar area. A two-dimensional axissymmetric finite element calculation of the electrical field distribution is shown in Figure 5.9. Field strength pattern of the coplanar electrodes. (In this case a gap distance of 10 mm and an applied voltage of 100 kV), because of the rough illustration of the field strength in figure 5.9, Naidu [26].

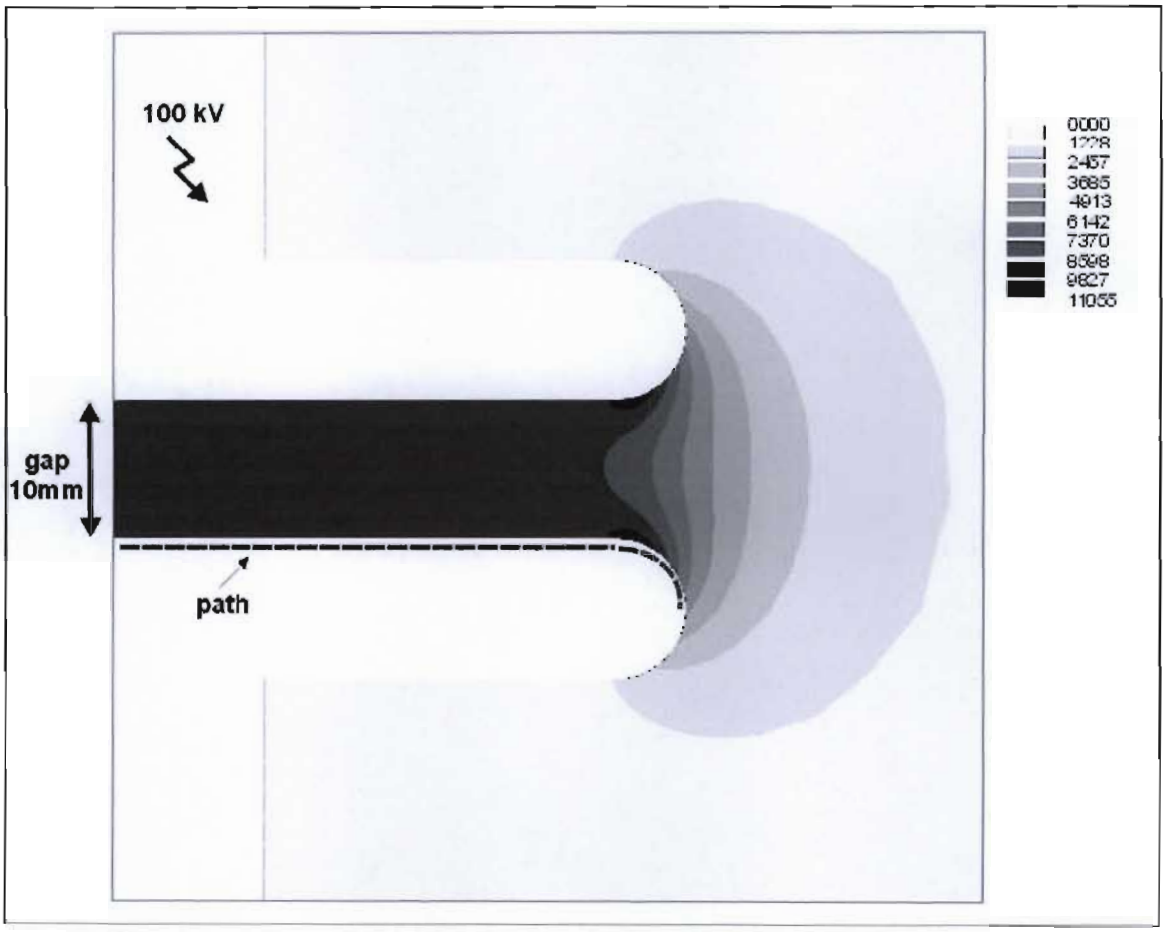

Figure 5.9 Field Distribution simulations for uniform parallel plates

5.13 Temperature Effects

This is along the path on the surface of the electrodes which are shown detailed in Figure 5.9. The Electric field distribution along the path for an applied voltage of 100 kV (gap distance = 10 mm and d = 100 mm). An additional result of the simulation leads to the conclusion that the influence of the gap length relating to the Effective Area is along the path on the surface of the electrodes are shown detailed in Fig 5.9. Electric field

distribution along the path of figure 5.9 for an applied voltage of 100 kV (gap distance = 10 mm and d = 100 mm).
An additional result of the simulation leads to the conclusion that the influence of the gap length relating to the Effective Area is the temperature affects density and hence pressure at higher temperatures or other effects occur

- Thermal ionisation
- Thermionic emission
- Electrode distortion by the heat.

5.14 Moisture / Humidity

The presence of moisture tends to reduce the breakdown voltage (Eb). For gaps exceeding 10 cm at NTP, the breakdown voltage increases linearly with P_d to the limits of the Paschen's law. In air, the equation developed experimentally by Schumann and modified by Bruce referred to by Naidu [26] takes into account the effect of moisture to reduce breakdown voltage.

5.15 Corona discharges

If the electric field is uniform, a gradual increase in voltage across the gap produces a breakdown of the gap in the form of a spark without any preliminary discharges On the other hand if the field is non-uniform, an increase in voltage will first cause a discharge in the gas to appear at points with highest electric field intensity, namely at sharp points or where the electrodes are curved. This form of discharge is called corona discharge and can be observed as a bluish luminescence. This phenomenon is always accompanied by a hissing noise, and the air surrounding the corona region becomes converted into ozone. Corona is responsible for considerable loss of power from HV lines and leads to deterioration of the insulation due to bombardment of ions and the chemical formed during discharges. On HV conductors, corona appears different in colour for positive and negative impulses. When the voltage is positive, corona appears as bluish white sheath over the conductor surface. When the voltage is negative, it appears like reddish glowing spots distributed along the wire, Naidu [26].

5.16 Breakdown in Non-uniform Fields

In non-uniform fields e.g. in point-plane, sphere-plane gaps or coaxial cylinders, the field strength and hence the effective ionization coefficient $\overline{\alpha}$ varies across the gap. The electron multiplication is governed by the integral of $\overline{\alpha}$ over the path ($\int \overline{\alpha} dx$) at low pressures the Townsend criterion for spark takes the form

$$\gamma[\exp(\int_0^d \overline{\alpha} dx) - 1] = 1 \qquad (5.32)$$

Where d is the gap length. The integration must be taken along the line of the highest field strength. The expression is valid also for higher pressures if the field is only slightly non-uniform. In strongly divergent fields there will be at first a region of high values of E/p over which. $\alpha / p > 0$. When the fields fall below a given strength E_c the integral $\int \alpha dx$ ceases to exists. The Townsend mechanism then loses validity when the criterion relies solely on the γ effect, especially when the field strength at the cathode is low. In reality breakdown (or inception of discharge) is still possible if one takes into account Photoionisation processes. The criterion condition for breakdown (or inception or discharge) for the general case may be represented by modifying the expression (5.90) to take into account the non-uniform distribution of $\overline{\alpha}$ or

$$\exp \int_0^{X_c < d} \alpha dx = N_{cr} \qquad (5.33)$$

Where N_{cr} is the critical electron concentration in an avalanche giving rise to initiation of a streamer (it was shown to be approx. 10^8) is the path of avalanche to reach this size and the d gap length. Hence equation (5.10) can be written as

$$\exp \int_0^{X_c < d} \alpha dx = \ln N_{cr} \approx 18 - 20 \qquad (5.34)$$

Equation (5.11) is applicable to the calculation of breakdown or discharge inception voltage, depending on whether direct breakdown occurs or only corona, Naidu [26].

5.17 Concluding Remarks

From a practical engineering point of view, rod-rod and sphere-sphere gaps are of great importance, as they are used for the measurement of high voltages and for the protection of electrical equipment as is the aim of this thesis.

The breakdown voltages for positive and negative polarity are compared by,Naidu [26] and it is clear from the analysis that negative breakdown voltages are higher than positive breakdown voltages. The breakdown voltage was also observed to be dependant on humidity in the air. In the case of rod gaps, the field is non-uniform and for sphere gaps, the field is uniform if the gaps are small compared with the diameter of the sphere. In the case of sphere gaps, the breakdown voltages do not depend on humidity and are also independent of the voltage waveform. The formative time lag is very small ($\sim 0.5\ \mu s$) even with a 5% overvoltage.

Hence sphere gaps are preferred for peak voltage measurements. The post breakdown phenomena as discussed in Naidu [26], is of technical importance as this is the phenomena that occur after the actual breakdown. Glow and arc discharge are the post breakdown phenomena and there are many devices that operate over this region. In a Townsend discharge, the current increase gradually as a function of the applied voltage. Further to this point, only the current increases and the discharge changes from the Townsend type to the Glow type. Further increase in current result in a very small reduction in voltage across the gap corresponding to the normal Glow region. The gap voltage again increases when the current is increased more, but eventually leads to a considerable drop in the applied voltage. This is the region of the arc discharge. The phenomena that occur in the region are the post-breakdown phenomena of Glow and Arc discharge. The above phenomenon indicates that for the lower voltage range, the gap draws a considerable arc at the lower voltages typically less than 250 kV.

A detailed review of the above theory indicates that the following factors will influence the breakdown behaviour of a spark gap

a) Applied voltage
b) Gap size
c) Air density (pressure and temperature)
d) Humidity for rod –rod gaps

e) Degree of non-uniformity which is a direct contribution from shape of rod tips.
f) Type of metal used for the rods
g) Tip to gap ratio

Precautions for the simulation and laboratory tests would be to ensure that the above conditions are noted and normalization be done before results are interpreted.

CHAPTER 6 MODELING AND SIMULATION RESULTS

6.1 Model Circuit Set Up For Simulation

The proposed method of transformer protection involves placing a rod – rod gap in parallel with the surge arrester on the transformer. The voltage input for the simulation was set at 110 kV. This value is a typical test voltage applied for ease of scale. Also based on the concluding remarks of chapter 3, section 3.8.

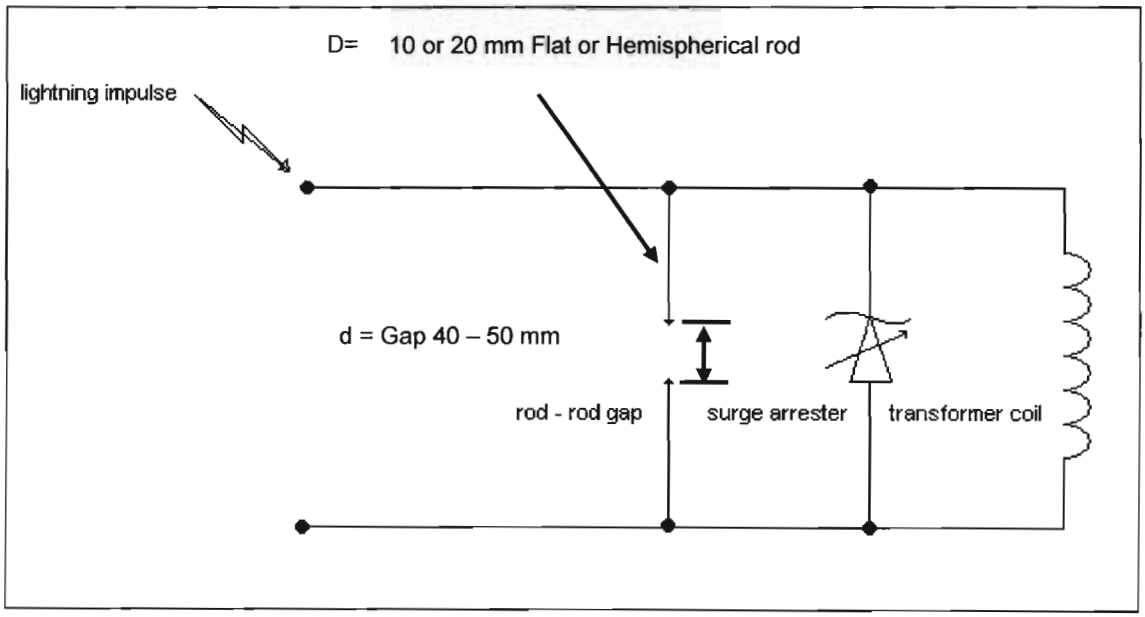

Figure 6.1 Transformer protection using rod – rod gap

6.2 The Rod – Rod Gap Configurations Analyzed

a) The following Flat rod – rod gaps were tested: d = 40mm, 50mm and 60mm; D = 10mm and 20mm.

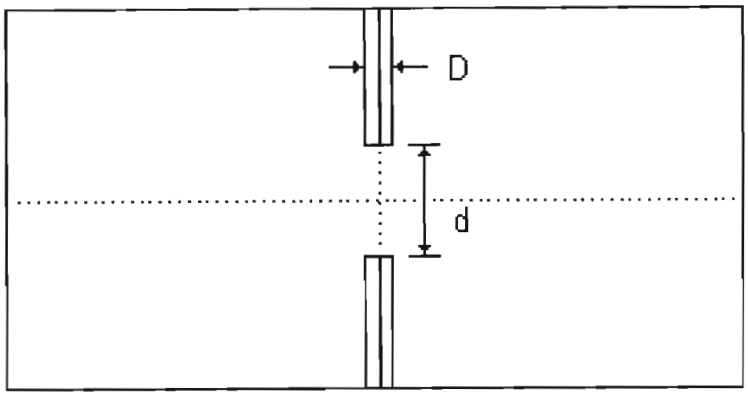

Figure 6.2 Flat Rod – Rod Gap

b) The following Hemispherical rod – rod gaps were tested: d = 40mm, 50mm and 60mm; D = 10mm , 20mm

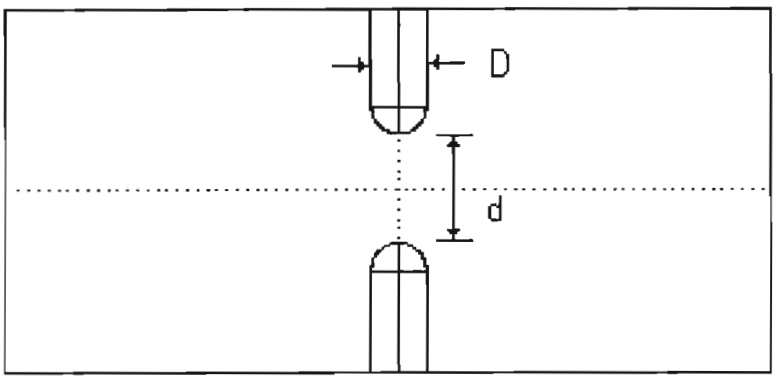

Figure 6.3 Hemispherical Rod – Rod Gap

6.3 Femlab Modelling and Analysis

The Femlab model navigator offered several options with respect to modeling modes and space dimensions. The 3D Electrostatics generalized mode was best suited and used.

6.4 Analysis of the FEMLAB Simulation studies

Each of the geometries was modeled using the electrical parameters as detailed in Annexure B and these were solved using the Femlab linear solver. The characteristic of interest was the electric field within the gap. The field was represented as a line plot along a straight line which passed through the gap as shown below.

6.5 Infinite Space

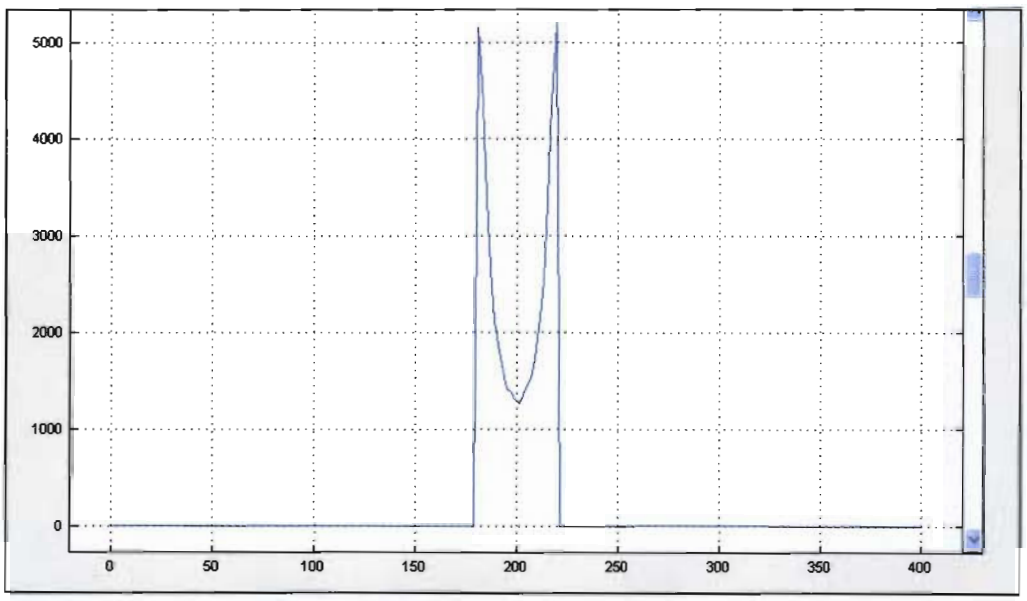

Figure 6.4 Electric field Flat rod gap, d = 40mm, D = 10mm.

As expected the electric field within the gap was symmetrical about the mid-point of the gap.

V/mm

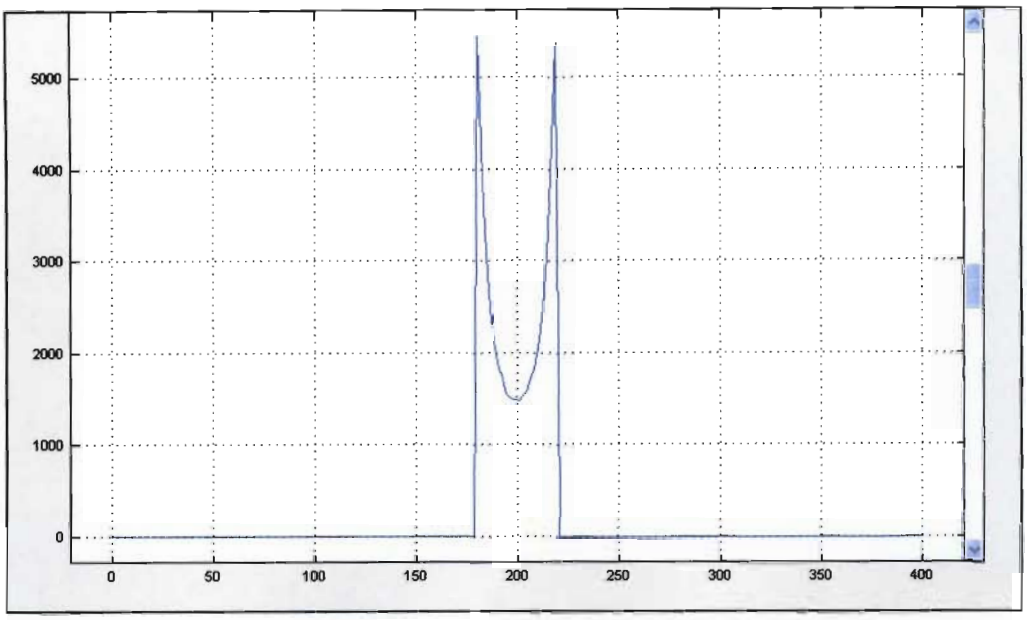

Figure 6.5 Hemispherical rod gap, d = 40mm, D= 20mm

The result for the electric field is symmetrical about the mid-point of the gap.

6.6 Nearby Earth Plane Effects

In order to establish the effects of grounded objects in the vicinity of the rod – rod gaps, simulations were carried out by placing a vertical ground plane in parallel to the rods and gaps as shown in Figure 6.6

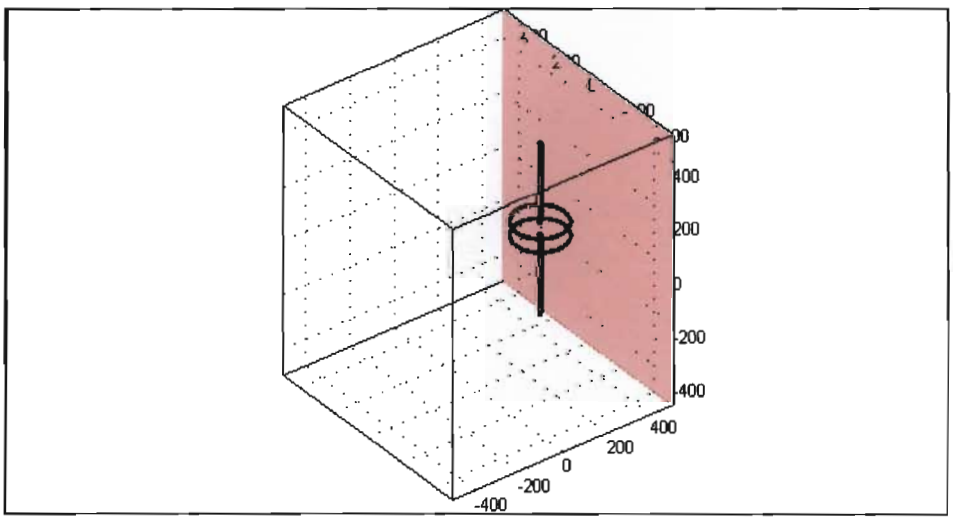

Figure 6.6 Earth plane 3D- drawing

The simulation results revealed that ground planes do have a significant effect on the gap breakdown as is seen in figure 6.7.

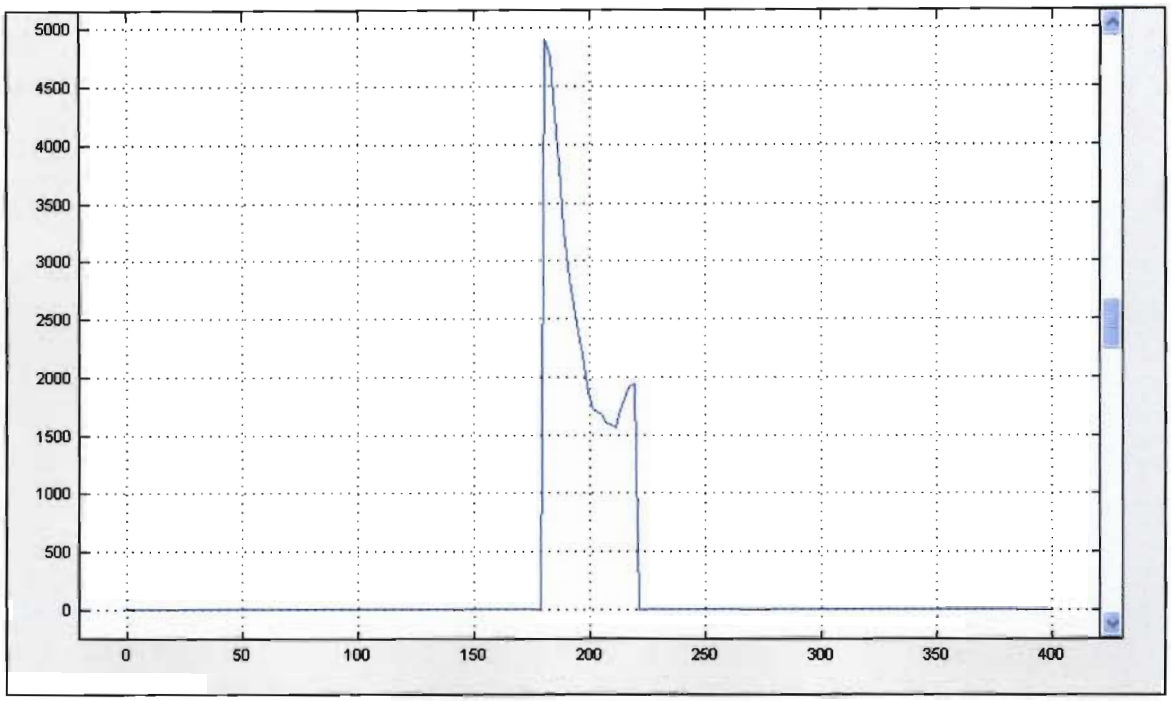

Figure 6.7 Electric field Flat rod gap with earth plane

It is generally accepted that in order for a grounded object not to affect the performance of a rod – rod gap, it should be at least 2.5d away. This is not the case, as was revealed with the multitude of laboratory tests done. The gap between the earth plane and the rod gap was increased by 12 times (12d) rod diameter and the earth plane effects were still noticeable. Attempts were made in order to find a suitable distance using the FEMLAB simulation but for gaps larger than 3D, the software was ineffective.

6.7 Determining Breakdown Voltage of the Rod – Rod Gaps

In order to determine the breakdown voltage of each rod – rod gap, the field line values obtained from the FEMLAB output file were iterated across the gap. A Matlab m-file was created in order to simplify the calculation of breakdown voltages. The iterations were used to find the breakdown voltage by comparing values at STD obtained from the simulation and normalizing using the $\alpha\eta$ curves shown in Appendix D. The code is detailed in Appendix D2.

6.8 Matlab Algorithm to solve the M-file for breakdown

- Input the applied voltage, V applied, ie. The voltage at which the Femlab simulation was performed.
- Input the rod – rod gap length in mm, d.
- Determine the distance to the centre of the first 2 regions of integration, a and b. (assume symmetry)
- Input the electric field at distance a and b in V/mm, Ea and Eb. (read from ASCII data captured from Femlab Electric Field Line Plot)
- Input pressure in bar, p.
- Convert all data to standard units.
- Define regions of α/p and η/p curves (Appendix C: α/p and η/p curves).
- Perform iteration until streamer criteria is met.

The accuracy of the calculation is dependent on the assumption that the electric field across the rod – rod gaps were perfectly symmetrical. Where it was apparent that the electric fields were not symmetrical, the Matlab m-file was altered to compensate for this fact and therefore still produce a viable approximation

6.9 Results of the FEMLAB Simulation for Breakdown Voltages

Table 6.1 FEMLAB No earth plane Simulation Breakdown Voltages

Rod Diameter mm	Rod Gap mm	Gap Interface configuration	FEMLAB Simulation Breakdown Voltage no Earth Plane kV
10	40	Flat	108
10	50	Flat	132
10	60	Flat	182
20	40	Flat	98
20	50	Flat	104
20	60	Flat	153
20	40	Hemispherical	115
20	50	Hemispherical	135
20	60	Hemispherical	181

The data in table 6.1 is a summary of the simulation values obtained from the FEMLAB software. Chapter 7 discusses the data in detail

Table 6.2 FEMLAB With earth plane Simulation Breakdown Voltages

Rod Diameter [mm]	The Spark Gap size [mm]	Tip Geometry	Earth Plane Distance when tested [kV]	Simulated Break Down Values with Earth plane [kV]
20	40	Flat	100	94
20	40	Flat	100	94
10	40	Flat	200	95
20	40	Flat	200	96
10	40	Flat	90	98
10	40	Flat	100	99
20	50	Flat	125	100
20	50	Flat	225	107
20	50	Flat	85	112
20	60	Flat	225	109
20	60	Flat	90	108
20	60	Flat	125	108
20	60	Hemispherical	90	117
20	60	Hemispherical	125	120
20	60	Hemispherical	225	125
10	60	Flat	250	183
10	60	Flat	150	186
10	60	Flat	110	140

The data in table 6.2 is a summary of the simulation values obtained from the FEMLAB software

6.10 Concluding remarks

The analysis of the results provided in table 6.1 and 6.2 is dealt with in detail in chapter 7. The various graphs show the break down voltage values with an input impulse wave of 1.2/50 μs and the relationship that the voltages have with gap variation as well as the influence of a nearby earth plane is analysed and concluded on.

CHAPTER 7 RESULTS AND DISCUSSIONS

7.1 Laboratory Set Up

7.1.1 Method Used To Apply the Impulse Voltage to the Gaps

The laboratory impulse generator has eight stages with each capacitor C_1 rated at 50 nF and 125 kV. The equivalent circuit is as shown in Fig 7.0 below. The load capacitor C_2 is at 1000 pF. A series resistor R_s is used between the source and the gap to limit the breakdown current and to provide some damping of the high frequency oscillations. The resistance is typically between 100 to 1000 kΩ for AC or DC voltages, and no more than 500 Ω for impulse voltages in the circuit

C_1	=	50 nF	Capacitance of the generator
C_2	=	1000 pF	Capacitance of the Load
R_s	=	100 -1000 kΩ	Charging resistors
G	=	20mm to 50mm	Impulse generator spark gap
R_1, R_2			wave shaping resistors
D			Rod gap spacing under test

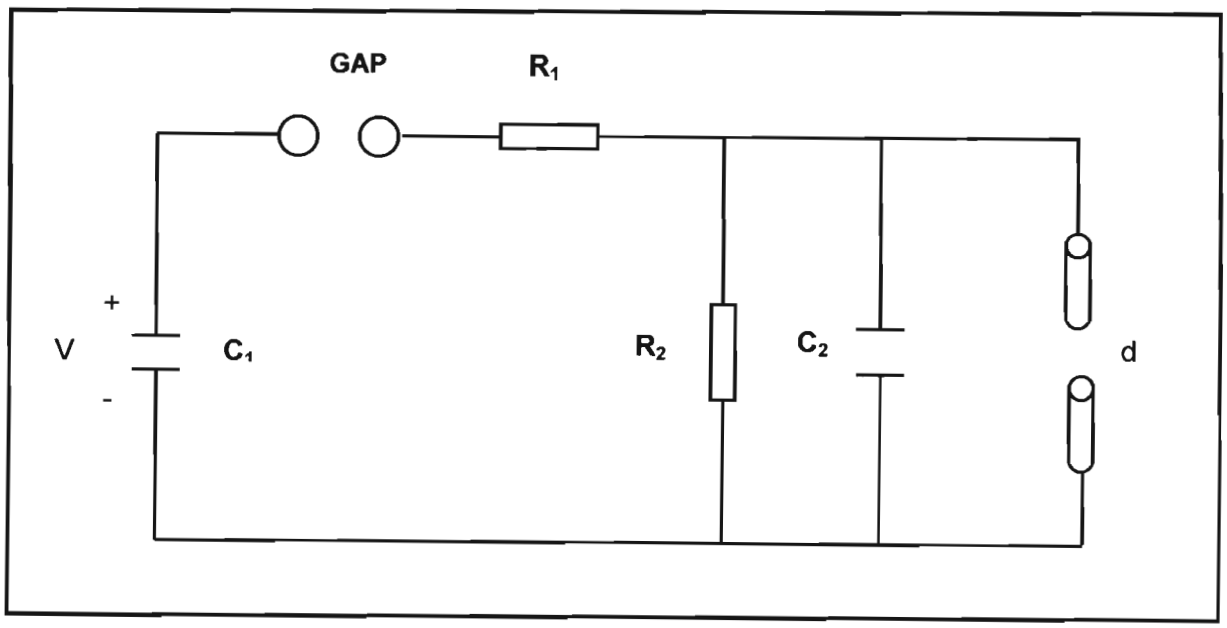

Figure 7.0 **Equivalent Marx circuit arrangement for Impulse generator**

For the spark gap tests a *positive polarity voltage* with wave shape 1.2/50 μs impulse was used to flash the rod gaps. The laboratory results were then normalized for pressure, temperature and humidity using the Alhpa-Neta curves at 760 torr and 20^0 C. For impulse tests the 50 shot up and down test were utilised. The rod gap tests were done using mild steel rods mounted on adjustable steel brackets. The earth plane effects were simulated by placing a metal sheet on an insulated stand in the vertical plane parallel to the set of vertical rods. The gap settings were spaced using a tape measure in mm. No readings were captured for the breakdown times; hence no analysis is available for timing of the breakdown voltage.

7.1.2 Test Specimens Used In the Laboratory Tests

The calibration results for various sphere gaps obtained in the literature review were used to hypothesize a corresponding range of rod specifications that have breakdown voltages within the protective margin as calculated in chapter 3.4. The most suitable range was determined to be within 96 kV to 144 kV. The corresponding rod specification range based on Qureshi [30] and sphere gap calibration values from Rogowski [31] was determined to be between 5mm to 20mm in diameter and gaps of lengths 30mm to 60mm would produce break down values in the 96 kV to 144 kV range. Hence, two rods with diameter dimensions of D =10mm and D = 20mm were selected for the experiments. Both the rods were of mild steel and were ground off to produce a hemispherical tip as in Figure 7.1 and flat cut edge as in Figure 7.2. The rods were not smoothed for practical reasons so as to cater for the worst case conditions that would generally occur during manufacturing or surface erosion when installed. The rough surface would generally result in a non-uniform field which is representative of practical manufacturing processes, Naidu [26].

Figure 7.1 hemispherical rod, D = 20mm

Figure 7.2 Flat rod, D= 20mm

7.2 The Results Expected for Gap Performance

The previous chapters have provided the theory on the breakdown mechanisms and factors influencing non-uniform breakdown. The effects of materials and lightning effects of reflected waves on transformer windings were also discussed. This chapter is based on the theory of previous chapters and references will be made were the theory is to be adopted.

7.3 Analysis of the Simulation and Laboratory Results

The results for the two rods sizes 10mm and 20 mm diameter are compared with the aim of choosing a rod geometry (Hemispherical or Flat) and gap (40mm, 50mm, 60mm) that will breakdown within the theoretical range 96 kV to 120 kV at sea-level conditions. It is critical that the $V_{10\%}$ value is less than 120 kV as well. Selecting the smaller breakdown value in the range will provide a buffer band and may result in nuisance tripping which is preferred over plant damage. The maximum values achievable are discussed in chapter 3.4.

7.4 Analysis of the effects of an earth plane

Both Naidu [26] and Kuffel [23] describe the effects of a nearby earth plane. The experiments conducted by Kuffel however were based on 5mm to 1m sphere gaps with rods of diameter 50mm. This thesis is limited to using rods without spheres and gaps ranging from 40mm to 60mm Naidu [26]. Thus there are no experimental values available to compare an earth planes influence on breakdown voltage for rod gaps.

7.5 Approach for the Analysis

The laboratory tests and the simulation results were analysed to confirm that the simulation software produces breakdown values that approximately align but as expected will not be exactly the same as the laboratory values. A comparison of the simulated results against the laboratory derived results will be done for the two rod sizes 10mm and 20 mm and the three gap sizes tested ie 40mm, 50mm, and 60mm. For choice of diameter, this means 10mm verses 20mm rod, a 10mm rod with 40mm, 50mm and 60mm gap will be compared with a 20mm rod with 40mm, 50mm and 60 mm gap

respectively. The next step was to determine the nearby earth plane effects on the break down voltage. Each rod was tested under the influence of an earth plane for both the 10mm and 20 mm was compared with each other for the three gap sizes tested ie 40mm, 50mm, 60mm. The results were then based on the analysis of the above findings and previous chapters. The thesis was concluded by recommending the most appropriate rod diameter and gap size suited for the scope required. The plant risks associated and the effects of pollution will be considered when choosing the suitable diameter and gap in chapter 8

Table 7.1 *Simualted* $V_{50\%}$ values and standard deviation for rod gaps

Rod Diameter [mm]	Rod Gap [mm]	Earth Plane influence	Tip Shape	Standard Deviation of $V_{50\%}$ [kV]	Average Break Down Voltage corrected to STP [kV]
10	40		Flat	1.5	95
10	50		Flat	3.6	112
10	60		Flat	2.5	127
20	40		Flat	2.6	93
20	50		Hemispherical	0.6	107
20	50	Yes	Hemispherical	0	110
20	60		Flat	1.7	110
20	60	Yes	Flat	1.2	111
20	60		Flat	15	126
20	60	Yes	Flat	1.2	115

Table 7.1 shows results of the simulation conducted in FEMLAB. The average standard deviation for the battery of each result was calculated and ranges between 1.5 to 4kV. Therefore, when comparing results for higher or lower breakdown values, only differences larger than 4 kV will be taken as a variance between values as there is always some scatter expected as seen in Table 7.1 above for the hemispherical tip having a standard deviation of zero.

Table 7.2 *Laboratory* Breakdown Voltage tests – With earth plane

Rod Diameter [mm]	The Spark Gap size [mm]	Rod type Flat/Round	Earth Plane Distance when tested [mm]	U50 [kV]	U10 [kV]
10	40	Flat	200	95	79
10	40	Flat	90	95	79
10	40	Flat	100	96	76
20	50	Flat	125	107	83
20	50	Flat	225	108	84
20	60	Flat	225	109	88
20	50	Flat	85	110	90
20	60	Flat	90	111	87
10	50	Flat	125	113	95
20	60	Flat	125	113	99
10	50	Flat	110	114	88
10	50	Flat	225	115	105
20	60	Round	90	115	92
20	60	Round	125	117	97
20	60	Round	225	118	108
10	60	Flat	250	127	95
10	60	Flat	150	130	110
10	60	Flat	110	137	121

Where, $U10 = U50 - 1.3\sigma$, also the implied value of σ is rather large

Table 7.3 *Laboratory* Breakdown Voltage tests – no earth plane

Rod Diameter [mm]	The Spark Gap size [mm]	Rod type Flat/Round	U50 [kV]	U10 [kV]
10	40	Flat	93	84
10	40	Round	96	76
10	50	Round	103	85
20	50	Flat	107	74
10	50	Flat	108	97
20	60	Flat	112	92
20	40	Round	120	111
10	60	Flat	125	121
20	50	Round	125	104
10	60	Round	126	99
20	60	Round	144	111

Table 7.2 and 7.3 show the *positive polarity* breakdown voltage results from the 50 shot test achieved in the laboratory. The results are shown with and without earth plane influence respectively.

7.6 Comparison of the laboratory and simulation Tests

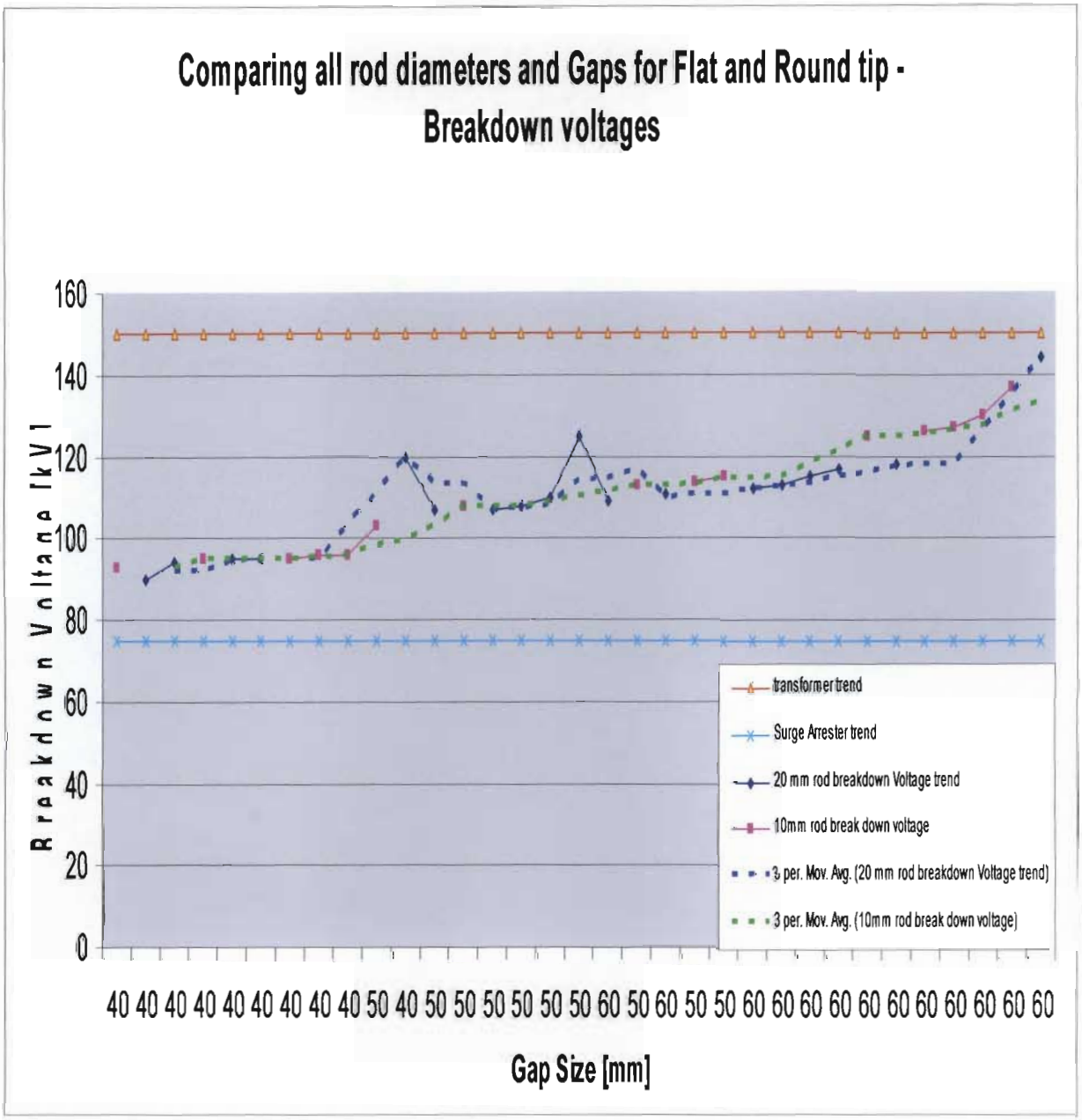

Figure 7.3 Comparison of All parameters versus breakdown Voltages U10/U50

Figure 7.3 above shows that with the chosen geometries and gap ranges the lowest breakdown voltage achievable is 85 kV and the highest achievable is 145 kV, which for the purposes of this thesis are within the range 96 kV to 120 kV required to select the optimal gap as discussed in Chapter 3.4.

7.7 Laboratory for 10mm Flat Vs round + Earth Plane

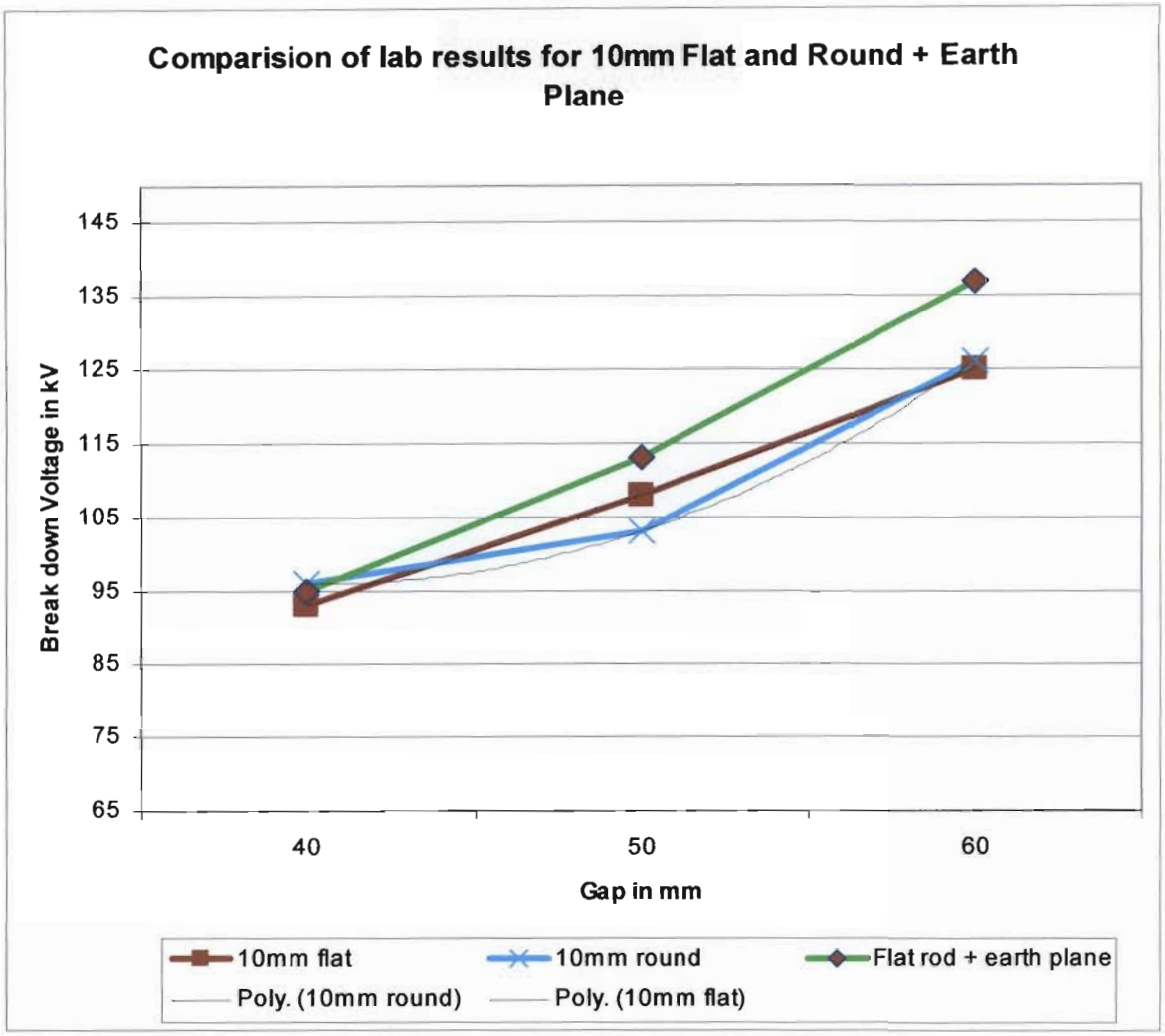

Figure 7.4 Laboratory results for 10mm Flat Vs Round + Earth Plane

Figure 7.4 show that the flat and hemispherical rods have a linear characteristic over the range of values tested. Both geometries have no advantages over each other in this set of results as the average linear values coincide. Note, a peculiar result for the earth plane influence, ie the result has a higher breakdown voltage than is expected. The earth plane generally results in lower breakdown values, Kuffel [23].

A) The 10mm flat and round rods are only suitable with the 40mm and 50mm gaps even with the earth plane influence.

B) The higher breakdown influence of the earth plane can result in the breakdown voltages being at higher values in the 50mm gap thus operating outside the chosen range

SIMULATED RESULTS VS LABORATORY FOR 10MM FLAT + EP

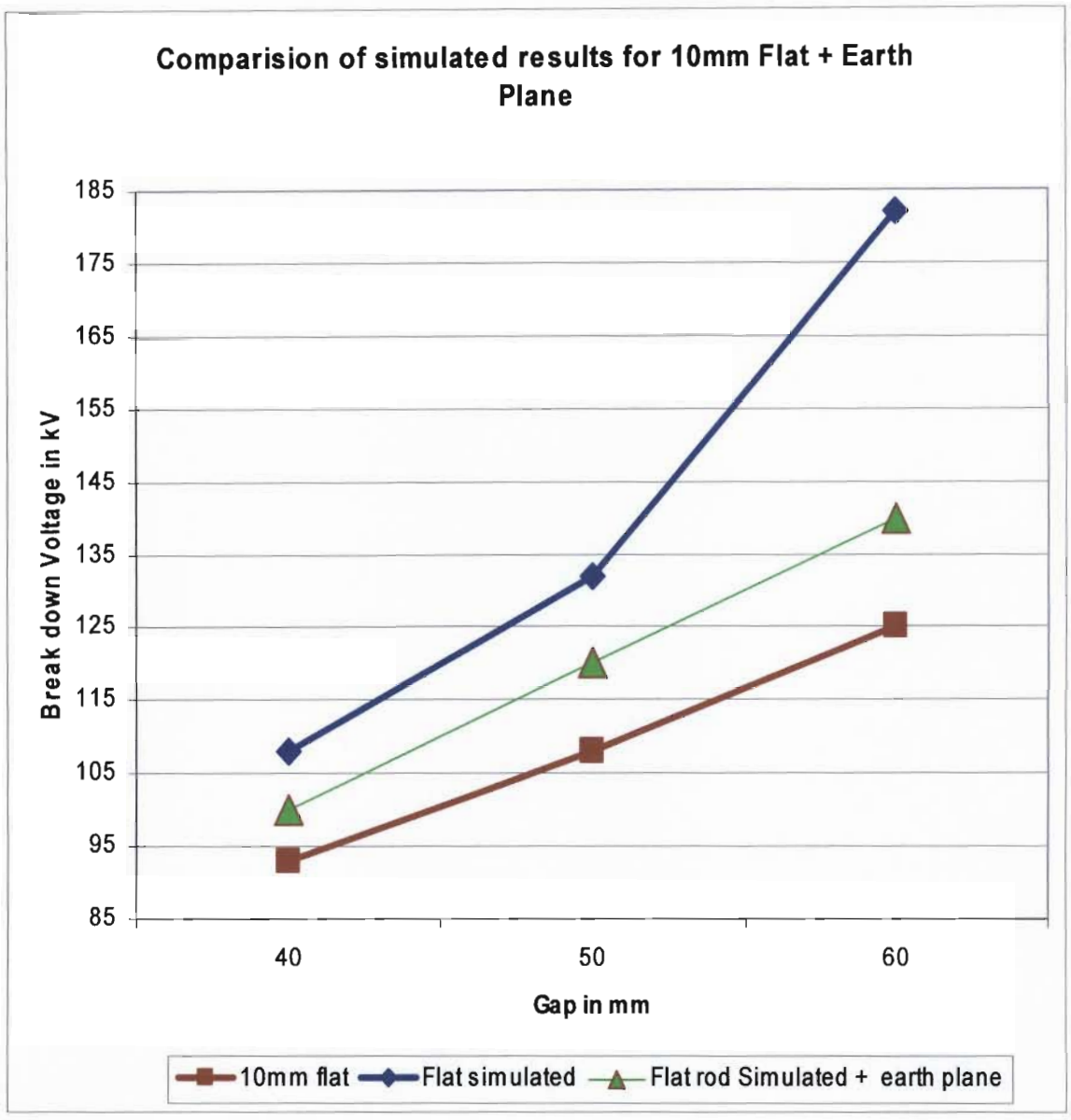

Figure 7.5 Simulated results Vs Laboratory results for 10mm flat + Earth Plane

Figure 7.5 above shows the simulated results are consistent and have an average delta V_b of approximately 10 %. The simulated earth plane result conforms to Kuffel [23] ie the breakdown voltage of the gap with earth plane influences are lower.

a) The flat 10mm rod is only suitable with a 40mm gap, even with earth plane influence.

7.8 Simulated results Vs Laboratory for 10mm round + EP

Figure 7.6 Simulated results Vs Laboratory for 10mm round + earth Plane

Figure 7.6 above shows the simulated results are consistent and have an average delta V_b of approximately 12 %. The breakdown voltages are higher and do not conform to Kuffel [23].

a) The increased earth plane breakdown voltage results however tends to indicate that rods with smaller diameters tend to breakdown at higher voltages when influenced by earth planes.
b) The round 10mm rod is only suitable with a 40mm gap.

7.9 Laboratory results 20mm Flat Vs Round Rod + Earth Plane

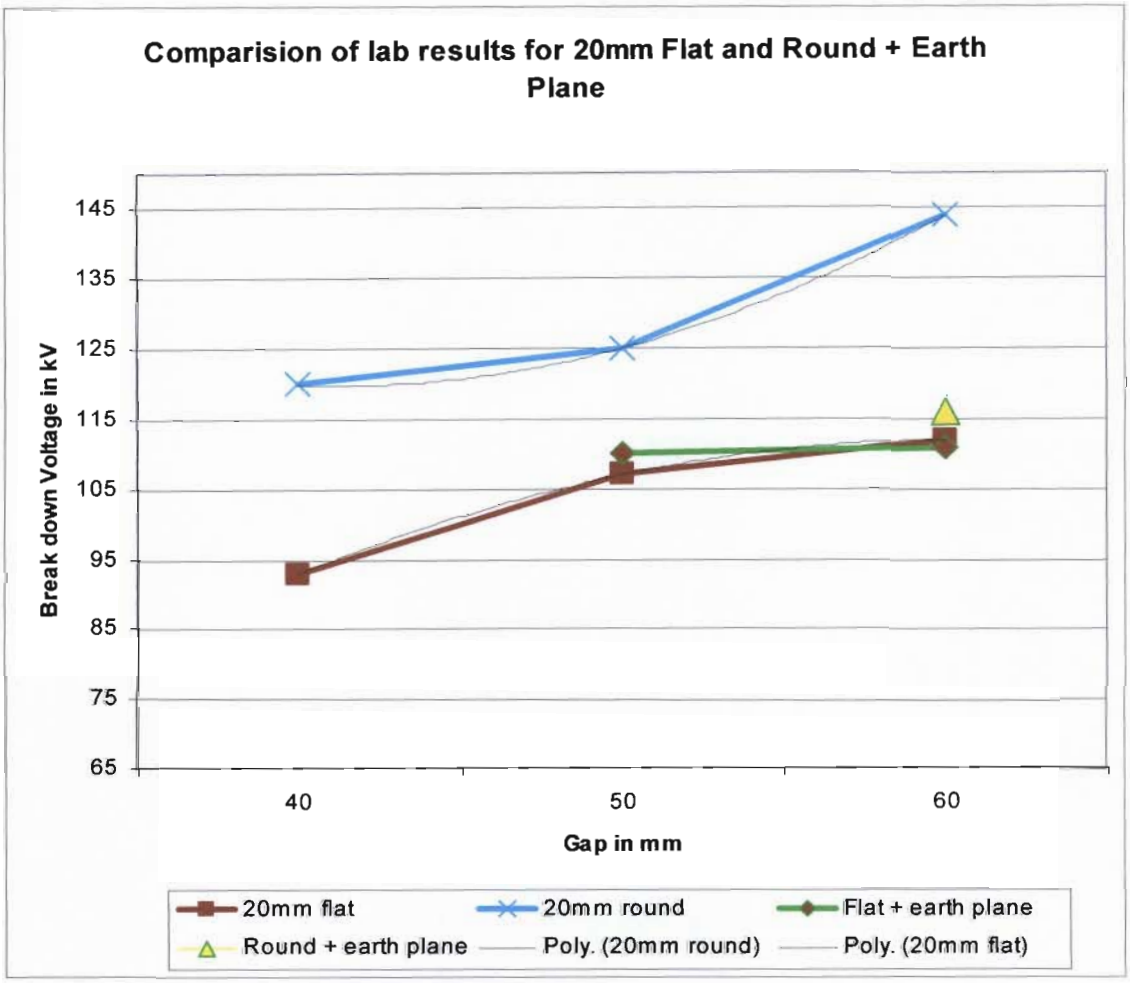

Figure 7.7 Laboratory results 20mm Flat Vs round + Earth Plane

The laboratory results in figure 7.7 above for the 20mm round and cut show a distinct performance variance of delta V = 15 %. The results are consistent for the range of values tested. The results show that earth-plane influence has not produced a lower breakdown values but a neutral one

a) The 20mm round rod is not suitable for gap sizes 50mm and 60mm mm and as the breakdown values are far out of the range required, these shall be excluded.

b) The Flat rod has two gaps sizes 50mm and 60mm within the required constraints, including the increased breakdown voltage due to earth plane influence.

7.10 Simulation Vs Laboratory for 20mm Flat Rod + earth Plane

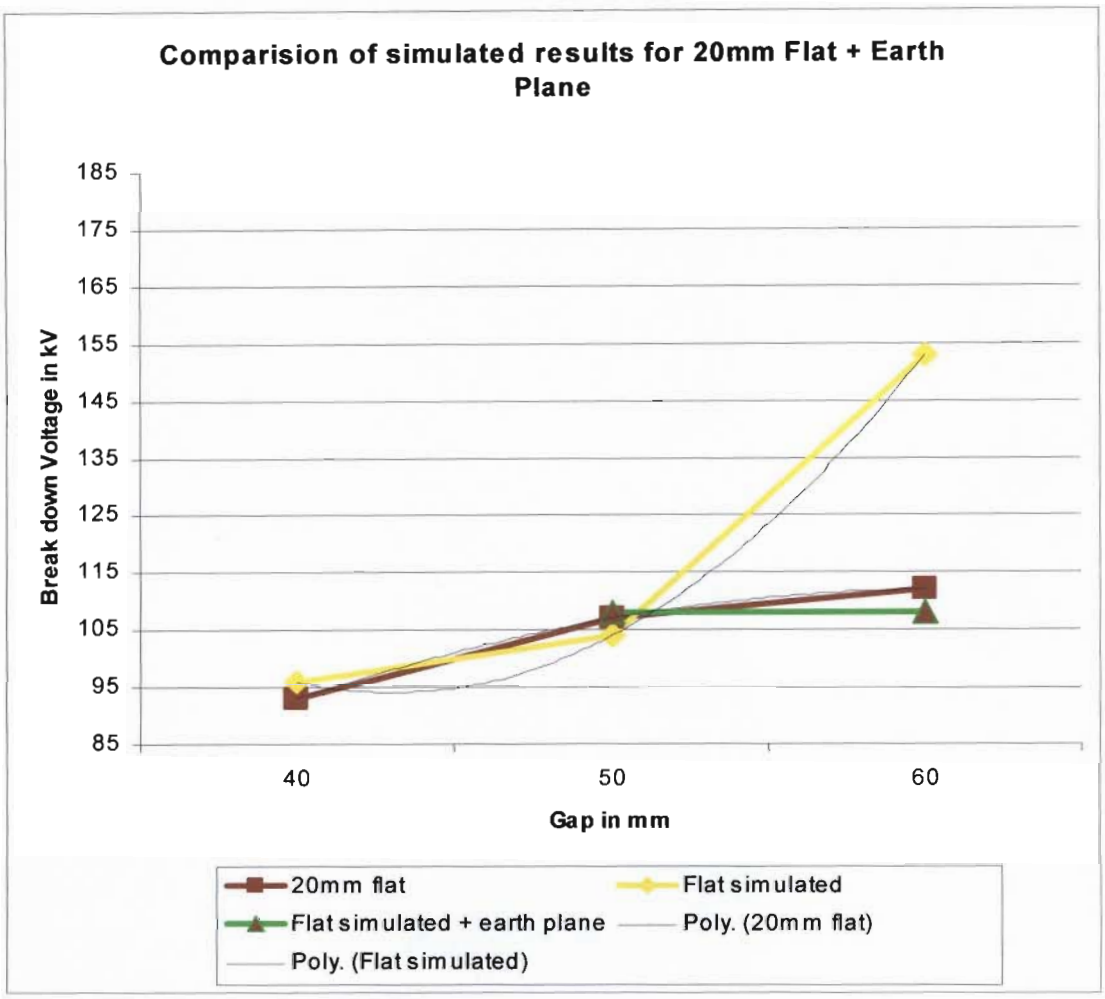

Figure 7.8 Simulated Vs laboratory for 20mm Flat + Earth Plane

The laboratory and simulated values in figure 7.8 above agree for the 40mm and 50mm gaps, including the influence of the earth plane. The 60mm gap has a significant deviation of delta V_b = 30 % between the simulated and laboratory tests. The earth plane values are lower than the tests without earth plane influence.

a) The 20mm rod, with 40 mm and 50mm gap are both within the suitable range, and can be considered.
b) The 20mm flat with a 60mm gap shall be excluded.
c) The earth plane breakdown is lower than expected.

7.11 Simulated Vs Laboratory for 20mm Round Rod + Earth Plane

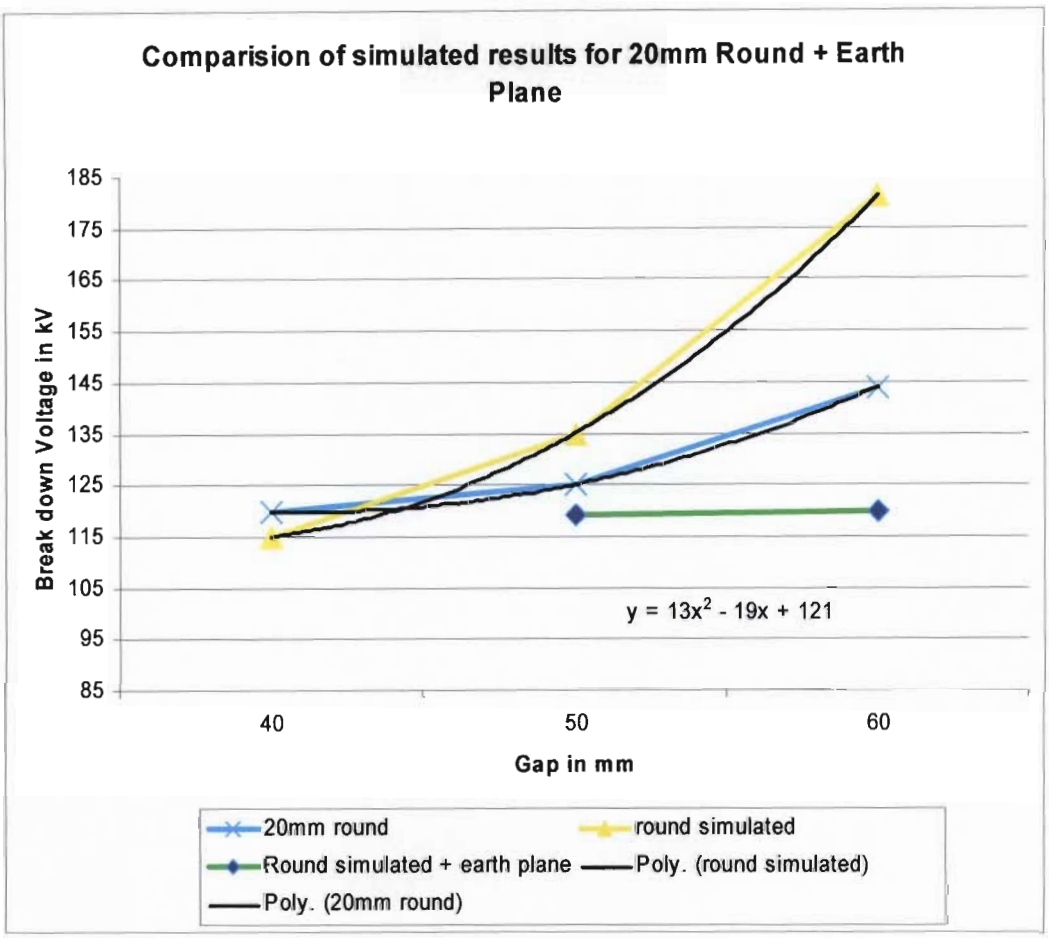

Figure 7.9 Simulated Vs Laboratory for 20mm Round rod + Earth Plane

The laboratory and simulated values in figure 7.9 above agree for the 40mm gap, including the influence of the earth plane. There is a marked divergence for the 50mm and 60mm gap. The simulated earth plane values are distinctly lower for the round rod.

a) The results shown here provide confidence only for the 20mm round rod with a 40mm gap that agrees with Kuffel [23], ie lower breakdown when in earth plane influence.
b) The range within which all the gap operates is between 114 kV and 124 kV. These values fall outside the suitable range selected; hence it certainly indicates that the 20mm round rod cannot be a choice.

7.12 Laboratory results 10mm Vs 20mm Flat rod + Earth plane

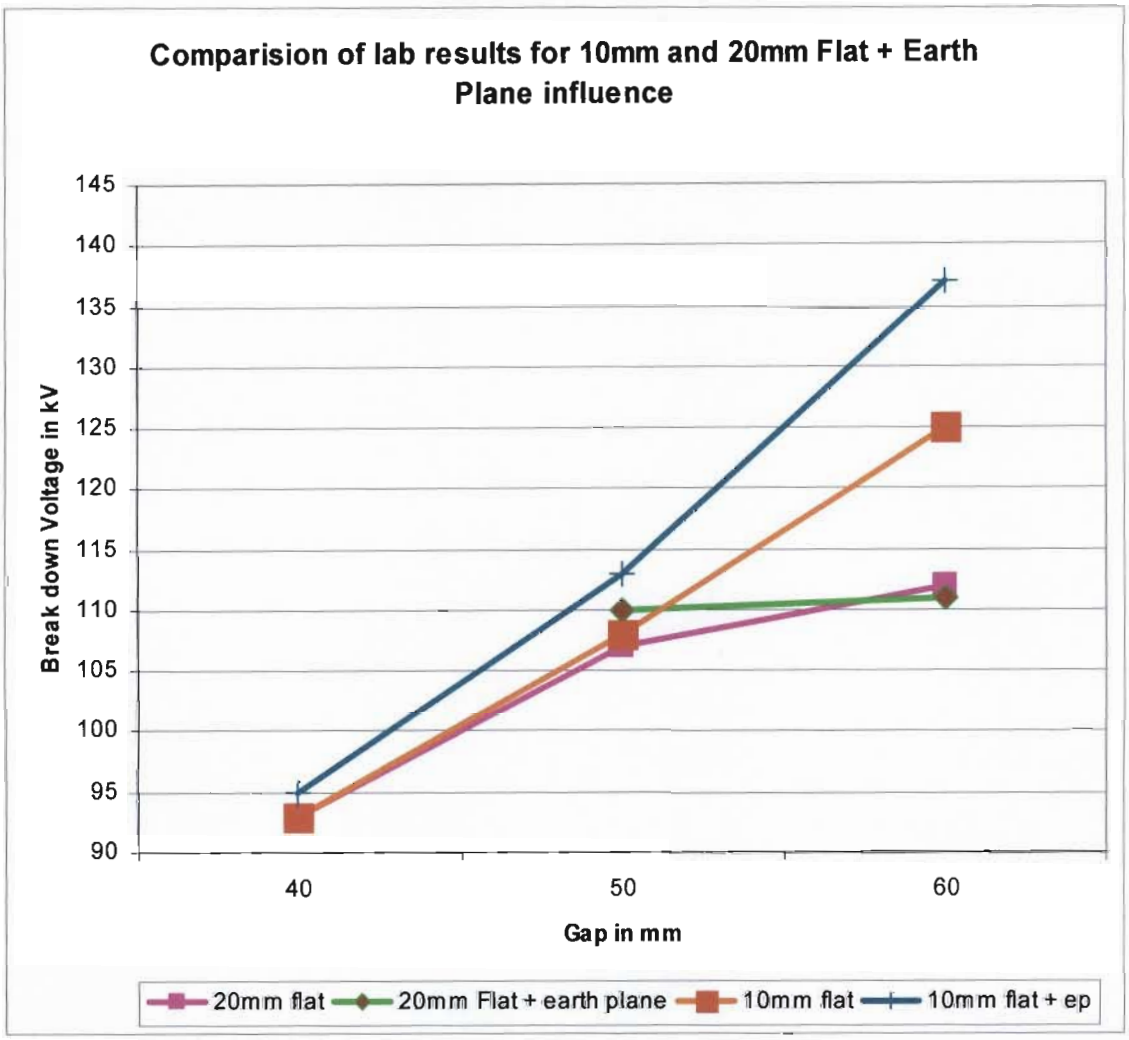

Figure 7.10Laboratory results 10mm Vs 20mm Flat rod + Earth Plane

The laboratory and simulated values in figure 7.10 above for the 10mm and 20mm rods coincide in breakdown voltage for the 40mm and 50mm gaps, including the influence of the earth plane. There is a marked divergence between the two rod diameters for the 60mm gap.

a) When comparing the 10mm flat rods to the 20mm flat rod and earth plane influences, the 20mm Flat rod is more suitable for the range required, as seen even with the earth plane influence, the breakdown voltages are suitable.
b) The simulated earth plane values are lower for the round rod.
c) The flat rod earth plane values are higher; hence the 10mm flat is not suitable.

7.13 Laboratory results 10mm Vs 20mm Round rod + Earth plane

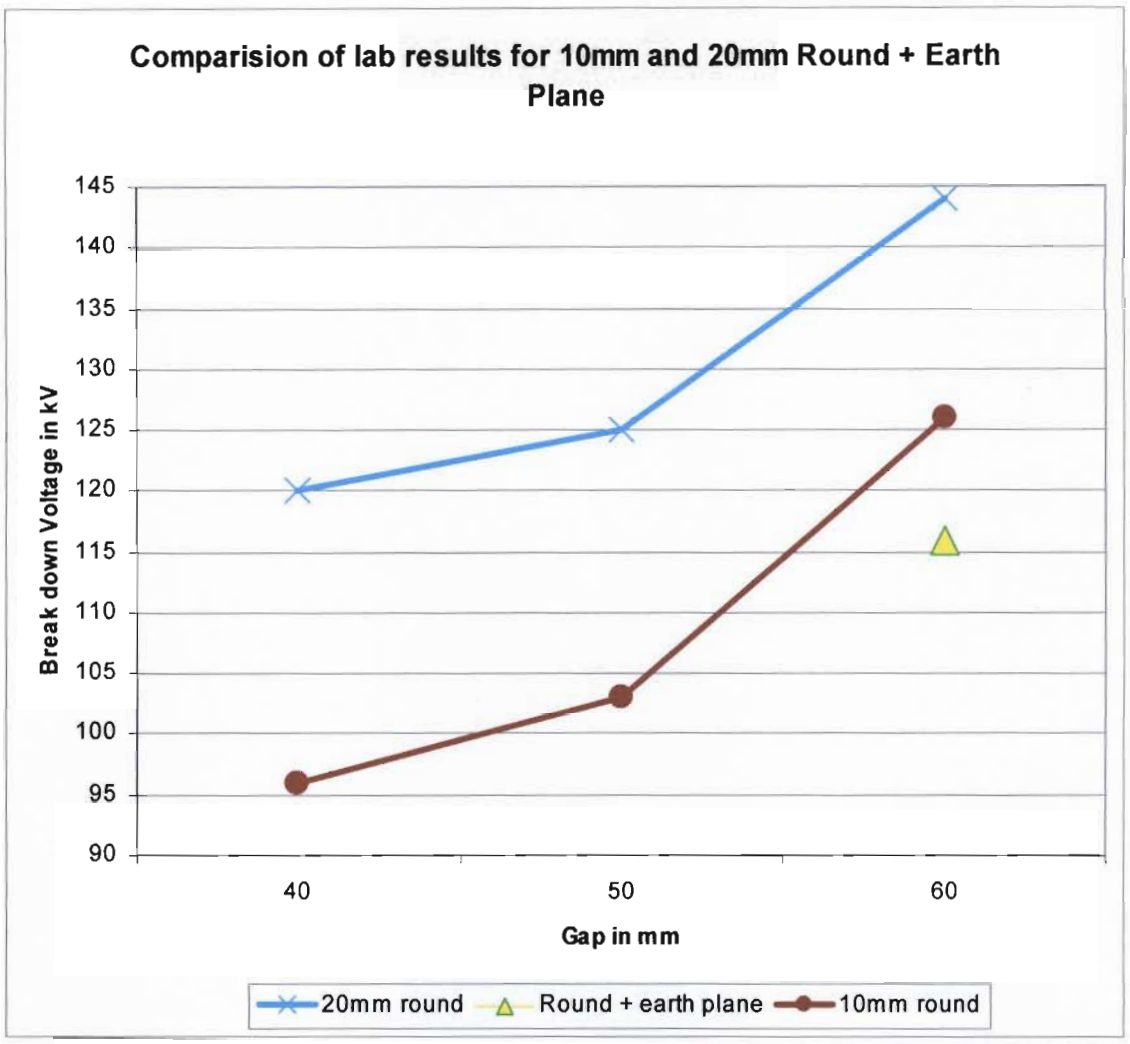

Figure 7.11 Laboratory results 10mm Vs 20mm Round rod + Earth Plane

The laboratory results in figure 7.11 above for the 10mm and 20mm round rods show a distinct performance variance of delta V_b = 20 % across the range. The results are consistent for the range of values tested. The results show that earth-plane influence has produced a lower breakdown value

a) The 20mm round rod is not suitable for all gap sizes as the breakdown values are far out of the range required, these shall be excluded.
b) The Flat 10mm rod has two gaps sizes 40mm and 50mm within the required constraints, including the increased breakdown voltage due to earth plane influence.

7.15 Calibration values of Breakdown Results from Various Sources

Table 7.4a Summary Of All The Voltage Breakdown Values For The Rod Gaps

Rod Diameter [mm]	The Spark Gap size [mm]	Flat Round	Earth Plane Distance when tested [mm]	The value for the 2.5d	U50 [kV]	U10 [kV]	σ
20	40	Flat	100	100	90	86	3
10	40	Flat	0	100	93	84	7
20	40	Flat	100	100	94	75	15
10	40	Flat	200	100	95	79	12
20	40	Flat	200	100	95	74	16
20	40	Flat	0	0	95	76	14
10	40	Flat	90	100	95	79	12
10	***40***	***Flat***	***100***	***100***	***96***	***76***	***15***
10	***40***	***Round***	***0***	***100***	***96***	***76***	***15***
10	***50***	***Round***	***0***	***125***	***103***	***85***	***14***
20	***50***	***Flat***	***125***	***125***	***107***	***83***	***19***
20	***50***	***Flat***	***0***	***0***	***107***	***74***	***25***
10	***50***	***Flat***	***0***	***0***	***108***	***97***	***8***
20	***50***	***Flat***	***225***	***125***	***108***	***84***	***18***
20	***60***	***Flat***	***225***	***150***	***109***	***88***	***16***
20	***50***	***Flat***	***85***	***125***	***110***	***90***	***15***
20	***60***	***Flat***	***90***	***150***	***111***	***87***	***18***
20	***60***	***Flat***	***0***	***150***	***112***	***92***	***16***
10	***50***	***Flat***	***125***	***125***	***113***	***95***	***14***
20	***60***	***Flat***	***125***	***150***	***113***	***99***	***11***
10	***50***	***Flat***	***110***	***125***	***114***	***88***	***20***
10	***50***	***Flat***	***225***	***125***	***115***	***105***	***7***
20	***60***	***Round***	***90***	***150***	***115***	***92***	***18***
20	***60***	***Round***	***125***	***150***	***117***	***97***	***15***
20	***60***	***Round***	***225***	***150***	***118***	***108***	***8***
20	***40***	***Round***	***0***	***100***	***120***	***111***	***7***
10	60	Flat	0	150	125	121	3
20	50	Round	0	125	125	104	16
10	60	Round	0	150	126	99	21
10	60	Flat	250	150	127	95	25
10	60	Flat	150	150	130	110	15
10	60	Flat	110	150	137	121	12
20	60	Round	0	150	144	111	26

$$\sigma = 1.62 \times V_{ave}(nB - A^2)/n^2) + 0.029))$$

$$U_{50\%} = V_0 + V_{ave}(A/n + 0.5)$$

$$U_{10\%} = U_{50\%} + 1.3\sigma$$

Table 7.4b Breakdown Values Various Sources With Sphere Gaps

Configuration Round/Flat Diameter [mm]	Theoretical Femlab results Voltage Breakdown values [kV]	From references in text, Voltage breakdown values [kV]	From references in text Voltage breakdown values [kV]	Lab results no- earth Plane Voltage breakdown values [kV]	Lab results with-earth plane break down values [kV]
Flat, D = 10mm					
d = 40mm	108			93-96	95
d = 50mm	132			108-115	125
d = 60mm	182			125-130	137
Flat, D = 20mm					
d = 40mm	104			90-95	
d = 50mm	98			107-108	110
d = 60mm	153			109-112	150
Hemispherical, D = 20mm		Grounded spheres used	Un-grounded spheres		
d = 40mm	115	106-110	107-132	120	
d = 50mm	135	123-136	128-137	125	
d = 60mm	181	181-199	177-214	118-144	115-117

The complete battery of breakdown voltage tests are shown in Table 7.4a and the calibration breakdown voltage values tabulated in table 7.4b have been taken from various sources including Naidu [26], Kuffel [23], Rogowski [31]. The values are tabulated against the values obtained from the laboratory and simulation exercise. The values listed reveal that there is a fairly consistent trend in the values obtained by simulation and laboratory work. The differences are easily attributed to the fact that most calibration tests are done using large spheres with close to uniform gaps. Despite this, there is a fair amount of correlation between the results obtained and those from the literature. Another comparison that is supported by the work done by Qureshi [30] using rod gaps at medium voltage.

The slight differences are also contributed by having too many variables like the pressure, temperature, rod material that are all inherent in gap. As discussed in chapter 3, the breakdown values for air gaps are scattered and values do vary between tests dependant on the factors that influence breakdown.

7.16 Concluding remarks

To ensure that the breakdown occurs within the suitable range ie between 96 kV to 120 kV and the influence of the earth plane is accommodated, the following combinations of rods and gaps are acceptable

a) A 10mm round or flat with a 40mm gap
b) A 20mm round with a 40mm gap
c) A 20mm flat with a 40mm or 50 mm gap.

CHAPTER 8 CONCLUSION

A comparison of experimental results for rod gaps from different labs is quite difficult, because they are influenced by a wide range of parameters like electrode material, surface finish, surface area, conditioning state of the surface and the geometry of the electrode arrangement. The aim of this thesis is to find a simulated solution supported with laboratory tests and a relation between the breakdown voltage and different electrodes parameters. The results obtained via simulation and laboratory test have been compared with bench mark calibration values from various literature and the percentage variances reported in Chapter 7.15

The breakdown voltages and the performance of rod gaps were studied by evaluating the 50 % breakdown voltage $V_{50\%}$ for gap sizes of 40mm, 50mm and 60mm and for rod diameters of 10mm and 20 mm. The volt-time (V-t) curves, average breakdown times corresponding to $V_{50\%}$, and scatters in breakdown voltage and breakdown times were not included in the laboratory experiments. To understand and compliment the laboratory results detailed theory is discussed in previous chapters. The breakdown voltage is influenced by the voltage polarity, gap length, the surface finish. The presence of the dust film or moisture on electrodes or of air borne pollution does not influence significantly, gaps smaller than 60 mm hence the work done by Qureshi [30], can be used as a further bench mark.

The results have been analysed with emphasis on the effect of rod end shape and rod gap size as well as performance of the gaps in the presents of a nearby earth plane using single gaps. Multiple gaps were not considered for laboratory tests. For protective gaps, the rod end profile, its radius, gap length and gap configuration (single or multiple gaps, and horizontal or vertical gaps), are the main design parameters. For rod gaps which have to operate outdoors in areas frequently subjected to atmospheric dust pollution, the choice should be of geometric influenced by dust pollution so as to have

reliable performance under all atmospheric conditions. Since, the dust pollution has similar effect for single or multiple gaps as well as for horizontal and vertical gaps, the main design parameters are the rod radius, its end profile and gap length.

From the results in Chapter 7, a conclusion can be drawn that rods with cut ends and smaller diameter are preferred since these offer immunity towards dust pollution related influences, Qureshi [30]. Therefore, the selected rod radius should be as small as possible to minimize the pollution effect on the gaps performance. The 10mm diameter rod is thus the most suitable for this purpose. A smaller size will not only be non-standard manufacture size but also it should not be so small that the gap is always coronating under normal AC voltage. For 12 kV systems, rod as small as 4~5 mm^2 in diameter have been successful and can be used with confidence from a corona point of view, Qureshi [30]. For higher voltage systems, the radius could be increased. As corrosion is a factor that should be considered, the 10mm was preferred as oppose to smaller diameters.

Dust films that adhere to electrodes are the main controlling factors that change the breakdown voltage. The pollution effects on the breakdown values decreases with the increase in gap spacing. Gaps exceeding 60mm have a more severe affect when polluted as compared with gaps between 6mm to 60mm. Polluted gap operates in much shorter time due to the effect of atmospheric pollution. The vertical gaps break down values of $V_{50\%}$ increases almost linearly for gaps larger than 40mm and with spacing of less than 40 mm the trend is nonlinear, thus the 40mm was the smallest gap size considered and 60mm the largest size considered, Qureshi [30].

The smaller than 40mm gap, in the presence of dust pollution can cause unnecessary interruptions of supply due to the sensitivity of adjustment. Similarly under negative polarity, the gaps in the range of (2 × 40mm) to (2 × 60 mm) can exhibit poor insulation co-ordination as they will operate at a voltage level which is 10 kV to 205 kV or higher

than anticipated. Although this is the case a gap larger than 60mm will result in a breakdown that was above the protective level required for the transformer.

The shape was selected based on Qureshi [30], findings that flat rods or cut ends and smaller diameters are to be preferred in areas with high pollution since these offer immunity towards pollution related influences. The second reason for the flat rod was that due to the smaller diameter of 10mm, the earth plane influences and the breakdown did not vary significantly from that of the 20mm rod or that of the hemispherical rod. The other consideration was the practicality of a cut end or flat rod was the simplicity to manufacture and maintain. Rods damaged in the field due to corrosion or spark erosion can be easily maintained by simply square cut-off and adjusting the gap sets to the required gap.

Selection of Protective Gap

Since, the dust pollution has similar effect for single or multiple gaps as well as for horizontal and vertical gaps, the main design parameters are the rod radius, its end profile and gap length. From these results, it can be concluded that rods with cut ends and smaller diameter are preferred since these offer immunity towards dust pollution related influences. Therefore, the selected rod radius should be as small as possible to minimize the pollution effect on the gaps performance. At 11kV and 22 kV gaps larger than 4~5 mm^2 in diameter must be used with confidence from corona point of view. For higher voltage systems, the radius could be increased.

The most optimal rod that is able to comfortably meet the grading requirements is a 10mm mild steel flat rod with a 50mm gap.

The final statements are that of caution, that the surge arrester technology is by far the best method for surge control and dissipation. The use of spark gaps to protect transformers is a solution that should be considered as a last resort and as an exception. There is no suitable spark gap substitute for surge arresters. Field staffs are to monitor transformers and change out arresters as soon as possible.

REFERENCES

1. Anderson R. B. and Eriksson A. J. (1980): "Lightning parameters for engineering application", Electra No.69, CIGRE, pp 65-101.
2. Britten A. C. (1992): "Insulation Co-ordination of Lines", Chapter 8, Eskom and CSIR Course Handouts.
3. Burger N. (1998): "Report on the failure of distribution transformers in the Southern Region", Eskom Report, Southern Region.
4. Chatterton B. G. (1999): "Revised Distribution transformer cost analysis and network performance index impact", Eskom Project Report.
5. Chatterton B. G., Geldenhuys H. J., Ferguson I., Stephen R. G. and Hoch D. A. (1999): "Distribution pole mounted transformer failure project 1999 short report, CIGRE/CIRED Working Group 33-01, Eskom Distribution Technology and University of Natal, South Africa.
6. Chatterton B. G. (2002): "The use of surge arresters in parallel for the lightning protection of pole mounted Distribution transformers in Eskom"
7. Cobine, Dillon J. (1958): "Gaseous Conductors: Theory and Engineering Applications", Dover Publications, New York.
8. Craggs J.D., Meek J.M. (1954): "High Voltage Laboratory Technique", Butterworth Scientific Publishers, London.
9. Craggs J.D., Meek J.M. (1953): "Electrical Breakdown in Gases", The Clarendon Press, Oxford.
10. Darveniza M., Mercer D. R. and Parnell T. M. (1968): "The lightning protection of distribution transformers", Transformers and Lightning, Institute of Engineers, Australia, pp193-204.

11. Darveniza D. and Uman M. A. (1984) : "Research into lightning protection of distribution systems – Results from Florida field work 1978 and 1979", IEEE Transactions on Power Apparatus and Systems, Vol 4, pp 103.

12. Ericksson A. J. (1986): "The incidence of lightning strikes to power lines", IEEE Transactions on Power Apparatus and Systems, New York.

13. Ericksson A. J., Geldenhuys H. J., Kroninger H. and Hefer S. M. (1986): "A study of lightning stresses on metal oxide surge arresters", Paper 33-08, CIGRE Session, Paris.

14. Gaunt C. T., Britten A. C. and Geldenhuys H. J. (1989): "Insulation co-ordination of unshielded distribution lines from 1 kV to 36 kV", The High Voltage Co-ordinating Committee Task Force on the Lightning Protection of Distribution Lines, SAIEE.

15. Geldenhuys H. J. (1992): "The role of earthing", Chapter 5, Lightning Workshop Handout Notes, Eskom and CSIR Course.

16. Geldenhuys H. J., Lagesse R. B., Britten A. C., Sadurski K. J. and Van der Merwe W. C. (1992) : "Practical insulation co-ordination of wood pole distribution lines in lightning areas", IEEE Transactions on Power Apparatus and Systems, Swaziland, pp 503-508.

17. Hileman A. R., Roguin J. and Weck K. H. (1990): "Metal oxide surge arresters in AC systems – Part 5: Protection performance of metal oxide surge arresters", Electra No. 133, pp133 -143.

18. Heine P. and Lehtonen. M. (2003): "Voltage Sag Distributions Caused by Power System Faults," IEEE Transactions on Power Apparatus and Systems, Vol. 18, pp. 1367-1373.

19. Linck H., Gehring E. H., Kotter F.R. and Rohlfs A.F. (1967): "Report on industry survey of protective gap applications in HV systems", IEEE Transactions on Power Apparatus and Systems, Vol 86, pp1432 -1437

20. Amestrand S.A., Linck H., Seabrook R.E. and Carrara G. (1974): "Characteristics of protective gaps", IEEE Transactions on Power Apparatus and Systems, Vol 93, pp196 - 205

21. Link H., Gehring E. H., Kotter F.R. and Rohlfs A.F. (1968): "Impulse, Switching Surge, And 60Hz Sparkover Tests By Three Laboratories On A 500 kV Ring To Rod Protective Gap", IEEE Transactions on Power Apparatus and Systems, Vol 87, pp 713 - 721

22. IEC 60060-2 (1994): "High Voltage test techniques – measuring systems" , second edition:

23. Kuffel, E. (1995): "The influence of nearby earth objects and polarity of voltage on dc breakdown of sphere gaps" IEE, Proc. Part A, pp 108, 302.

24. Lowden E. (1989): "Practical transformer design handbook", 2nd ed., Tab Books, Blue Ridge Summit, ISBN 0-8306-3212-3.

25. Maxwell J. C. (2000): "Electricity and Magnetism" , 3rd edition, Vol 1,

26. Naidu M. S. and Kamaraju V. (1995): "High Voltage Engineering", 2nd ed., McGraw Hill, ISBN 0-07-462286-2.

27. NRS 039 (1995): "Guide for the application of gapless metal-oxide surge arresters in distribution systems", NRS Rationalised user specification, South Africa.

28. NRS 048 (1996): "Electricity Supply Quality of Supply", NRS Rationalised user specification, South Africa.

29. Parrish D. E. (1991): "Lightning-caused distribution transformer outages on a Florida Distribution system", IEEE Transactions on Power Delivery, Vol. 6, No.2.

30. Qureshi M. I., Al-Arainy A. A. and Malik N.H. (1999): "Performance Of Protective Rod Gaps For Medium Voltage Networks In The Presents Of Dust Particles Under Lightning Impulses", IEEE Transaction on Power Delivery, Vol 14, pp 1311 - 1316.

31. Rogowski (1926): "Arch.F.Elekt", Vol 16, pp 16.

32. SAIEE (1989): "The lightning protection of distribution lines", Conference Proceedings.

33. Schwab A. (1969): "High Voltage Experimental Technique".

34. SCSASAAL9 (1999): "Distribution Earthing Standard Part 2: Section 1 MV and LV Reticulation Earthing", Eskom Standard.

35. SCSASABE7 (2001): "General information and requirements for overhead lines up to 33kV with conductors up to Hare/Oak", Eskom Distribution MV Standard, Section 0.

36. SCSSCAAN5 (2000): "Specification for distribution class, metal-oxide surge arresters without spark-gaps", Eskom Distribution specification.

37. Schneider Technical library (2006): "Schneider Electric Technical booklet N°151"

38. Van Schalkwyk W. J. (2001): "The placing of line surge arresters and fuses on 11 and 22kV lines to protect equipment against lightning", M.Eng thesis, University of Stellenbosch, South Africa.

39. Chimklai S. and Marti J. R. (1995): "Simplified three phase transformer model for electromagnetic transient studies" ", IEEE Transaction on Power Delivery, Vol 10, pp 1316 - 1325

40. .Wedmore E. B. (1940): "Surge Phenomena –seven years research for the central electricity board".

41. The Alstom Technical Library (2006): "Alstom Prag Manual - Settings manual for network protection"

42. Leuven (1992): "Alternate transient program rule book", Leuven EMPT Centre.

43. Woivre V. , Ahmed A. and Burais N. (1993): "Transient overvoltage study and model for shell-type power transformers", IEEE Transaction on Power Delivery, Vol 8, pp 212 - 222

44. Morched A., Marti L. and Ottenvangers J. (1993): "A high frequency model for the EMPT", IEEE Transaction on Power Delivery, Vol 18, pp 1615 – 1626.

45. Kelly R. (1996): "Lightning surge propagation from medium voltage to low voltage distribution networks" MSc(Eng.) Thesis, Wits.

46. Holdalen H. K. (1997): "Lightning induced voltages in low voltage systems with emphasis on lossy ground effects"

47. Kreuger F. H. (2002): "Industrial High voltage co-ordination, measuring and testing"

48. IEEE Standard C62.22 (1991): "Guide for the application of metal-oxide surge arresters for alternating current systems."

49. IEC 60011-1 (2006): "Insulation co-ordination, definition, principles and rules", eighth edition.

50. IEC 60028 (1995): "International standard for the resistance of copper" , second edition:

51. IEC 60052 (2002): "Voltage measurements by means of standard air gaps", third edition.

APPENDICES

APPENDIX A: EASTERN REGION TRANSFORMER FAILURES PLANT REPORT 2006

The graph shows that the transformer failure rate for Newcastle in November 2005, was 6.87 % and November 2006 was 4.64 % The average for all areas over the same periods was 5.19% and 3.84% respectively.

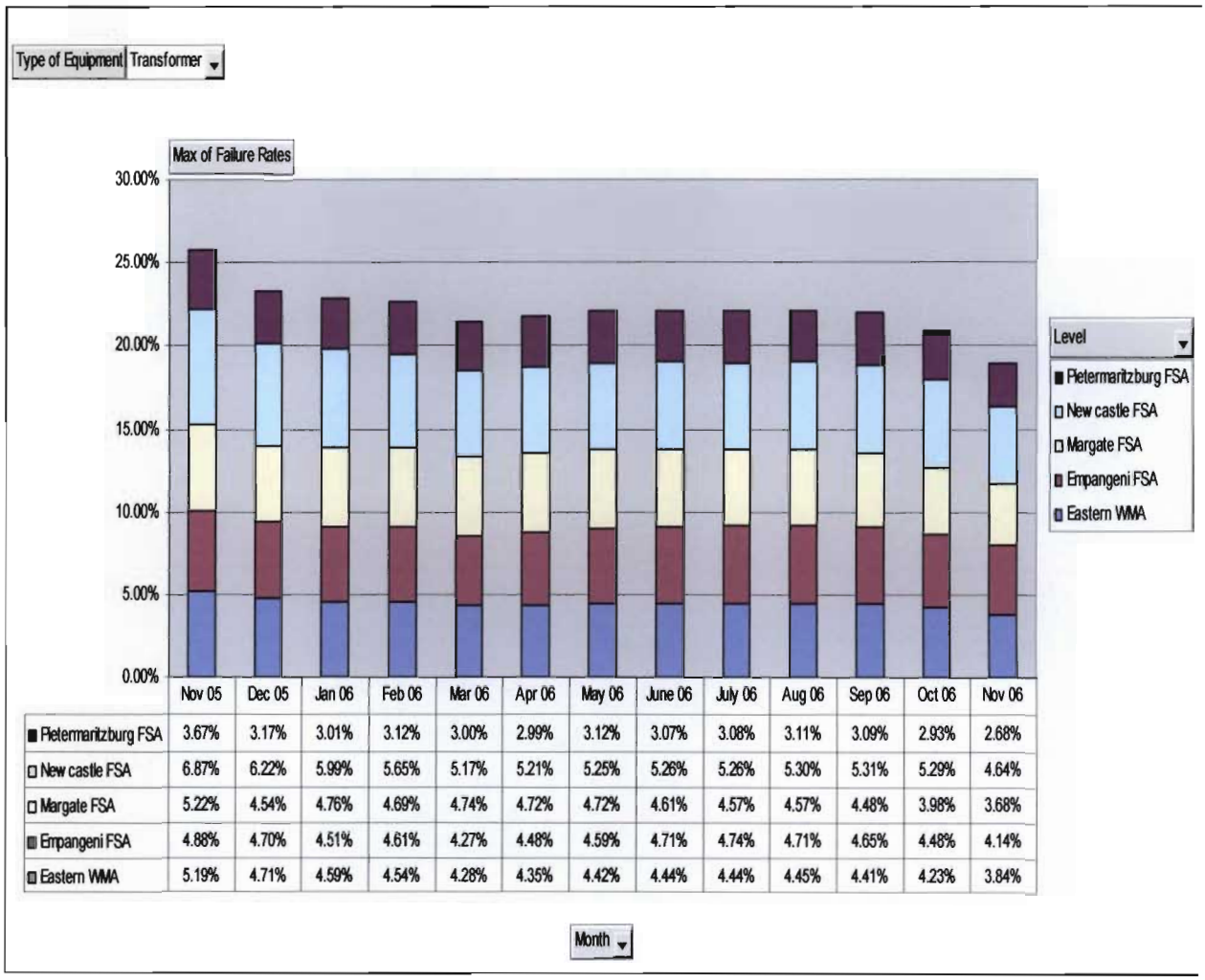

	Nov 05	Dec 05	Jan 06	Feb 06	Mar 06	Apr 06	May 06	June 06	July 06	Aug 06	Sep 06	Oct 06	Nov 06
Pietermaritzburg FSA	3.67%	3.17%	3.01%	3.12%	3.00%	2.99%	3.12%	3.07%	3.08%	3.11%	3.09%	2.93%	2.68%
New castle FSA	6.87%	6.22%	5.99%	5.65%	5.17%	5.21%	5.25%	5.26%	5.26%	5.30%	5.31%	5.29%	4.64%
Margate FSA	5.22%	4.54%	4.76%	4.69%	4.74%	4.72%	4.72%	4.61%	4.57%	4.57%	4.48%	3.98%	3.68%
Empangeni FSA	4.88%	4.70%	4.51%	4.61%	4.27%	4.48%	4.59%	4.71%	4.74%	4.71%	4.65%	4.48%	4.14%
Eastern WMA	5.19%	4.71%	4.59%	4.54%	4.28%	4.35%	4.42%	4.44%	4.44%	4.45%	4.41%	4.23%	3.84%

Figure A 1 Transformer failure over a one year period

APPENDIX B: THE SOFTWARE USED TO CONDUCT THE SIMULATION

B1 FEMLAB software used to model the Electric Field

The PDE solution Formulation for Electrostatics modeling in 3D

The solution for the *3D Electrostatics in a generalized* application mode the solution is solved as follows:

$$-\nabla \cdot ((\sigma + \varepsilon_0 / T)\nabla V - (\mathbf{J}^e + \mathbf{P}/T)) = \rho_0 / T \qquad \text{[B1.1]}$$

This equation assumes the constitutive relation

$$\mathbf{D} = \varepsilon_0 \mathbf{E} + \mathbf{P}$$

In the *In-plane electrostatics, generalized* application mode, we assume a symmetry where the electric potential varies only in the *x* and *y* directions, and is constant in the *z* direction. This implies that the electric field, **E**, is tangential to the *x-y* plane. Given this symmetry, we solve the same equation as in the 3D case.

In the *Axissymmetric electrostatics, generalized* application mode we consider the situation where the fields and the geometry are axially symmetric. In this case the electric potential is constant in the φ direction, which implies that the electric field is tangential to the *r-z* plane.

Writing the equation in cylindrical co-ordinates, and multiplying it by *r* to avoid singularities at *r* = 0, the equation becomes

$$-\begin{bmatrix} \frac{\partial}{\partial r} \\ \frac{\partial}{\partial z} \end{bmatrix}^T \cdot \left(r(\sigma + \varepsilon_0 / T) \begin{bmatrix} \frac{\partial V}{\partial r} \\ \frac{\partial V}{\partial z} \end{bmatrix} - r(\mathbf{J}^e + \mathbf{P}/T) \right) = r\rho_0 / T \qquad \text{[B1.2]}$$

B2 Results of the FEMLAB Electrostatic Analysis

The theory used is as discussed above. The equation B1.1 is solved,

$$-\nabla \cdot ((\sigma + \varepsilon_0 / T)\nabla V - (\mathbf{J}^e + \mathbf{P}/T)) = \rho_0 / T \qquad \text{[B2.1]}$$

Where:

V = applied voltage

σ = isotropic conductivity

ε_0 = isotropic permittivity

ε_r = isotropic relative permittivity

ρ_0 = space charge density

B3 Steps for FEMLAB Simulation set up for Gap Modeling

a) Set up of the drawing window and then choose the following options

1. Model navigator
2. 3D – because in 3D place.
3. Electromagnetic
4. Electrostatics
5. Cannot model in 3D
6. Choose – work plane settings and
7. Choose either xy ; y3 ; 3x
8. Default to yx plane = 0
9. To draw a cylinder select x =0

b) Completing the drawing

10. Draw in a rectangle.
11. Draw a second rectangle by in by coping rectangle 1
12. The space between rectangles is d. Select x = 0 and y= gap size.
13. Press control to select both objects.
14. Go to draw; then select revolve.
15. Then in revolve settings for both P1 and P2.

D = 0
D2 = 360

} Angle of rotation

X = 0
Y = 0

} Revolution axis's; point on axis

Axis direction second point

X = 0
Y = 1

} * revolve one at a time

To draw block around entire gap, select from draw menu

Block

Style – solid

Base – centre

X, Z length = 1000

16. D = diameter of rod
    d = distance between rods (gap)
17. If D = 20mm; draw rectangle = 10mm; when revolved = 20mm.
18. Two modes to work in draw mode; pencil with triangle – Set Square, Subdomain is Ω at end. In Ω mode you will not be able to edit drawing only in draw mode.
19. To draw a boundary all round; in draw, select block.
    In sub-domain settings select block right on top. Style solid; free space – define as q.
    - Base centre ; xyz = 700
    - Select 700 ie 340; 340 on either side.
    - Choose a block that will give you a maximum all round (equal 3D space around rod).
    - If we set top rod at potential we expect lines to flow out of the rod
    - Set (bottom) of it to earth potential; it will force lines into rod.
    - If we set V_t at potential, we line core out, because we at zero potential it will force lines back into rod.

20. Define material of rods.

Go to physics; sub-domain settings; object

1. being the entire cube (free space)
2. being the lower rod (metal, load metal)
3. being the structural steel (automatically all setting populate)

21. Conductivity of free space = 1

Go to initial (init)

- Electric potential at zero V tie the
- Bottom rod is ground
- Top electrode at 110 000 V or 110kV

22. Sub-domain setting for object 1 is air so leave blank

- To move vertical rods further or closer to earth plane ; go to draw mode ; shift and select both objects ; use the arrow sign icon on left centre. Select x, y, z to move big red square on extreme left.

23. Next is physic boundary setting

- Select big red square on left to select surfaces; just above it is select lines.
- Select box and set as five sides as electric insulation and one side as earth plane/ground.
- All surfaces on upper rod to be electric potential. All on lower rod to be earth/ground plane (or) V = V0 = 0kV
- Go to boundary at pick electric potential as we have set V= V0 = 110kV, has been defined in previous settings, sub-domain settings.
- Under boundary settings electrostatic, boundary sources and constraints V0 = 10kV right at bottom.
- If you need to redefine axis; axis and grid settings select axis and change
- Ground rod = 0; potential – 110kV

24. To Mesh

- Go to mesh

- Select initialize mesh
- Mesh parameter
- Predefined sizes
- Move between draw and mesh to see object mesh
- Once mesh generated go to solve.

25. To solve
    - Go to solver
    - Run solver
    - Input initial guess
    - If it leads to undefined problems go to mesh select course mesh
    - Re-mesh
    - Go back to solve – resolve.
26. Once solver is complete – go to post processing – this is the information that we initially were looking for in the first place.
27. Post Processing

    Cross-section plot parameters; slice; predefine quantities your way select any of these; select electric field normal.

    When breakdown occurs you have complete ionization across the gap, the potential that you had at potential rod must now equal to the potential at your ground rod. If the two peaks are not the same it implies that complete breakdown has not occurred, which is fine. We put in a value of 100kV and expected breakdown at 110kV so complete ionization did not occur.

B4 Developing the Femlab geometry

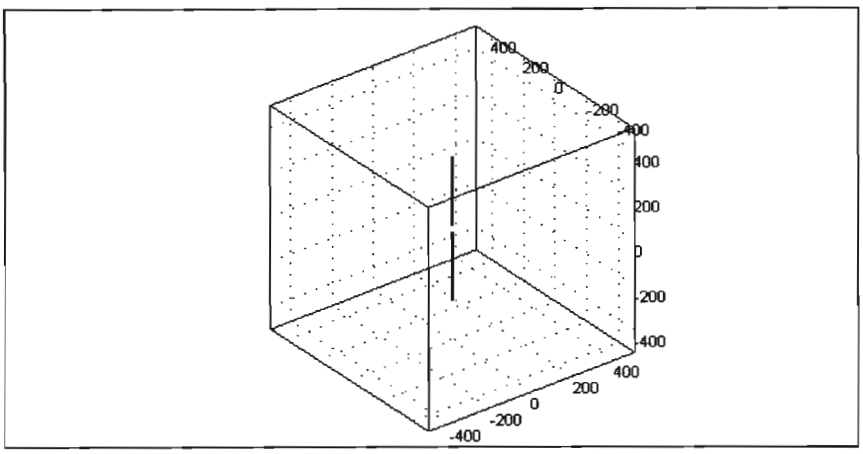

Figure B4.1 Showing completed 3-D geometry of Flat / Hemispherical rod - rod gap.

B5 Sub-domain and Boundary Settings

The potential difference equation which was applied to each of the sub-domains was:

$$-V.((\sigma + \varepsilon_0 \varepsilon_r / T)\nabla V - J^e) = \rho_0 / T \qquad \text{(B4.1)}$$

where V = applied voltage

σ = isotropic conductivity

ε_0 = isotropic permittivity

ε_r = isotropic relative permittivity

ρ_0 = space charge density

The constitutive relation that was applied to each of the sub-domains was:

$$D = \varepsilon_0 \varepsilon_r E \qquad \text{(B4.2)}$$

Where

D = electric flux intensity

E = electric field intensity

B6 The sub-domains were defined as follows:

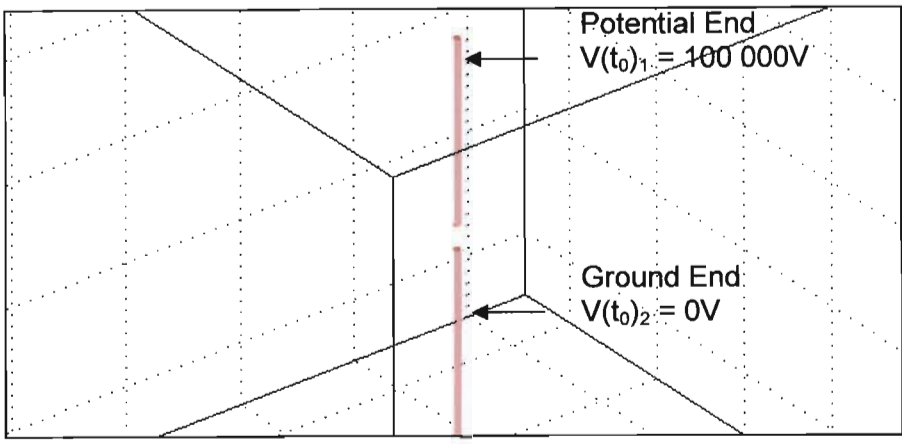

Figure B4.2 Showing Potential End and Ground End sub-domains for Flat / Hemispherical rod – rod gaps.

Table B4.1 Subdomain settings applied

Sub-domain	Potential End	Ground End	Potential Ring	Ground Ring	Cube
Material	Structural steel	Structural steel	Copper	Copper	Air
$V(t_o)$ V	100000	0	100000	0	0
σ	4.032e6	4.042e6	5.998e7	5.998e7	0
ε_r	1	1	1	1	1
ρ_0	0	0	0	0	0
Boundary	Electric potential	Ground	Electric potential	Ground	Electric insulation

APPENDIX C: FEMLAB ELECTRIC FIELD LINE PLOTS OF BREAKDOWN VOLTAGE

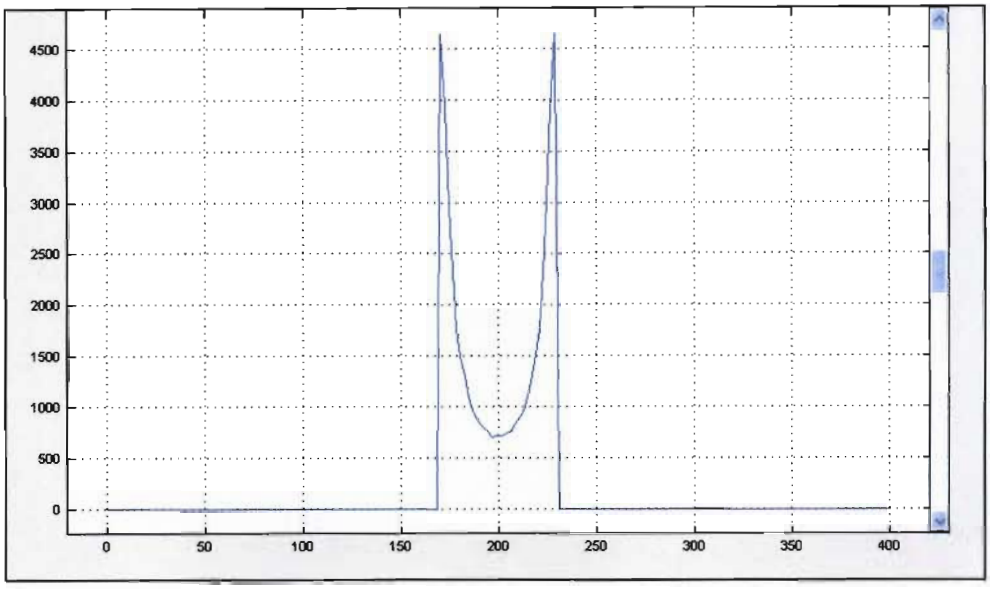

Figure C1 Electric Field Line plot for Flat rod – rod gap, D = 10mm, d = 50mm.

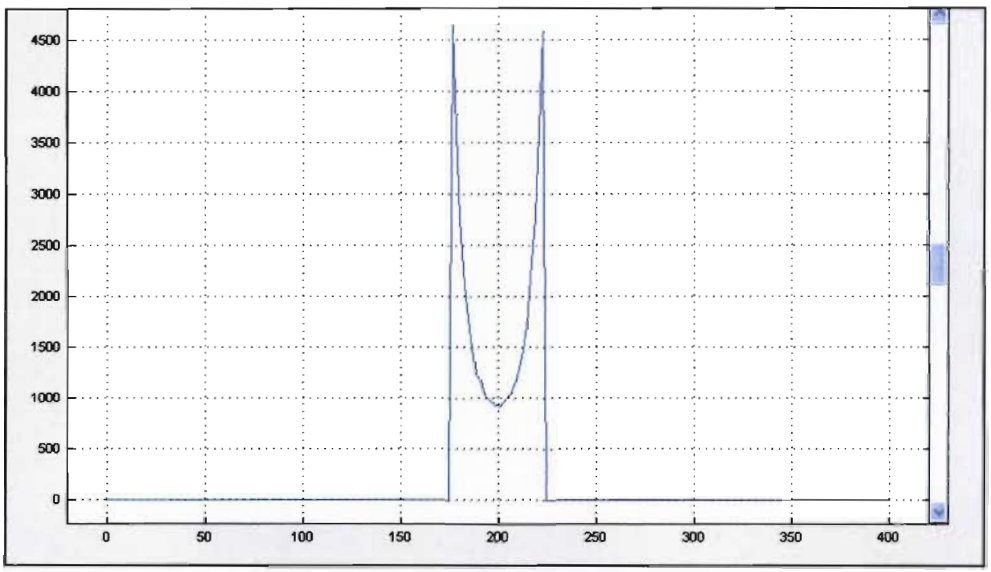

Figure C2 Electric Field Line plot for a Flat rod – rod gap, D = 10mm, d = 60mm.

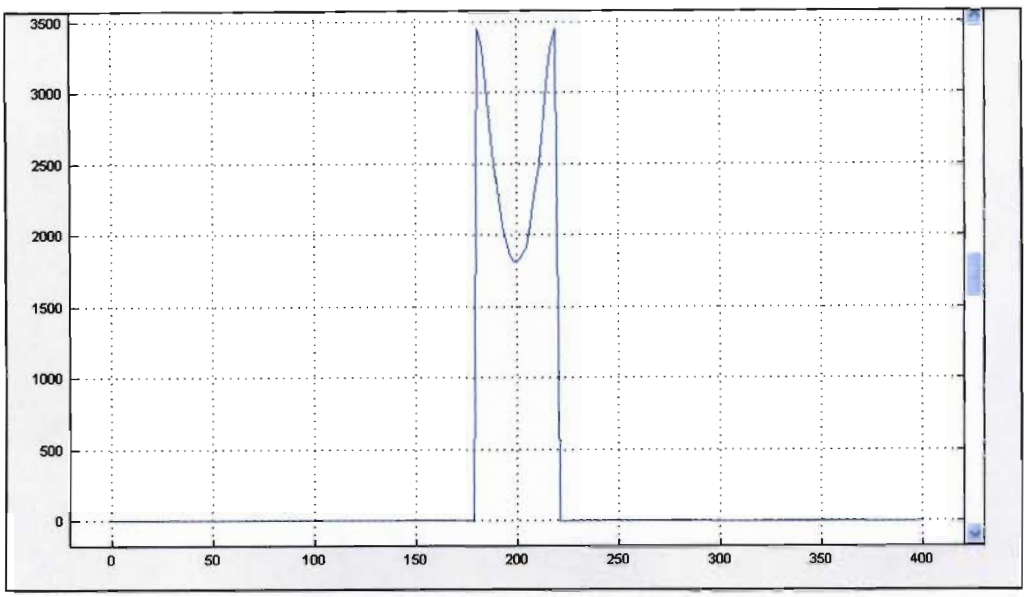

Figure C3 Electric Field Line plot for a Flat rod – rod gap, D = 20mm

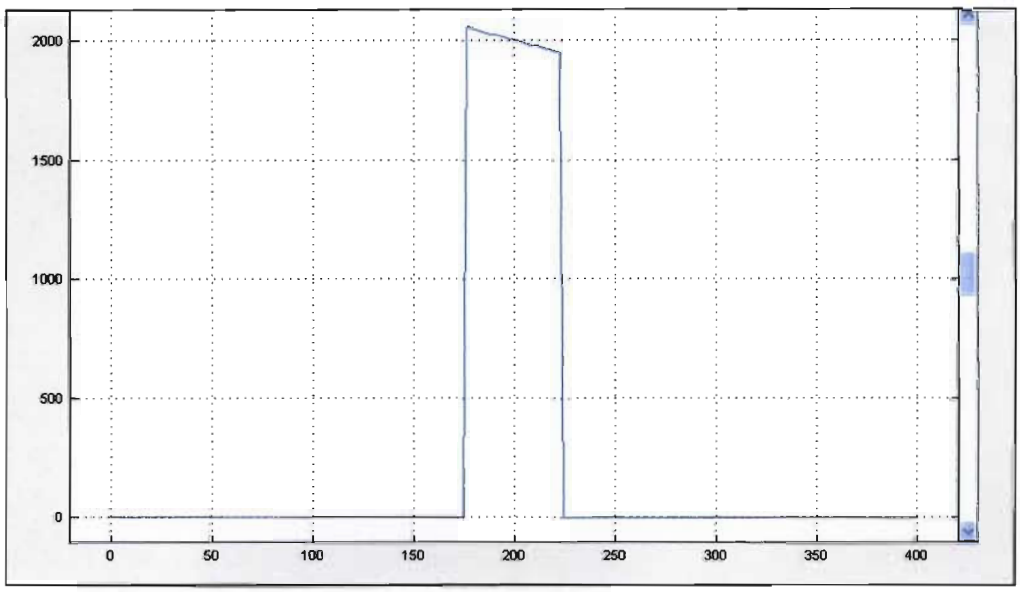

Figure C4 Electric Field Line plot for Flat rod – rod gap, d = 40mm.

Figure C.4: Showing line plot of electric field within a Flat rod – rod gap, d = 50mm. Note: Unsymmetrical about mid-point of gap.

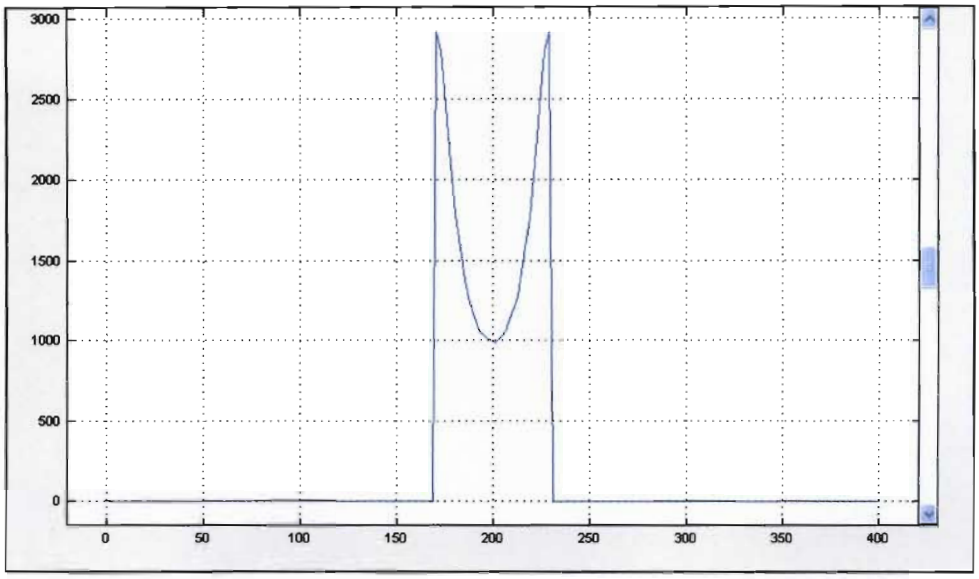

Figure C5 Electric Field Line plot for Flat rod – rod gap, d = 60mm.

Hemispherical rod – rod gap, D = 20mm

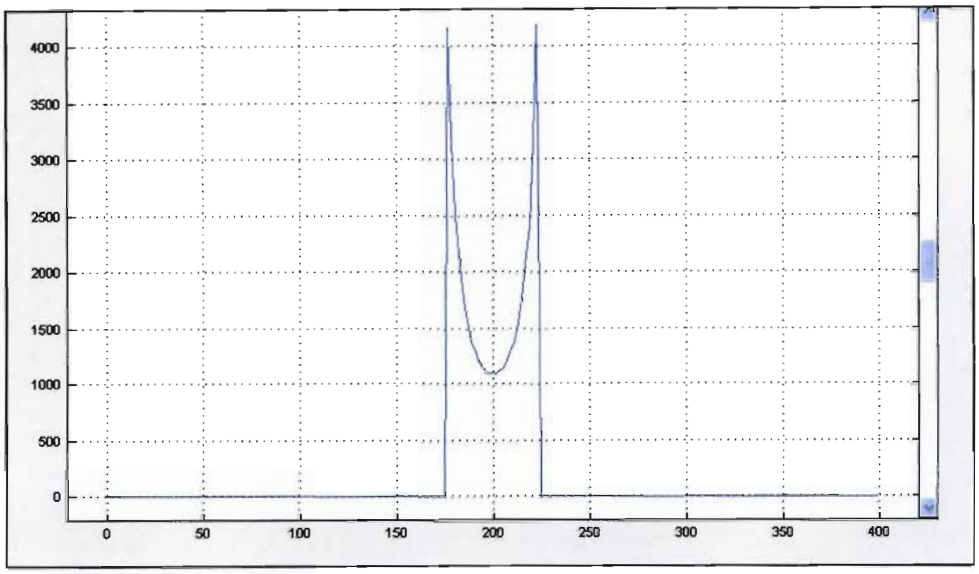

Figure C6 Electric Field Line plot for Flat rod – rod gap, d = 50mm.

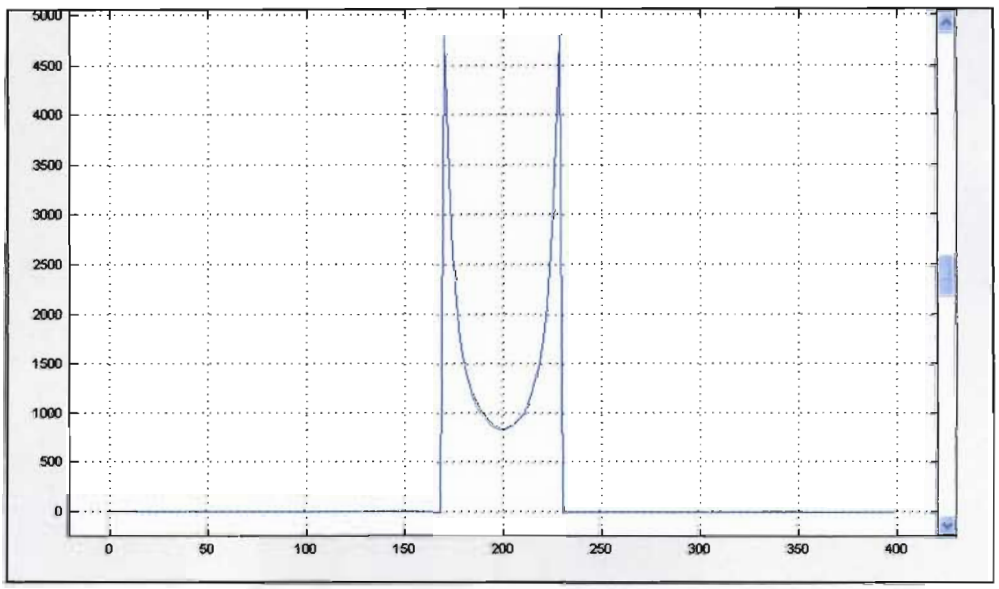

Figure C7 Electric Field Line plot for Flat rod – rod gap, d = 60mm.

APPENDIX D: FEMLAB GRAPHS DERIVED USING MATHLAB SOFTWARE CODE

D1 Software code to calculate Breakdown Voltage

```
Vapplied = input ('Enter the Voltage applied (V): ');
d = input ('Enter the sphere gap length (mm): ');
delta = d/3;
a = (d/2) - delta;
b = d/2;
distance_a = a
Ea = input ('Enter value of electric field at distance a (V/mm): ')
distance_b = b
Eb = input ('Enter value of electric field at distance b (V/mm): ')

Ea_p = (10*Ea)/760;
Eb_p = (10*Eb)/760;

Ea_p_new = Ea_p;
Eb_p_new = Eb_p;

ans = 0;
V = Vapplied;

if (Ea_p_new < 25)
   alpha_a = 0;
   neta_a = 0.005;
end
if (Ea_p_new >= 25) & (Ea_p_new < 32)
   alpha_a = (571.4285714*10^-6)*Ea_p_new - (13.08571429*10^-3);
   neta_a = (-57.14285714*10^-6)*Ea_p_new + (6.428571429*10^-3);
end
if (Ea_p_new >= 32) & (Ea_p_new < 44)
   alpha_a = (2.06666667*10^-3)*Ea_p_new - (60.93333333*10^-3);
   neta_a = (116.6666667*10^-6)*Ea_p_new + (866.6666667*10^-6);
```

```
end
if (Ea_p_new >= 44) & (Ea_p_new < 55.5)
   alpha_a = (5.391304348*10^-3)*Ea_p_new - (207.2173913*10^-3);
   neta_a = (3.636363636*10^-6)*Ea_p_new - (9.999999998*10^-3);
end
if (Ea_p_new >= 55.5)
   alpha_a = (9.166666667*10^-3)*Ea_p_new - (416.75*10^-3);
   neta_a = (3.636363636*10^-6)*Ea_p_new - (9.999999998*10^-3);
end

alpha_neta_a = (alpha_a - neta_a) * 760;
sigma_a = alpha_neta_a * (delta/10);

if (Eb_p_new < 25)
   alpha_b = 0;
   neta_b =0.005;
end
if (Eb_p_new >= 25) & (Eb_p_new < 32)
   alpha_b = (571.4285714*10^-6)*Eb_p_new - (13.08571429*10^-3);
   neta_b = (-57.14285714*10^-6)*Eb_p_new + (6.428571429*10^-3);
end
if (Eb_p_new >= 32) & (Eb_p_new < 44)
   alpha_b = (2.06666667*10^-3)*Eb_p_new - (60.93333333*10^-3);
   neta_b = (116.6666667*10^-6)*Eb_p_new + (866.6666667*10^-6);
end
if (Eb_p_new >= 44) & (Eb_p_new < 55.5)
   alpha_b = (5.391304348*10^-3)*Eb_p_new - (207.2173913*10^-3);
   neta_b = (3.636363636*10^-6)*Eb_p_new - (9.999999998*10^-3);
end
if (Eb_p_new >= 55.5)
   alpha_b = (9.166666667*10^-3)*Eb_p_new - (416.75*10^-3);
   neta_b = (3.636363636*10^-6)*Eb_p_new - (9.999999998*10^-3);
end

alpha_neta_b = (alpha_b - neta_b) * 760;
sigma_b = alpha_neta_b * (delta/10);
```

```
ans = 2*sigma_a + sigma_b;
while (ans < 18) | (ans > 18.8)

   if (ans < 18.32)
      V = V + 1000;

      Ea_p_new = Ea_p*(V/Vapplied);
      Eb_p_new = Eb_p*(V/Vapplied);

if (Ea_p_new < 25)
   alpha_a = 0;
   neta_a =0.005;
end
if (Ea_p_new >= 25) & (Ea_p_new < 32)
   alpha_a = (571.4285714*10^-6)*Ea_p_new - (13.08571429*10^-3);
   neta_a = (-57.14285714*10^-6)*Ea_p_new + (6.428571429*10^-3);
end
if (Ea_p_new >= 32) & (Ea_p_new < 44)
   alpha_a = (2.06666667*10^-3)*Ea_p_new - (60.93333333*10^-3);
   neta_a = (116.6666667*10^-6)*Ea_p_new + (866.6666667*10^-6);
end
if (Ea_p_new >= 44) & (Ea_p_new < 55.5)
   alpha_a = (5.391304348*10^-3)*Ea_p_new - (207.2173913*10^-3);
   neta_a = (3.636363636*10^-6)*Ea_p_new - (9.999999998*10^-3);
end
if (Ea_p_new >= 55.5)
   alpha_a = (9.166666667*10^-3)*Ea_p_new - (416.75*10^-3);
   neta_a = (3.636363636*10^-6)*Ea_p_new - (9.999999998*10^-3);
end

alpha_neta_a = (alpha_a - neta_a) * 760;
sigma_a = alpha_neta_a * (delta/10);


if (Eb_p_new < 25)
```

```
    alpha_a = 0;
    neta_a =0.005;
end
if (Eb_p_new >= 25) & (Eb_p_new < 32)
    alpha_a = (571.4285714*10^-6)*Eb_p_new - (13.08571429*10^-3);
    neta_a = (-57.14285714*10^-6)*Eb_p_new + (6.428571429*10^-3);
end
if (Eb_p_new >= 32) & (Eb_p_new < 44)
    alpha_a = (2.06666667*10^-3)*Eb_p_new - (60.93333333*10^-3);
    neta_a = (116.6666667*10^-6)*Eb_p_new + (866.6666667*10^-6);
end
if (Eb_p_new >= 44) & (Eb_p_new < 55.5)
    alpha_a = (5.391304348*10^-3)*Eb_p_new - (207.2173913*10^-3);
    neta_a = (3.636363636*10^-6)*Eb_p_new - (9.999999998*10^-3);
end
if (Eb_p_new >= 55.5)
    alpha_a = (9.166666667*10^-3)*Eb_p_new - (416.75*10^-3);
    neta_a = (3.636363636*10^-6)*Eb_p_new - (9.999999998*10^-3);
end


alpha_neta_b = (alpha_b - neta_b) * 760;
sigma_b = alpha_neta_b * (delta/10);

ans = 2*sigma_a + sigma_b;

end

if (ans > 18.8)
        V = V - 1000;

        Ea_p_new = Ea_p*(V/Vapplied);
        Eb_p_new = Eb_p*(V/Vapplied);

if (Ea_p_new < 25)
    alpha_a = 0;
```

```
    neta_a =0.005;
end
if (Ea_p_new >= 25) & (Ea_p_new < 32)
    alpha_a = (571.4285714*10^-6)*Ea_p_new - (13.08571429*10^-3);
    neta_a = (-57.14285714*10^-6)*Ea_p_new + (6.428571429*10^-3);
end
if (Ea_p_new >= 32) & (Ea_p_new < 44)
    alpha_a = (2.06666667*10^-3)*Ea_p_new - (60.93333333*10^-3);
    neta_a = (116.6666667*10^-6)*Ea_p_new + (866.6666667*10^-6);
end
if (Ea_p_new >= 44) & (Ea_p_new < 55.5)
    alpha_a = (5.391304348*10^-3)*Ea_p_new - (207.2173913*10^-3);
    neta_a = (3.636363636*10^-6)*Ea_p_new - (9.999999998*10^-3);
end
if (Ea_p_new >= 55.5)
    alpha_a = (9.166666667*10^-3)*Ea_p_new - (416.75*10^-3);
    neta_a = (3.636363636*10^-6)*Ea_p_new - (9.999999998*10^-3);
end

alpha_neta_a = (alpha_a - neta_a) * 760;
sigma_a = alpha_neta_a * (delta/10);


if (Eb_p_new < 25)
    alpha_a = 0;
    neta_a =0.005;
end
if (Eb_p_new >= 25) & (Eb_p_new < 32)
    alpha_a = (571.4285714*10^-6)*Eb_p_new - (13.08571429*10^-3);
    neta_a = (-57.14285714*10^-6)*Eb_p_new + (6.428571429*10^-3);
end
if (Eb_p_new >= 32) & (Eb_p_new < 44)
    alpha_a = (2.06666667*10^-3)*Eb_p_new - (60.93333333*10^-3);
    neta_a = (116.6666667*10^-6)*Eb_p_new + (866.6666667*10^-6);
end
if (Eb_p_new >= 44) & (Eb_p_new < 55.5)
```

```
    alpha_a = (5.391304348*10^-3)*Eb_p_new - (207.2173913*10^-3);
    neta_a = (3.636363636*10^-6)*Eb_p_new - (9.999999998*10^-3);
end
if (Eb_p_new >= 55.5)
    alpha_a = (9.166666667*10^-3)*Eb_p_new - (416.75*10^-3);
    neta_a = (3.636363636*10^-6)*Eb_p_new - (9.999999998*10^-3);
end


alpha_neta_b = (alpha_b - neta_b) * 760;
sigma_b = alpha_neta_b * (delta/10);

ans = 2*sigma_a + sigma_b;

end

end

Sigma = ans
Break_Down_voltage = V
```

D2 A/P AND H/P CURVES

In order to perform the breakdown voltage calculation in a timely and optimum manner it was decided that the α/p and η/p curves be manipulated using Matlab. The curves were divided into 5 and 4 linear regions respectively and the linear equations for each region was then determined.

α/p

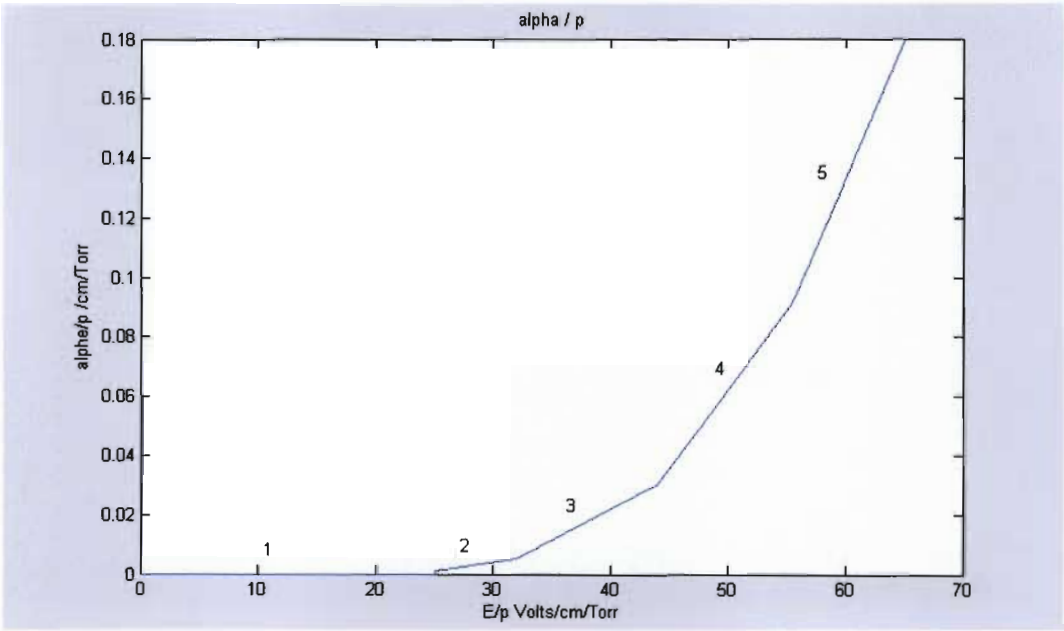

Figure D.1: Showing regions of α/p curve.

1: $\alpha/p = 0$

2: $\alpha/p = 571.4285714 * 10^{-6} * E/p - 13.08571429 * 10^{-3}$

3: $\alpha/p = 2.066666667 * 10^{-3} * E/p - 60.93333333 * 10^{-3}$

4: $\alpha/p = 5.391304348 * 10^{-3} * E/p - 207.2173913 * 10^{-3}$

5: $\alpha/p = 9.166666667 * 10^{-3} * E/p - 416.75 * 10^{-3}$

η/p

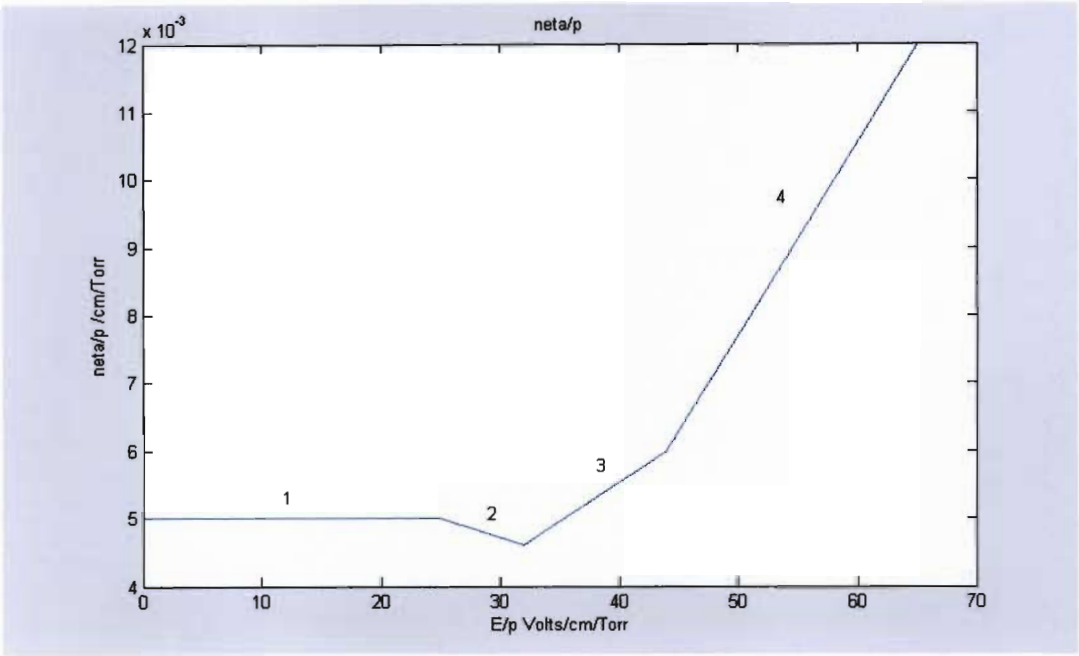

Figure D.2: Showing regions of η/p curve.

1: $\alpha/p = 0.005$

2: $\alpha/p = -57.14285714 * 10^{-6} * E/p + 6.428571429 * 10^{-3}$

3: $\alpha/p = 116.6666667 * 10^{-6} * E/p + 866.6666667 * 10^{-6}$

4: $\alpha/p = 3.636363636 * 10^{-6} * E/p - 9.999999998*10^{-3}$

APPENDIX E: THE DERIVATION OF A SOLUTION FOR ABRUPTLY CHOPPED WAVE

E1 The theory derived from an equivalent transformer circuit.

From the ordinary transformer theory it is known that transformer windings oscillate in a great number of space harmonics, the character of which is mainly determined by the transformer connections. Whereas the damping effect is negligible for the fundamental frequency, it increases rapidly with higher orders of harmonics, and test results show that it is sufficient to limit the calculation of transference to the fundamental harmonic. The calculations carried out for impulse waves using Heaviside's unit step function shape, that is, waves which rise to unity when time equals zero and which remain constant at unity for all subsequent values of time ***t***.

As the Laplace transforms methods is simpler than Heaviside's operational calculus, the following equation describes the transmitted wave

Taken as an L-C parallel combination, Let **E** be the voltage to earth impressed at the line terminal of the winding under consideration (owing to the relatively high surge impedance of transformer windings **E** will generally be approximately twice the voltage of the travelling wave), also, let ***e*** be the voltage to earth at a point in the winding a distance **x** from the neutral end.

Then,

$$e = EU(t) \qquad (4.2)$$

Thus the reflected wave is

$$e'(s) = -\left(+1 - \frac{2\alpha}{n-m}\left(\exp(-mt) - \exp(-nt)\right)\right)EU(t) \qquad (4.3)$$

and the transmitted wave is

$$e''(s) = -\left(+1 - \frac{2\alpha}{\left(\omega_0^2 - (\alpha/2)^2\right)}\left(\exp(-\alpha/2t)\sin\sqrt{\omega_0^2 - (\alpha/2)^2}\,t\right)\right)EU(t) \qquad (4.4)$$

and the constraints are:

$$If\ \omega_0^2 > \frac{\alpha}{2}^2 \qquad (4.4)$$

From equation 4.4 the transmitted wave reaching the transformer will be either a double exponential (standard impulse type) or damped sinusoidal wave and the steepness of the wave front gets reduced as show in figure 4.3, Wedmore [40].

Thus the full solution becomes:

$$e\left[\frac{x}{l} - \frac{2\alpha^2}{\pi^2 + \alpha^2} Sin \frac{\pi x}{l} \cos \varpi 1t + \right.$$

$$\frac{2\alpha^2}{2(4\pi^2 + \alpha^2)} Sin \frac{2\pi x}{l} \cos \varpi 2t - ..... +$$

$$+(-)^m \frac{2\alpha x^2}{m\pi(m^2\pi^2 + \alpha^2)} Sin \frac{m\pi x}{l} \cos \varpi mt - .....+ \quad ...(4.7)$$

Thus the voltage gradient at any point in the winding and at any instant may be found by differentiating equation 4.7 above with respect to x.